Multi Bunch Beam Generation using a Mode Separated Photocathode RF Gun

Abhay P. Deshpande

The Graduate University for Advanced Studies (Sokendai)
School of High Energy Accelerator Science
2010

Acknowledgments

Any work that one performs needs a lot of support from many people in and around the individual. I am glad that I received great support from my family, friends and colleagues whenever I planned to do some thing. However, how many times does one get to appreciate and thank these supporters? Fortunately, I get this space for myself and I wish to thank many people for their help and encouragement over years.

First I wish to thank Prof. Junji Urakawa, my thesis advisor, for his encouragement and vision. He makes it a point not to assign any work or not to push in researchers towards his own ideas. Instead he left me to choose my own area of work and insisted on finding a topic for myself and focused to teach me how to achieve good quality work. I thank you sincerely for the guidance.

I wish to thank Prof. M. Kawai who introduced me to KEK. I also wish to thank Prof. Shin-ichi Kurokawa who guided me from time to time and made my journey from India to KEK smooth and comfortable.

At LUCX facility, I found many new friends with whom I shared most of the time in past 3 years. I wish to thank Dr. Masafumi Fukuda. Most of the work done at KEK was with Fukuda-san and I did enjoy working with him. I wish to thank Sakae Araki who taught me not only technical things but also Japanese language and many other things. I also wish to thank Dr. Kazuyuki Sakaue, Dr. H. Shimizu, Dr. Y. Honda, Dr. N. Terunuma, Dr. T. Omori, Dr. Alex Aryshev, Dr. M. Takano, Prof. N. Sasao (Okayama University), Prof. M. Washio (Waseda University), Dr. S. Liu (IHEP, China) and all other members of LUCX collaboration for discussions and guidance at various stages. I wish to acknowledge the active support from Dr. T. Higo in all aspects of structure design and Prof. K. Floetmann (Desy) for guidance for ASTRA code. I wish to thank Takatomi-san and Kudo-san for manufacturing support.

LUCX is a sub-group of ATF at KEK. Most of us share work on ATF and take shifts on ATF especially as support members. I wish to thank Dr. H. Hayano, Dr. Kuroda, Dr. Kubo, Dr. Okugi, Dr. T. Naito, Dr. S. Boogert (UK), Dr. Phillip Bambade (France), Dr. Deepa-Angal Kallinin (UK), Dr. M. Kuriki (Hiroshima University) and other members of ATF from whom I learnt a lot. I also wish to thank support staff at ATF for the kind support.

My life at KEK went very smooth mainly because of good attention of Ms. Kimiyo Ikeda. She sorted out not only official things but also apartment renting and other routine life issues for me. I have pestered her with large number of forms for my daughter who went to a Japanese play school. I admire Ikeda-san for her kindness and I thank her sincerely. I also thank Ms. H. Sasaki, Ms. H. Kusama and Ms. Y. Ono for the kind support. In Tsukuba I found many good friends and I wish to appreciate Hetti, Dushyant, Sho Yano, Mariajose, Maarja, Tanya and Dr. Simin for all the party time and emotional support. Indians at KEK Dr. Kailash Ruwali, Puneet Jain, Puneet Tyagi and Vijay Chouhan helped any time I asked for.

I did many other activities during my stay for Sokendai. I initiated first student magazine “FLAVOR” in English for Sokendai students. For all such activities, I got good support from Sokendai staff at KEK and

Hayama. I wish to thank Ms. Miyai, Ms. Omura and Mr. Y. Aizawa at KEK office for their support. I wish to thank Prof. Hirata and Dr. M. Iwase from Hayama for constant support in all activities I initiated.

In India, I work for SAMEER, R&D Lab of Govt. of India. I wish to thank Director SAMEER and my boss R. Krishnan for permitting me to take Ph.D. work at KEK. I wish to thank Shri. S. S. Bhide, my ex-boss, who introduced me to accelerators and patiently taught me basics of electron linac. Even today, he is keen to listen to me and teach me. Thanks to all my colleagues and friends at SAMEER and to Vasim Khan (now at Manchester University) for rigorous discussions.

My astronomy group, Khagol Mandal, has been an integral part of my life for past 20 years. It was a tough decision to be less active at KM and I wish to thank all my friends and well wishers at KM for their support. I wish to thank Dilip Joshi who has been most instrumental in all things that I did or will do. He is the source of inspiration for me, and many of my friends, to think out-of-the-way and to work hard to achieve the goal. “Failure is not a crime, to not to try is!” That’s what he taught me and I am indebted to him for everything. I also wish to thank Varsha Shukla and Sujata Babar for their kindness and support.

It will be capital mistake if I don’t mention my best friend Dr. Tanuja Dixit. I wish to thank you for constant support (and tolerance!) that you showed for past 15 years.

My mother followed all my plans with great interest and always insisted that I should take up new work and challenges. I wish to express my gratitude to my mother, brothers, sister-in-law for their understanding. I express my gratitude and thanks to my mother-in-law and all extended family and special thanks to Bhashu. My sweet niece Aboli grew up so much in 3 years and I missed her all the time.

My wife, Sujata is my biggest supporter, admirer, critic and she checks all aspects of my personality. She took up post-doctoral work at Tsukuba University in parallel to my work and managed my odd working hours, her own research and our daughter; not to mention the social life that we built up here. She has a good understanding of physics and is keen to listen to new ideas and criticize shallow thoughts. There is no way that I can thank you. I promise you to perform much better in future and make you happier.

Most of the work I did is at the cost of the time that would have been for my daughter Chitra. She was 3 months when I left her in India and grew up with out me. She came to Japan and yet stayed almost without me due to odd working hours that I kept. I am very happy to finish my work at KEK and that I will be soon back to India with my kid.

I wish to dedicate my thesis work to my father-in-law Prakash Kardile who passed away last year. I would miss the party he would have thrown to mark return of us all to India.

Thank you every one.

Abhay Deshpande

abhaypd@gmail.com

Sept. 2010, Tsukuba, Japan

Index

List of figures

Chap. 4

Chap. 5

Chap. 6

Appendix 1

Appendix 2

List of tables

Appendix 2

Table A2.1: Gun and linac parameters

Table A2.2: Measured linac parameters for existing 15 MeV linac tube

Table A2.3: RF gun cavity parameters

Table A2.4: Parameters of X-ray source

Abstract

The Accelerator Test Facility (ATF) at KEK designed the RF gun with Cs_2Te photo-cathode for the Laser Undulator Compact X-ray source (LUCX) and ATF linac. The first gun made at KEK was based on Brookhaven National Laboratory (BNL) gun design. Subsequently many improvements were made and an improved gun design was established. Based on the improved gun, eight guns were made by KEK and installed at various institutions in Japan. The expertise thus evolved at KEK for the RF guns from 2002 to 2008. The next request was now to further reduce the beam emittance and make beam energy spread stable over wider range in laser injection phase. It was also essential to increase the charge per bunch and number of bunches per train for increasing the x-ray flux from the LUCX. Around 2005, the Linac Coherent Light Source (LCLS) group at Stanford Linear Accelerator Center (SLAC) suggested that by increasing mode separation, more stability over injection phase variations could be achieved. LCLS group changed their own design to increase the mode separation up to 15 MHz. Following this approach, we decided to increase the mode separation. An advantage in our case is that we also made a new profile for the new gun to achieve high Q (unloaded quality factor) and high shunt impedance.

In this thesis we discuss the evolution of the design of the new gun structure and the procedure which we established to fabricate and process the RF gun. We show the experimental results of measurements and details of the tuning process to achieve the desired frequency at π mode of 2856 MHz with mode separation of 8.6 MHz maintaining the field balance at 1.0. The new gun has higher Q, higher shunt impedance and large mode separation than any gun made at KEK as well as the LCLS gun or the BNL gun. The observed dark currents are also less than earlier gun.

Our experience with new large mode separation gun coupled with 130 MV/m fields and Cs_2Te cathode is a very essential experience for making Cs_2Te a well acceptable material for photo cathode guns.

Beam dynamics simulations were done to estimate the trends of parameter variations. At present, PARMELA, ASTRA, GPT are the three most widely used codes for beam dynamics simulations of the RF guns. We decided to use ASTRA for the beam dynamics simulations of new RF gun mainly because it is much simple to use, free-of-charge and has been bench marked using many new RF gun.

The main focus of beam quality measurement was to compare the parameters for new RF gun with those for the old RF gun, where ever possible. The dependence of emittance was measured as a function of solenoid field, laser injection phase, laser spot size and charge. These measurements played crucial role to fix the optimum operational parameters for the RF gun. We measured the emittance value of 1.89 π-mm-mrad at 1nC charge. Efforts are on-going to check system alignment to push this emittance down to 1.0 π-mm-mrad. Variation in energy spread over the injection phase was also a parameter that we focused upon. The larger mode separation helps to maintain low energy spread over wider phase range. This was observed after careful experimentation.

The thermal emittance issue is discussed in the thesis. We try to estimate the thermal emittance using an indirect method. Direct measurement was not possible due to various limitations of the present setup. We propose to measure the thermal emittance by direct method in near future and we are making changes in our setup accordingly. We conclude that the three step model as it exists today is not sufficient to explain the measured value of thermal emittance for semiconductor photocathode. Hence detailed study will be helpful to understand the complexities of factors involved, which affect the thermal emittance.

Another striking feature of the work done at LUCX is to establish the methods for generation of long multi bunch beam. We succeeded in generating 100-bunches with 0.5 nC per bunch at 40 MeV with peak to peak energy difference less than 0.7%. In other experiment we generate low energy beam of 5 MeV. In this case we succeed to generate 300-bunches with 0.55 nC per bunch with peak to peak energy difference less than 0.85%. These results are very important results for our efforts to make 8000-bunches per train as a first step. We hope to achieve this goal by the end of this year (2010).

At LUCX we are trying to establish the generation of very long pulse trains and we wish to achieve 8000 bunches per train. The future of compact x-ray sources will depend on how long trains with high charge and low energy difference. It will be possible in few years to get very high flux x-ray from such sources. The present thesis is focused on new design of large mode separation gun, fabrication and tuning of the gun. Then tuning this gun to get a low emittance beam and there after generate 300-bunches per train is described.

Chapter 1: Introduction

The Accelerator Test Facility (ATF) group at KEK designed the RF gun system with Cs_2Te photo-cathode for the Laser Undulator Compact X-ray source (LUCX) and ATF main linac. The first gun made at KEK was based on Brookhaven National Laboratory (BNL) gun design. Subsequently many improvements were made and an improved gun design was established. Based on the improved gun, eight guns were made by KEK and installed at various institutions in Japan. The expertise thus evolved at KEK for RF guns from 2002 to 2008. The next request was now to further reduce the beam emittance and make beam energy spread stable over wider range in laser injection phase. It was also essential to increase the charge per bunch and number of bunches per train for increasing the x-ray flux from the LUCX. Around 2005, the Linac Coherent Light Source (LCLS) group at Stanford Linear Accelerator Center (SLAC) suggested that by increasing mode separation, more stability over phase variations could be achieved. LCLS changed their own design to increase the mode separation up to 15 MHz. Following this approach, we decided to increase the mode separation up to 9 MHz. An advantage in our case is that we also made a new profile for the new gun to achieve high Q (unloaded quality factor) and high shunt impedance.

Our experience with new large mode separation gun coupled with 130 MV/m fields and Cs_2Te cathode is a very essential experience for making Cs_2Te a well acceptable material for photo cathode guns. In addition, we also produced 300 bunches per train and established the multi bunch generation. Our plan to achieve 8000 bunches per train will clearly establish the technology and method for future applications.

1.1: RF gun at LUCX

The Accelerator Test Facility (ATF) was proposed at KEK and started operating around 1995 [1]. The original ATF linac had a thermionic gun as the source. With the popularity of RF gun on rise, RF gun activity was started at ATF and an RF gun was successfully installed thus replacing the thermionic gun from ATF linac. At present, we can generate 1 to 20 bunch beam at the ATF RF gun. A similar gun was made at the Laser Undulator Compact X-ray Source (LUCX) facility at KEK [2, 3]. The parameters were tested successfully and the gun was found working well. A 3 meter long travelling wave linac was later on added to generate 45 MeV electron beam with 100 bunches per train [4].

The main reason to construct LUCX was to initiate the study of Inverse Compton Scattering using multi bunch beam. Collaboration was formed and efforts were initiated to make a collision chamber. This chamber is a 2-mirror system to build up the laser peak power and then to collide the laser pulses with the electron beam. Due to this chamber; the peak power of laser becomes high and the flux of x-rays obtained after the collision increases. This novel idea was tested successfully in 2009 [5, 6].

The next stage is to initiate efforts which will help to increase the flux of the x-rays. The LUCX setup was not sufficient to obtain a high flux and so many up gradations were necessary.

1.1.2: New RF gun design:

RF photocathode gun work is on-going at LUCX for long time. The original gun design was based on the Brookhaven National Laboratory (BNL) RF gun [7]. After establishing the technology and operational experience, eight identical RF guns were made and at present are operational at many universities in Japan. Worldwide such efforts were made and the BNL gun was established as a standard model for the RF gun structures.

The BNL gun gives a low emittance beam and stable operation for low repetition rate. But as the demand to further reduce the emittance and increase the charge started increasing, it became essential to check new options and profiles which will help reduce emittance. In 2003, the Linac Coherent Light Source (LCLS) group at Stanford Linear Accelerator Center (SLAC) decided to change the gun profile to make the emittance further low. LCLS changed the gun cavity profile and they chose elliptical cavities with race track layout [8]. LCLS gun also has a dual feed to input RF power from two ports. It is proposed to operate at 120 Hz rep rate. The emittance value will go down due to profile changes. The most important feature for the LCLS gun is the

increased mode separation from 4 MHz to 15 MHz. LCLS suggested to increase the separation between the operational (π) mode and the lower (Zero) mode. They predicted that this will make emittance more stable over large laser injection phase variations. Following their approach, Lawrence Livermore National Laboratory (LLNL) also increased the mode separation of the gun from 4 MHz to 12 MHz [9]. The Swiss Light Source (SLS) also initiated design studies for similar concept [10]. Most recently, Pohang Light Source has proposed similar changes [11, 12].

Following the same approach, it was decided to make a new RF gun at LUCX with increased mode separation. We decided to increase the mode separation from 3 MHz to 9 MHz. We also decided to make high Q and high shunt impedance structure [13]. This will increase the energy of beam coming out of the gun. So we achieve high mode separation, high Q and high shunt impedance. This makes this design very useful for many applications.

1.2: What happens if the mode separation increases?

It has been shown that large mode separation in RF photo cathode gun can enhance the performance of the RF Gun [1]. Mode separation is the difference between π mode frequency and Zero mode frequency. In the standard BNL gun, the mode separation was 4 MHz. At LUCX old gun we achieved a separation of about 3.5 MHz.

To see the effect of increased mode separation we recall the standing wave cavity model and perform some basic analysis. When the RF gun is excited at π mode frequency, the zero mode fields can also get excited. The zero mode fields on cathode can degrade the emittance.

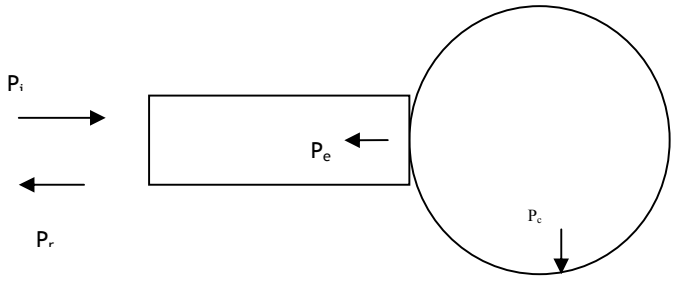

Fig. 1.1: The standing wave cavity model

In the figure, P_i is the incident power; P_r the reflected power, P_e is the emitted power and P_c is the power dissipated in the cavity. Let ω_o be the resonant frequency and Q_0 the unloaded quality factor. The fields inside the cavity E are related to the power P as:

$$P = kE^2$$

where *k* is a constant of proportionality. We define E_i as the incident field; E_r the reflected field and E_e as the emitted field. Using the standard wave cavity model we can state that, the fields in the cavity at time t,

$$E_e + t_F \frac{dE_e}{dt} = \frac{2\beta}{(1+\beta)} E_i$$

where the filling time t_f is given by as $t_F = \frac{2Q_L}{\omega_0}$ and β is the coupling constant

Solving the above equation,

$$E_e = \frac{2\beta}{(1+\beta)} E_i \,(1 - e^{-t/t_F})$$

We define:

$$\beta = \frac{P_e}{P_c}$$

$$\therefore\ P_C = \beta P_e$$

$$P_C = \beta k E_e^2$$

$$= \frac{4\beta}{(1+\beta)^2} P_i^2 (1 - e^{-t/t_f})^2$$

Now for a standard cavity, shunt impedance is defined as:

$$R_0 T^2 = \frac{V^2}{P_c}$$

Q is defined as: $Q_L = \frac{Q_0}{1+\beta}$

Therefore the energy gain can be,

$$V = (1 - e^{-t/t_F}) \sqrt{(\frac{R}{Q_0}) \omega_0 t_F \frac{2\beta}{(1+\beta)} P_i}$$

Thus we can calculate the cathode fields for operation in π mode. Now we define that the zero mode as: $f_0 = f_\pi - \Delta f$ where Δf is the mode separation. We then define the tuning angle as:

$$\tan(\psi) = 2Q_L \frac{\Delta f}{f}$$

The magnitude of zero mode fields will vary with the tuning angle ψ. Thus zero mode fields will be much less as compared to π mode for higher Δf [14]. In other words, the magnitude of zero mode cathode fields will be a function of Δf. This is shown in Fig. 1.2.

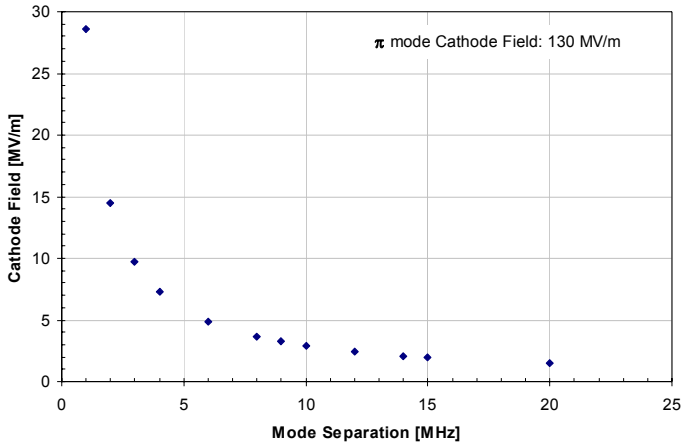

Fig. 1.2: Zero mode cathode fields as a function of mode separation. The π mode field is 130 MV/m

Thus by increasing the mode separation, the zero mode fields on cathode can be reduced. This will help to reduce the effects of zero mode fields on the beam dynamics. In particular this will be more effective when the klystron pulse length is long. The simulated field pattern for the standing wave fields at π and 0 modes is shown in Fig. 1.3

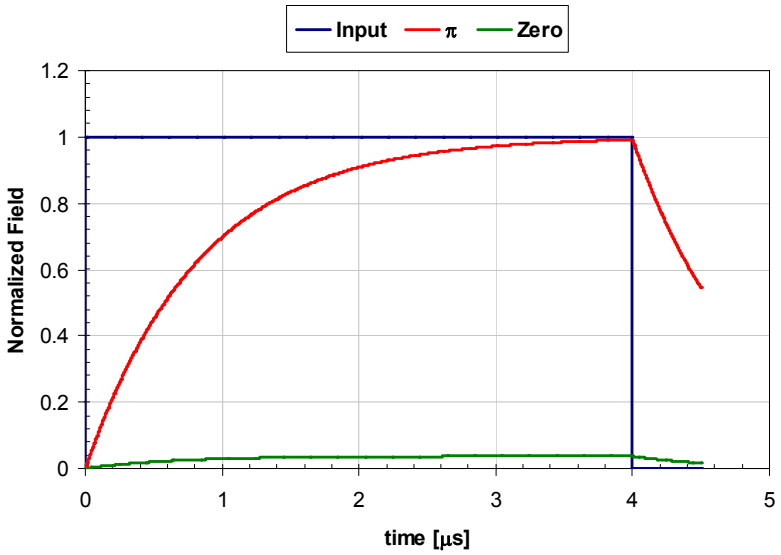

Fig. 1.3: Fields inside a standing wave cavity

By two frequency model simulations, it has been shown that by increasing the separation, the minimum of emittance and energy spread is more stable over injection phase variations [10, 15].

With this motivation we designed the RF Gun at LUCX to achieve higher mode separation. We have designed the cavities to achieve a mode separation of 8.6 MHz as against 3.5 MHz of original cavity.

1.3: Other features

We experimentally found that the increased mode separation gun is more stable over the injection phase variations. The emittance and energy spread varies less with the phase. This was predicted by simulations by other groups. Our experimental results are described in chapter 5. We have achieved a low emittance beam and the energy spread is stable over the injection phase variation. We also changed the profile to achieve higher shunt impedance and higher quality factor. This has helped us to achieve high gradient at the cathode which helps to reduce the emittance.

One of the most important differences between our gun and LCLS gun is that we use Cesium-Telluride (Cs_2Te) cathode while the LCLS uses copper as photo cathode. The quantum efficiency (QE) of Cs_2Te is much higher than that of copper and so we get a very high charge beam. We have achieved a very low dark current and very high field gradient.

1.4: Scope of current work

The work done in past 2 years at LUCX is focused to design, fabricate and test the new RF gun. Once we achieve a stable value of low emittance, we plan to investigate the parameters that limits in achieving further low emittance at high charge. This will help us to further reduce the emittance value.

Generation of multi bunch beam is other important area on which we are focusing. Our aim is to achieve a long pulse trains with high charge. We propose to achieve a very low peak to peak energy difference in bunch train. At present we have achieved peak to peak difference less than 0.8% and we wish to push it further down. This will be a very good achievement and will boost our research to produce multi pulse x-rays using inverse Compton scattering.

Chapter 2 gives an outline of LUCX setup and the devices that we handle and tune. It also lists our measurement methods and the procedures we invented to make measurements straight forward and easy to initiate. The key of our stable operations lies in the fact that the machine

design is simple and the operation is with least possible troubles. We have done lots of efforts to maintain and up grade the system.

Chapter 3 provides the details of the changes made in the structure design to increase the mode separation. We have opted for curved geometry. One of the main issue was location of brazing joint in the full cell. The design was discussed and fabrication drawings were made. Eventually the RF gun was fabricated in KEK workshop. We faced no serious issues in the brazing joint which is not centered on full cavity. This joint, the tuning and other details are also described in chapter 3.

The beam dynamics simulations of new gun were done using a code ASTRA. Chapter 4 summarizes the beam dynamic simulation result of the new gun structure. After making the gun, it was installed in the existing LUCX facility. Detail measurements were done for the new gun and operation parameters were finalized. Measurement results are summarized in Chapter 5. In the same chapter we describe our procedure for conditioning the gun.

It has been proposed to generate a very long pulse train under the Quantum Beam Project at Japan [16]. In phase 1, using a super conducting linac 160,000 bunches per train will be accelerated. To get a first hand experience of generation and acceleration of long pulse trains, simulations were done to establish multi bunch generation mechanism. In particular, we proposed to generate 8000 bunch per train at 5 MeV and 100 bunches per train at 40 MeV. 40nC in 100 bunches at 40 MeV was successfully accelerated and the results are listed in Chapter 6. The most difficult part was the acceleration of 8000 bunches. The linac offers a high loading so we removed the linac and thus made system of low energy operation. After careful tuning, we succeeded in generating and accelerating 300 bunches per train with total charge of 160 nC. The limit of 300 came from the limitation of the Pockels cell. This result is one of the most striking results of the work done here. This result makes way for longer train acceleration and we have already made plans to accelerate up to 8000 bunches in one train by the end of year 2010.

The work done at LUCX is already opening up new work areas. The experience of multi bunch generation, in particular, is very valuable. This is mainly because the future linacs will demand long bunch-trains, with high charge and high rep rates to push the limits of the compact sources. The flux from such sources at present is just short of second generation sources. With maturity of laser technology and with long bunch-train expertise, the compact machines will reach a higher flux. Thus this field will compete with light sources. The other main aspect of the compact

sources is that such sources are relatively cheaper than the synchrotron sources. Hence, these sources are becoming popular.

When we look from application point of view; the small setups are more favorable in medical, industrial or any university setup. Simple system with good design will help reduce the down time of any accelerator and thus serve the user in a much better way.

References:

[1] F. Hinode et al. ATF Design and Study Report, KEK Report 1995-4

[2] K. Hirano, M Fukuda et al., Nuclear Instruments and Methods in Physics Research, A 560 (2006) 233-239

[3] J. Gao, KEK ATF Internal Report, ATF-04-01, 2004.

[4] Liu S. et al., Nuclear Instruments and Methods in Physics Research, A 584 (2008) 1-8

[5] K. Sakaue et al., Rev. Sci. Inst. 80 (2009) 123304.

[6] K. Sakaue, Ph D Thesis, Waseda University 2009

[7] D. T. Palmer, Ph D Thesis, Stanford University 1998

[8] L. Xiao, D H Dowell et al. SLAC Pub 11213 (2005)

[9] S. G. Anderson et al, Proc. of PAC 2007, TUPMS028

[10] J.Y. Raguin, R.J. Bakker, Proceedings of FEL 2005, pp 324

[11] Y. Park, RF gun at PAL-Postech, AAWS-2010 http://kocbeam.kek.jp/

[12] J. H. Hong, I S Koo et al, Proceedings of IPAC 2010 TUPEC014

[13] Abhay Deshpande, J Urakawa et al Nuclear Instruments and Methods in Physics Research, A 600(2009) 361-366

[14] C. Limborg et al. LCLS Tech Note, LCLS-TN-05-3

[15] D. H. Dowell et al. Nuclear Instruments and Methods in Physics Research, A 528, 316-320 (2004)

[16] Quantum Beam Project, http://kocbeam.kek.jp

Chapter 2: The LUCX setup

LUCX is a research collaboration between KEK, Kyoto University and Waseda University. LUCX started as RF Gun Test Bench (RFGTB) when a RF gun was developed for experimental purpose. A 3 meter long travelling linac was then added and the generation of 100 multi bunch beam was achieved. The main focus of LUCX, of course, was to collide laser pulses with electron bunches from multi bunch beam for generation of multi pulse X-rays. This was achieved in 2009. The x-ray flux of LUCX was low, as expected, and hence an improvement effort is on-going. In the modified setup, a new RF gun, separate RF source for the gun and the linac and a four mirror cavity are planned. The ultimate aim of LUCX is to establish technologies to achieve the photon flux of order of 10^{10} or more photons/sec and thus become a comparable, compact and cheap light source.

In this chapter, we present the features of LUCX and explain the instrumentations that we design, tune and maintain to make precision measurements for various experiments.

The LUCX Logo (designed by K. Sakaue)

2.1: The LUCX Injector and accelerator

The Laser Undulator Compact X-ray Source facility, called LUCX, is the research facility at KEK for Inverse Compton Scattering experiment [1, 2, and 3]. LUCX is a 45 MeV linac test bench to think and try new ideas of acceleration, compensation and x-ray generation as shown in Fig. 2.1. The setup is shown in Fig. 2.9 later on in the chapter.

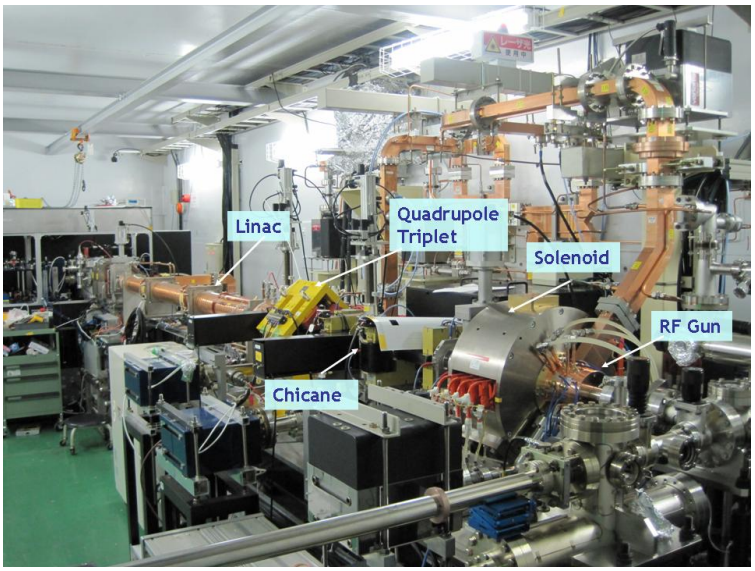

Fig. 2.1: The LUCX beam line

The LUCX accelerator has a RF photo cathode gun as the source followed by 3 meter long Travelling Wave Constant Gradient (TWCG) accelerator.

2.1.1: RF gun

The old RF gun at LUCX was a BNL Type IV gun with 3.5 MHz mode separation [4]. We changed this gun to new RF Gun with higher mode separation and curved internal surface. The details of new gun are listed in Chapter 3. The new gun is a two cell structure operating at π mode. Like most of accelerators the gun structure also is a cylindrical structure with TM_{010} as dominant mode. Such structures do have a dipole and quadrupole mode defects and hence the resultant emittance will be higher than similar frequency gun with corrections applied for these modes. To reduce the effect of dipole defects, dual feed configuration can be used. To reduce the effect of quadrupole modes, race track structures are proposed and used [5, 6 and 7]. Use of elliptical cells can reduce the surface fields. We have not, as yet, initiated elliptical and or race track structures to avoid fabrication difficulties. Our focus is to achieve ~ 1 π emittance with our gun design at 1 nC charge.

The operational principle of RF photo cathode gun is shown in Fig. 2.2. The incoming laser profile and power is a crucial parameter. We need to choose as high power with a choice of profile to suit our use. Once the laser power is fixed, the quantum efficiency of the photo cathode material will define the electron bunch charge and hence the second important choice to be done is the photo cathode material. The third key issue to decide is the cavity structure. We discuss the laser and photo cathode choice in this chapter while the structure details are listed in Chapter 3. The outgoing electron bunch parameters depend on the laser choice, the photo cathode material choice and the structure design. In addition to above, the surface conditions and the field at the cathode also affect the beam quality. To achieve a low emittance beam it is essential to monitor each of these parameters and hence the RF gun technology needs careful checking at each stage.

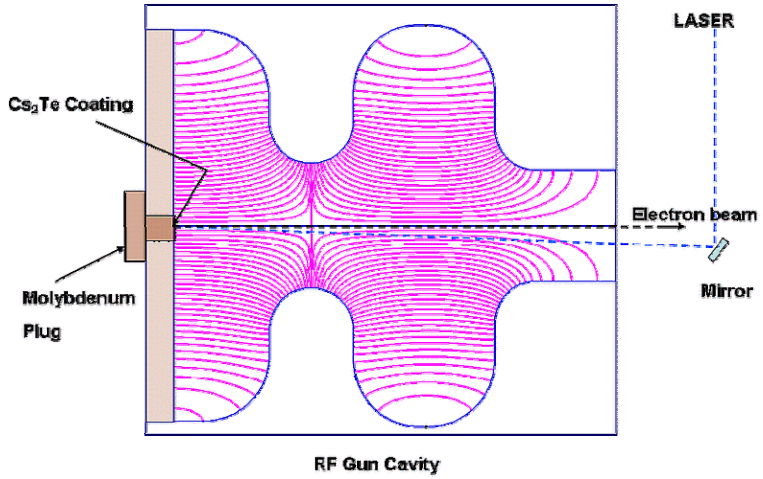

Fig. 2.2: Operation principle of RF gun

2.1.2: Photo cathode at LUCX

The photo cathode choice is one of the main decisions to be made when one chooses the RF gun technology. In RF gun the bunch charge depends on the laser power and the choice of photo cathode material. The user can choose a metallic photocathode or a semiconductor photocathode. The LCLS group uses Copper as photocathode material. The main disadvantage in this case is that the efficiency to conversion from photon to electron is very low for copper and hence to generate very high charge bunches, laser power goes high and so the cost of laser system rises. To achieve a high bunch charge, at LUCX we chose semiconductor material Cesium-Telluride (Cs_2Te) as the photocathode.

The Cs_2Te has comparatively low life time at peak quantum efficiency. The quantum efficiency (QE) of Cs_2Te decreases rapidly over time [8]. In our case we found the QE dropped to about 3

0.5% in about a month after the coating. In our earlier gun, the cathode lasted for around 3 yrs with ~ 0.3% QE in high fields of about 130 MV/m despite of long operations. The successful operation with Cs_2Te photo cathode in presence of fields over 130 MV/m at LUCX is a significant achievement to boost the user's confidence of many labs in the world to switch to Cs_2Te photocathode.

Our system uses a molybdenum plug inserted in the RF gun via load lock mechanism. As an initial conditioning before the Cs_2Te coating, the plug is inserted at the cathode position and subjected to high fields of over 130 MV/m. The plug is cleaned through this conditioning, and at the completion of the process it is transferred to the coating unit in a vacuum chamber. Once the plug is inside the coating chamber, a 10 nm thick coating of Telluride is applied. Then the Cesium deposition is commenced, and the quantum efficiency (QE) is monitored over time. The photo current peaks at some point, and then starts to fall. In our process, the coating is discontinued when a stable QE of nearly 4% is reached. Next, the QE is measured as a function of photon energy. Figure 2.3 shows the LUCX coating data in blue dots and the data from Powell in brown dots [9]. When we use this photo cathode in our gun with our laser system, we easily achieve a charge of around 1 nC per bunch and stable operation with a gradient of 110 MV/m or higher.

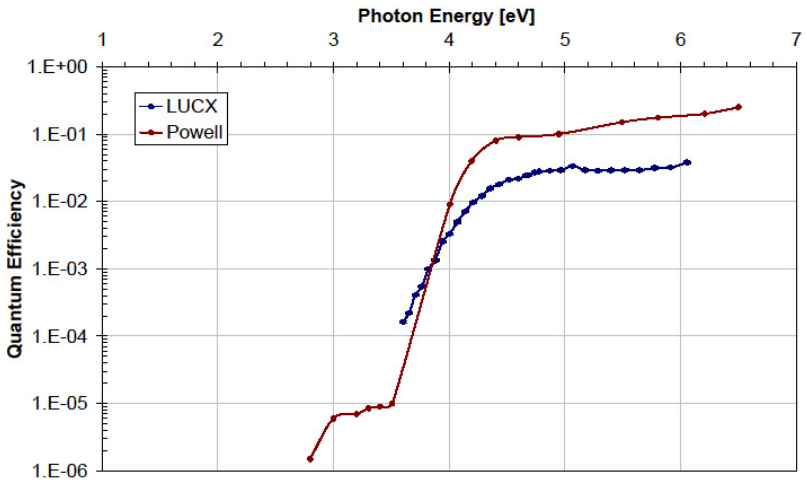

Fig. 2.3: Measured dependence of quantum efficiency on incident photon energy. The blue curve corresponds to the LUCX data. The brown points correspond to the data from Powell from Ref. 9

In our setup, we achieve high charge per bunch with our laser system and we achieved stable, long operations and hence the choice of Cs_2Te is well justified for us.

2.1.3: Laser system

Along with the gun structure and cathode, choice of laser system is a defining parameter. In RF gun, the laser strikes the photo cathode and an electron bunch is generated. The laser profile defines the bunch profile. The laser power defines the bunch charge. The phase at which laser is injected defines the bunch exit energy. The stability of laser defines the operational stability of the system. Hence, stable laser system with low jitter is needed.

Our laser system is a multi pulse laser system [10]. The seed laser is Time Bandwidth Neodymium Vanadate (Nd: YVO4) mode locked oscillator with a 357 MHz frequency. The average power is 7W at 1064 nm wavelength and pulse duration is 7ps (FWHM). The infrared (IR) pulses produced at 2.8ns (corresponding to 357MHz) pass through a Faraday isolator F1 into a Pockels Cell PC1. The Pockels cell chooses the number of pulses depending on the choice of user. In May 2010, we installed a new fast rise time Pockels cell and now it is possible to choose up to 8000 pulses for operation. The earlier Pockels cell had limitation of minimum 4 to maximum 300 pulses only. The selected pulses pass through double pass amplifier AMP1 and then through Pockels Cell PC2 to enhance the contrast ratio. Then it passes again through an Amplifier AMP2. The high-power pulses are then passed through non linear optics BBO crystals to produce the fourth harmonic. The final outcome is a 266 nm ultraviolet (UV) laser with a pulse length of 12.5 ps (FWHM). Figure 2.4 shows the schematic of laser system.

Table 2.1: Power of laser pulse at various stage

Oscillator output	7	W
Frequency	357	MHz
Power per pulse	19.6	nJ
2 Amplifier Double Pass	39	μJ
IR to UV conversion	3.9	μJ (Incident on photo cathode)
QE	0.3	%
No. of photons incident	5.25×10^{12}	
Bunch Charge	2.5	nC (variable)

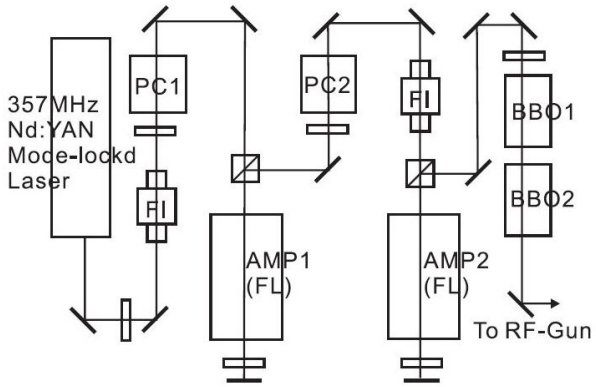

Fig 2.4: LUCX laser system (image courtesy K. Sakaue)

2.2: Travelling wave accelerator

The LUCX main accelerator is a 3 m long Travelling Wave Constant Gradient linac made by Mitsubishi Heavy Industries. The TWCG structure is a disc loaded structure operating at $2\pi/3$ mode. The end cells are matching cells in which power coupling slots are made. The power enters through a coupling slot in matching cell number 1 and exits through coupling slot at matching cell number 2 at exit. The bunch can be launched at any phase by varying the phase through phase shifter. To achieve a low energy spread we launch the bunch off-crest and hence have slightly low energy than we can achieve through this linac. Figure 2.5 shows the TWCG linac at LUCX while Fig. 2.6 shows the field pattern simulated using beam simulation code ASTRA for the linac. The parameters are listed in Table 2.2.

Table 2.2: Linac parameters

Frequency	2856	MHz
Mode of operation	$2\pi/3$	
Shunt Impedance	60	MΩ/ m
Attenuation	0.57	np
Filling Time	0.830	ms
Peak Field	20	MV/m
Number of accelerating cells	84	
Number of Coupler Cells	02	
VSWR	1.01	
Q	12000	
Group velocity	0.0204c- 0.0065c	

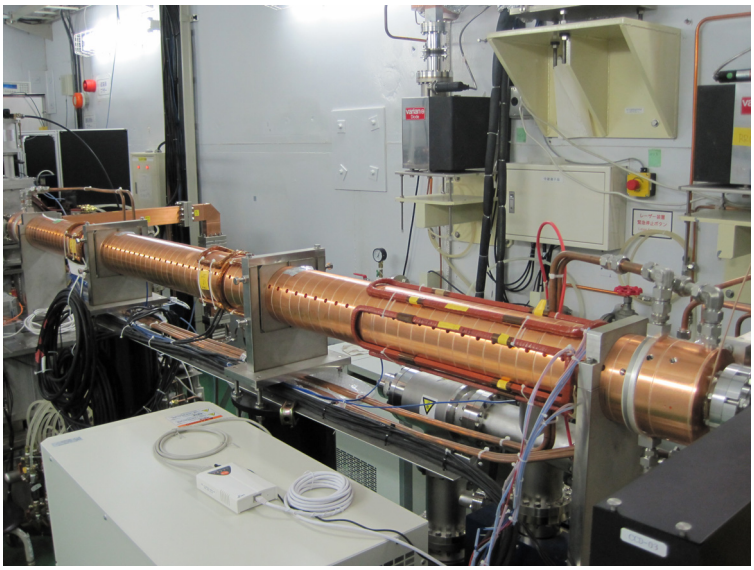

Fig. 2.5: TWCG linac at LUCX

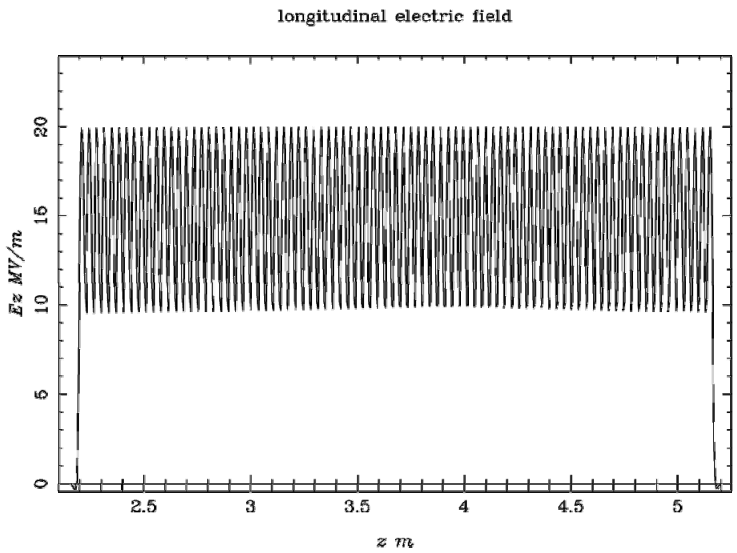

Fig. 2.6: Field pattern generated by ASTRA for TWCG structure

2.2.1: RF power system

In our setup we use 80MW Toshiba E3712 Klystron as RF source. The klystron has 4 μs pulse width. To achieve high power needed to compensate high charge multi bunch beam, we use a Resonant Ring Power Compressor (RRCS) type pulse compressor scheme [11]. This scheme is like the SLAC Energy Doubler (SLED) [12, 13] scheme with the main difference that SLED is a standing wave type resonator while RRCS uses travelling wave resonator. Using a phase switcher,

the phase of first 3 μs of RF pulse power is switched-off by 180 deg. During this time, the RF power builds up into the resonant ring and is stored in the cavity. At end of 3 μs, the phase is switched back and the stored power from cavity adds up with the power coming from klystron, at the linac port. We usually operate the Klystron at 41.7 MW power. Hence after using the RRCS instead of 4 μs, 41.7 MW RF power, we achieve 1 μs, 135.5 MW peak power at the output of RRCS. The input and output power structure is shown in Fig. 2.7. The multiplication factor in this ideal case is around 5.25 where as we actually achieved a multiplication factor of around 3.25.

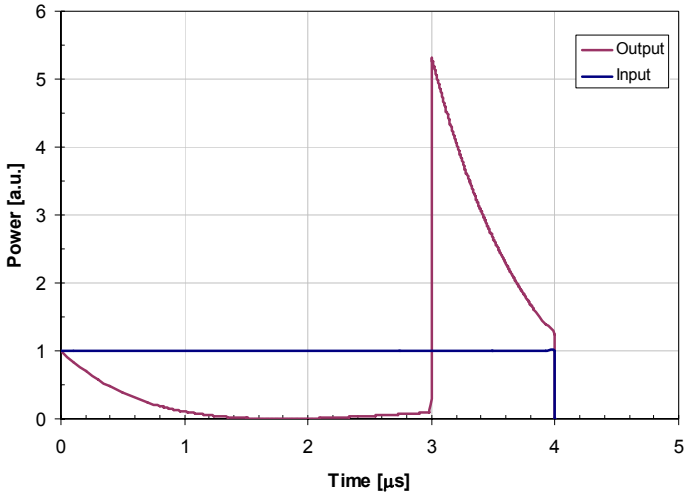

Fig. 2.7: RF pulse compression using RRCS. Input waveform comes from the Klystron and output is delivered to the linac port.

The power thus obtained from Klystron is further divided and attenuated before it goes to gun or linac. Of the 135.5 MW power, 30% i.e. 40.6 MW goes to linac. Of the remaining 94.8 MW, 50% goes to load and about 47.4 MW goes to RF gun. The existing power scheme is shown in Fig. 2.8.

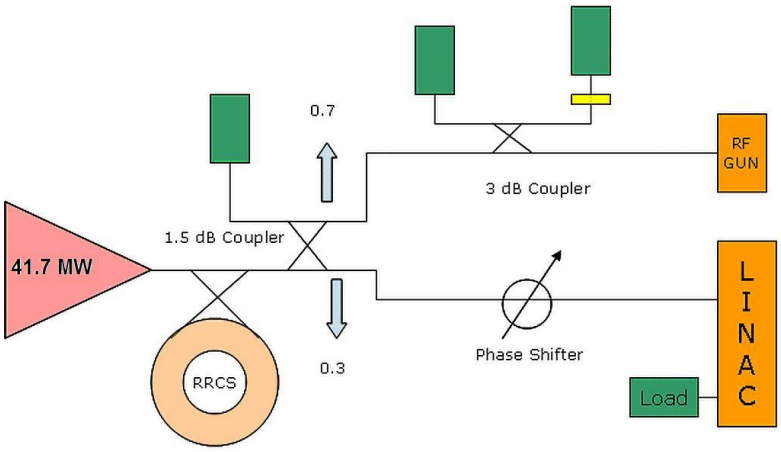

Fig. 2.8: LUCX RF Power distribution (image courtesy M. Fukuda)

2.3: Magnetic devices

The LUCX aims to focus beams to vertical size of less than 50 μm. To achieve this, high field quadrupole magnets are inserted in the beam line.

As shown in Fig. 2.9 on next page, at the RF gun exit, a solenoid is placed to help the emittance compensation. This solenoid focuses the electron beam to a minimum size, near the focal length, at which the linac should be placed. We have introduced a 4-magnet Chicane after the solenoid. This is needed to make space for a small mirror to incident laser on the photocathode nearly perpendicular to the surface. The chicane bends in horizontal plane and takes the beam off-axis and then brings it back on-axis. This bend, introduces a divergence to the beam, which may not be fully recovered if the chicane is not neatly aligned. Thus the x-y asymmetry is introduced which leads to different emittance values of x and y plane emittance in our case.

The chicane also serves as an energy slit in our case. If the energy spread is more than 1 MeV, some part of the beam is cut off. In multi-bunch case, the chicane ensures that peak energy difference is in acceptable range and this good quality beam is passed on to linac. If the energy difference is too high, chicane blocks some bunches and further tuning is expected to correct for the loss. Thus we ensure that a good quality beam appears at the entrance of the linac.

After the chicane, a quadrupole triplet (QA1G-3G) is inserted. This triplet can be used to ensure that the beam size at the entrance of the linac is small and that the beam has a round shape. After this triplet, the linac is placed to accelerate the beam to high energy. After the linac, two set of doublets are introduced. The first doublet, QD1G and QF1G, focuses the beam at the collision point (CP1G) to obtain 50 μm beam size in the vertical plane. Simulations show that this needs a large compression and hence a large field is needed at the quadrupole. As a consequence, the beam size increases rapidly after the minima at the collision point and the beam size will go on increasing continuously. Hence, the second set of doublet, QD2G and QF2G, is used to re-focus the beam to the dump.

The collision point is the location at which the electron beam collides with the laser. The outgoing electrons and the generated X-rays are in the same direction. Hence, X-ray detection will be impossible, unless we bend the beam. Therefore we use a bending magnet (BA1G) to bend the beam in vertically downward direction to the dump.

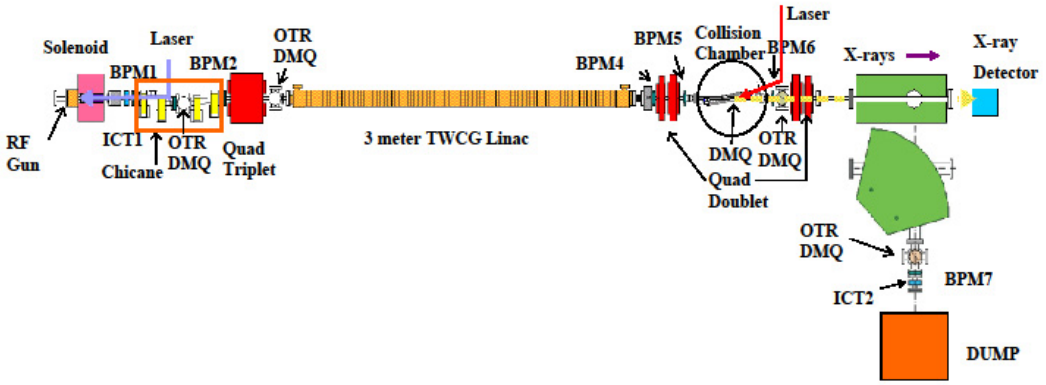

Fig. 2.9: Details of the old LUCX beam line. The beam line was modified in Mar 2010 after the collision chamber.

2.4: Diagnostic and measurement setup

The location of monitors, BPM and ICT are shown in Fig. 2.9. Various measurements are done using a combination of some diagnostic devices and magnets. We now list few essential things about some devices and the way they are used. This section follows closely earlier work at LUCX [10].

2.4.1: Current monitors

At LUCX we use Faraday Cup (FC) and Integrating Current Transformers (ICT) to monitor and measure the beam current. Faraday Cup is a destructive type measurement setup. It is essentially a high conducting, low Z metal cylinder with large thickness. Z is the atomic mass number. When the electron hits this metal cup a proportional current is produced. The FC is isolated and hence we get a direct measurement of electron beam charge.

In contrast, ICT is used to measure intensity of short bunches in a non-destructive way. The ICT is a circular hollow disc type structure through which the beam passes through all the time. When a bunch passes through the ICT, induced current flowing through ICT can be detected. The ICT integrates the signal with a time constant and hence losses are suppressed. With sufficient fast rise time ICT available commercially, ICT can be used to measure micro-bunch charge by proper choice of time constant. Thus ICT is very useful in accelerator applications.

2.4.2: Beam position monitor (BPM)

BPM, as the name suggests, is used to monitor the position of the beam to fix the beam orbit. At LUCX we use button type BPM's having four electrodes. When a bunch passes in between these buttons, an image charge is induced on the diagonally opposite electrodes. The induced charge is seen as a bi-polar signal pulse with the amplitude proportional to beam charge and the distance from the beam. If the beam is passing off-axis, asymmetric charge is induced in a pair of buttons and thus the beam position can be traced proportional to this asymmetry. Thereby we can fix the position of beam in that particular BPM. Plotting the position of beam, in successive BPM's, gives the entire beam orbit from the gun to the dump.

2.4.3: Beam profile monitor

We use two types of screen monitors to observe the beam. A highly sensitive alumina fluorescent plate (AF995R, Demarquest Co.) is selected for use as the screen material. The screen is made of 0.5% chromium oxide doped with alumina and reaches peak scintillation at a wavelength of 693 nm. A 100-μm thick screen is mounted on an inserting device at 45 deg relative to the beam. The main disadvantage of this type of screen is a slight enlargement of the scintillation indicating a larger beam size than that of the original beam. This disallows the use of the screen for precise beam size measurements. But with its high sensitivity to even pico-ampere charge, the screen is very useful for finding beams and monitoring dark currents. Thus, we use the screen mainly for tuning and use an optical transition radiation (OTR) screen for beam size measurements.

The Optical Transition Radiation (OTR) method is mainly used to image the transverse profile of beam. When the charged particle beam strikes a thin stainless steel plate, OTR radiation are seen both in forward and backward direction. By inserting the metal disc at 45 deg, the backward OTR can be diverted out of the beam plane, through a window onto a CCD camera. By observing these radiations, we can build the beam profile in transverse planes.

In both case, the screen is initially calibrated using a known distance pattern. It could be a marking on the screen or some small screw in the vicinity of the screen. The image of such known device is obtained with a known magnification and there by microns per pixel ratio is decided.

At LUCX we have 04 screens with OTR and DMQ setup. At all four locations, inserting device is common with DMQ and OTR screen mounted one below other. Selecting DMQ brings the screen

1 in front of the beam. Selecting OTR, the screen further moves down and stainless steel plate faces the beam.

Fig. 2.10 shows beam profile obtained at same location using a DMQ and OTR screen. The fit is obtained in each case and it shows the deviation in size obtained from both the methods.

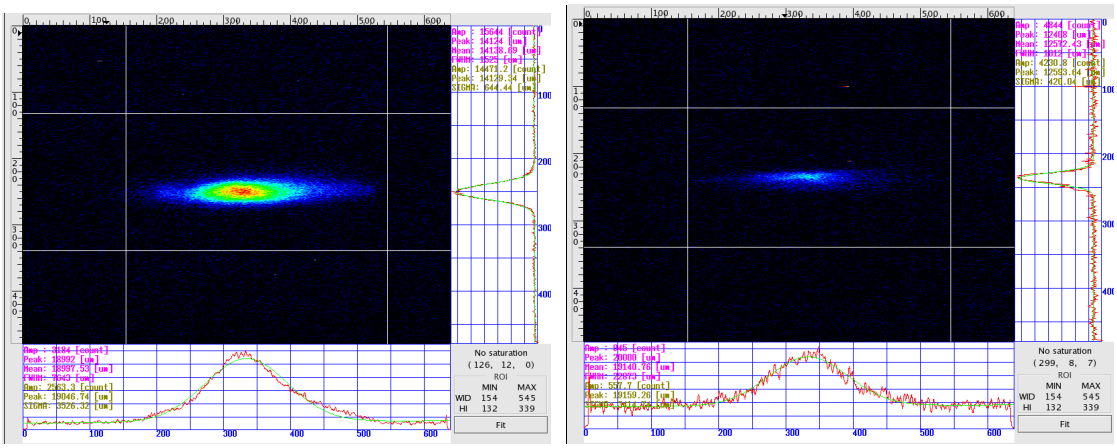

a b

Fig. 2.10: Beam profile images: (a) on DMQ screen at MS4G. The vertical beam size is 644 μm (rms) (b) at same location on OTR screen the vertical beam size is 425 μm (rms)

2.5: Beam energy spread measurements

The beam energy spread measurements are done using screen MS4G OTR. Initially, the beam profile is observed on this screen. The phase of injection for RF Gun is adjusted to minimize the spread. The linac phase is also set so as to obtain minimum energy spread on the screen. The crucial part is to calibrate the screen pixel to the energy spread. This is done by using the analyzer magnet and time delay units. To begin with, the analyzer magnet is set to current so that the beam appears at center of the screen. The beam injection is then delayed in steps. This changes the beam energy and the beam moves on the screen. Average value of beam position and the error is noted. For each case, the current of analyzer magnet is then varied to bring the beam to center position and corresponding energy is recorded. Thus we get screen pixel as a function of beam energy. This calibration is used to measure the energy spread.

Using the same screen MS4G OTR, the magnet and the BPM near the screen it is possible to find out bunch-to-bunch energy difference. This is not directly measured value but estimated using the BPM-magnet-screen combination. As before, energy spread for less number of bunch is measured using screen as discussed above. There after a multi bunch beam with 100 bunches is launched. We know the mean energy from 4 bunch measurement at which the analyzer magnet current is

fixed. The 100 bunches pass through the magnet and through the BPM. Since the energy of bunches is different from the mean energy, they trace a different path through the BPM and the position can be recorded. The difference in position is correlated to difference in energy and thus we can know the bunch-to-bunch energy variation. For 4 bunch mode, we can thus measure energy spread of the bunch while for 100 bunch beam we can not measure individual bunch energy spread but bunch to bunch energy deviation can be found. Thus we measure the peak to peak energy difference for multi bunch beam which is very important parameter. If the beam loading is compensated properly, the peak to peak variation for 100 bunches is less than 1%.

2.6: Start up and beam based alignment

Like any other accelerator, starting up the LUCX and setting base parameters is the most critical part. LUCX is shut down each day and hence on each day at start up we have established a procedure to ensure that the beam quality is nearly same as on the day before. Initial quality assessment and tuning is done to stabilize the machine and there after experiments can be done as per the plan of the day.

After warming up of the system, laser profile is measured as a starting point. The laser intensity is measured each day. The system is then turned on and all the magnets are switched off except the bending magnet. The beam is turned ON and beam current is measured. The first step is to ensure the beam center alignment with the solenoid magnet. This is done using a beam based alignment (BBA). The solenoid current is varied from optimum solenoid current by plus and minus 5 A. At each setting of solenoid, the BPM reading for x and y plane is registered. Then the solenoid current is changed by 5A and the deviation is BPM reading is checked. If the deviation is large, the position of laser incidence on cathode is varied using mirror control. This process is repeated many times till we find that the deviation for BPM in each plane is less than 0.01 mm over 15A current range.

Once the beam is aligned with respect to solenoid axis, phase plot is recorded. The injection phase is varied and corresponding charge is recorded. From this setting, the phase of injection is set for minimum energy spread location. There after the screen after the bending magnet, MS4G is put on and profile of beam is observed on this screen. The linac phase is adjusted so that the energy spread is minimized.

After these initial tuning, the beam is observed at screen after the collision point. The beam size is then measured using the OTR screen at MS3G. Emittance is measured at this location by using

the quadrupole doublet. The solenoid current is then varied in small steps and the emittance measurement is repeated. Eventually, solenoid current versus emittance is plotted to find out the best compensation setting. This is the setting for minimum emittance and most experiments are done with this position as the reference position.

References:

[1] K. Hirano, M Fukuda et al., Nuclear Instruments and Methods in Physics Research, A 560 (2006) 233-239

[2] Liu S. et al., Nuclear Instruments and Methods in Physics Research, A 584 (2008) 1-8

[3] K. Sakaue et al., Rev. Sci. Inst. 80 (2009) 123304.

[4] X. J. Wang et al. Nuclear Instruments and Methods in Physics Research A 375 (1996) 82-86

[5] L. Xiao, D H Dowell et al. SLAC Pub 11213 (2005)

[6] Y. Park, RF gun at PAL-Postech, AAWS-2010 http://kocbeam.kek.jp/

[7] J. H. Hong, I S Koo et al, Proceedings of IPAC 2010 TUPEC014

[8] S. H. Kong et al. J. Appl. Phys., 77(11), (June 1995)

[9] R. A. Powell et al. Phys. Rev. B, Vol. 8, Number 8 (Oct 1973)

[10] K. Sakaue, Ph D Thesis, Waseda University 2009

[11] S. Yamaguchi et al. KEK Pre-print 94-87 (1994)

[12] Z. D. Farkas, SLAC-TN-73-08 (1973)

[13] P. B. Wilson, SLAC-TN-73-15 (1975)

Chapter 3: RF structure design

The LCLS gun design group has shown that by increasing the separation of mode frequencies, it is possible to have a large range of injection phase variations over which the emittance minimum can be maintained to a low value. Technical report from LCLS has motivated Lawrence Livermore National Laboratory (LLNL) to switch from small mode separation to large mode separation. The LCLS group went from 4 MHz separation to 15 MHZ while the LLNL group went up to 12 MHz separation. Following these two references, we decided to adopt the strategy of increasing the mode separation at LUCX setup. We chose new design to increase the mode separation up to 9 MHz from the existing 3.5 MHz separation. This needed some changes in the cavity profile. It was also decided to alter the profile so as to get high Q structure with higher shunt impedance.

This chapter describes the evolution of the new gun structure and the procedure which we established to fabricate and process the RF gun. More importantly the chapter explains the experimental results of the measurements and details of the tuning process to achieve the desired π mode frequency of 2856 MHz with the mode separation of 8.6 MHz maintaining the field balance at 1.0. Though the current work is focused on comparison between old and new LUCX gun; yet a comparison with the modified gun at ATF, KEK is also considered at some point. The new design has higher Q than the original and the modified gun at KEK.

3.1: Comparison of old and new structure

LCLS gun design review group has shown that by increasing the separation of mode frequencies, it is possible to have a large range of phase variations over which the emittance minimum can be maintained to a low value [1]. Technical report from LCLS has motivated LLNL group to switch from low mode separation to high mode separation. The LCLS group went up to 15 MHZ from 4 MHz separation while the LLNL group went up to 12 MHz separation [2]. Following these two references, we decided to adopt the strategy of increasing the mode separation at LUCX setup. We chose to increase up to 9 MHz from the existing 3.5 MHz separation [3, 4]. This needed some changes in the cavity profile. It was also decided to alter the profile so as to get high Q structure with higher shunt impedance. We selected circular profile for the new structure.

The structure of the original LUCX RF gun (hereinafter, the "old gun") was close to the BNL type IV gun structure as shown in Fig. 3.1. Our main modification at KEK, after years of experience, was to replace the Helicoflex seal joint with a brazing joint. Another major change was to introduce the new 'deformation tuners' in the tuner region [5]. These tuners do not penetrate the gun cavity, but maintain a wall thickness of about 2 mm. A screw-type mechanism is used to move the tuner, and with it the cavity wall, up or down, and thereby change the cavity frequency. Each cell has four diametrically opposed tuners, and the cavity frequency can be changed up to ±1 MHz. The original LUCX RF gun cavity had a mode separation of 3.52 MHz and a field balance (E_{half} / E_{full}) of 1.30. Our target was to increase the mode separation to 8.6 MHz while maintaining filed balance of 1.0.

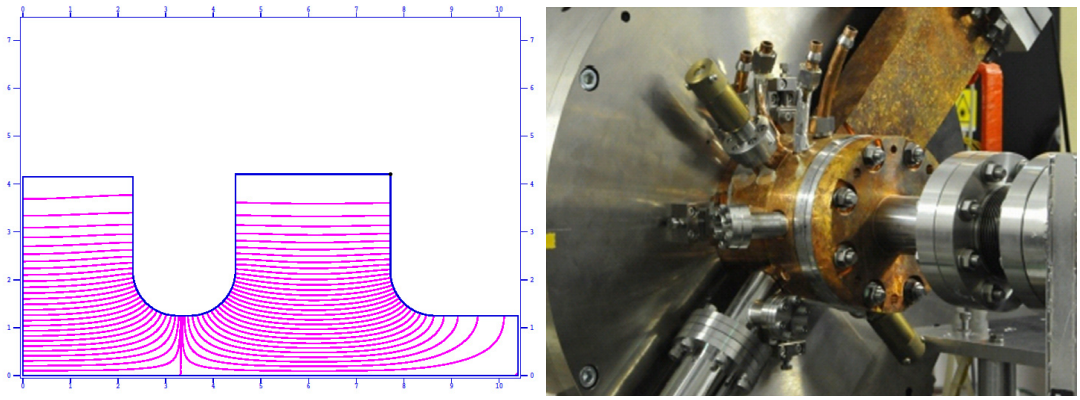

Fig. 3.1: Old RF gun field pattern and the mounted structure on LUCX

The mode separation was increased by increasing the coupling between the cells through two adjustments, namely, increasing the iris diameter and reducing the length of the drift tube

between the half cell and full cell. The new gun structure has 1.625 cells. Half cell was chosen to be 5λ/16 and full cell was exactly ½ λ. It was decided to maintain the field balance to 1.0. In order to increase the mode separation, the half cell to full cell iris diameter was increased in small steps. This changes the cavity coupling which in turn changes the mode separation. With increase in the iris diameter the mode separation increases. This can be seen from Fig. 3.2 below. The graph is obtained by varying the iris diameter in small steps from 25.0 to 28.0 mm. In each case, full cell and half cell frequencies are tuned so as to get π mode frequency near 2856 MHz and field balance is unity. It is clear from Fig. 3.2 that iris diameter plays an important role in deciding the mode separation.

After optimizing the iris diameter, the drift tube length between two cavities was minimized in order to get high mode separation.

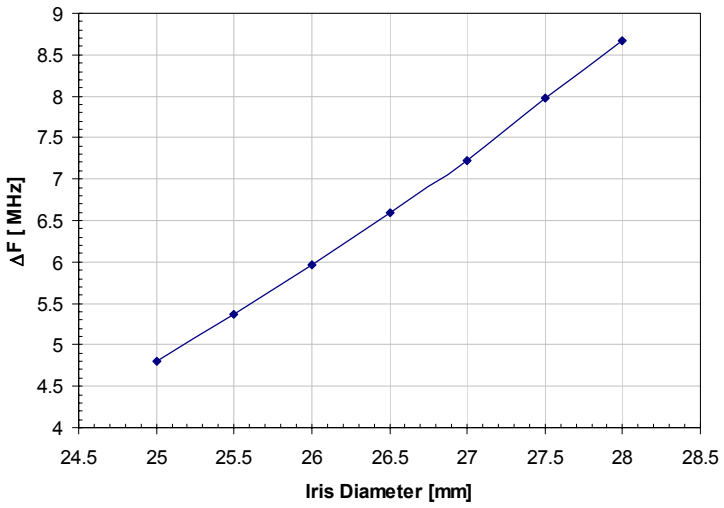

Fig. 3.2: Mode separation as a function of iris diameter

For a given iris diameter, we can vary the mode separation by changing the frequencies of individual cells. The mode frequencies depend on the average cell frequency and the coupling between cells. For fixed coupling, varying the cell frequencies can generate plot as shown in Fig. 3.3. The plot shows the graph for the new and the old gun design obtained from Super fish and circuit calculations.

In our case we decide to operate the gun at field balance 1.0. This is a good choice as it leads to high energy gain in full cell and hence to high energy at the output. A LUCX type of field balance, such that E_{half} is 1.3 times E_{full}, leads to high field in half cell at the cathode position. However it

leads to different kick at the full cell exit. This can be compensated by adjusting the solenoid field. But such a field balance leads to less energy gain in full cell and so the output energy of beam from the gun will be less in this case. In contrast, the RF Gun with field balance 1.0 can have similar low emittance like the 1.3 field balance gun but higher energy at the gun exit. This has been shown by Palmer et al [6]. For present case, the simulations show that 1.3 field balance gun operating at 120 MV/m will have 0.75 MeV less energy with identical gun at 1.0 field balance. Since there is no much benefit in the emittance reduction, we decided to tune to field balance 1.0 to get more energy at the exit of the gun.

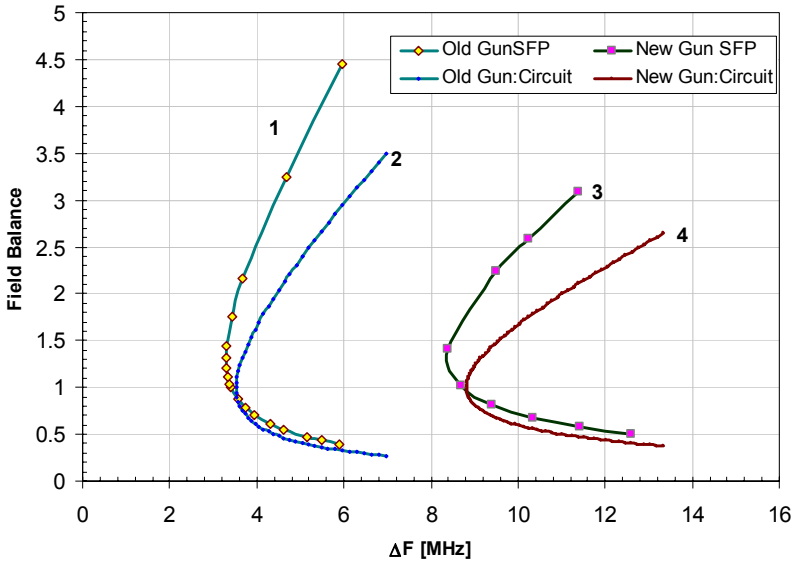

Fig. 3.3: Field balance as a function of mode separation for LUCX and new gun. Curve 1 is for old gun using Super Fish code and curve 2 is for old gun with circuit simulations. Curve 3 shows Super fish simulations for new gun while curve 4 shows circuit simulations for new gun.

The choice of operation point design is limited by the fact that for a given geometry high mode separation can be achieved at the cost of field balance. How ever as mentioned above, we selected to operate at around 1.0 field balance. Hence the cells were tuned to get mode separation of 8.67 MHz. The new RF gun cavities are cylindrical with curved surface. With respect to earlier cells a rise of around 3000 is expected in Q value. The high Q value can be achieved if the internal surface condition is reasonably good. This means the processing quality should be high with entire processing done in good clean environment. Such a cavity will reduce the dark currents from the gun and thus will help in enhancing the beam quality and serve the purpose of delivering stable beam over large run time.

The new cavity profile is shown in Fig. 3.4 while the π mode axial field profile as predicted by Super fish [7] is shown in Fig 3.5. The zero mode axial field pattern is shown in Fig. 3.6.

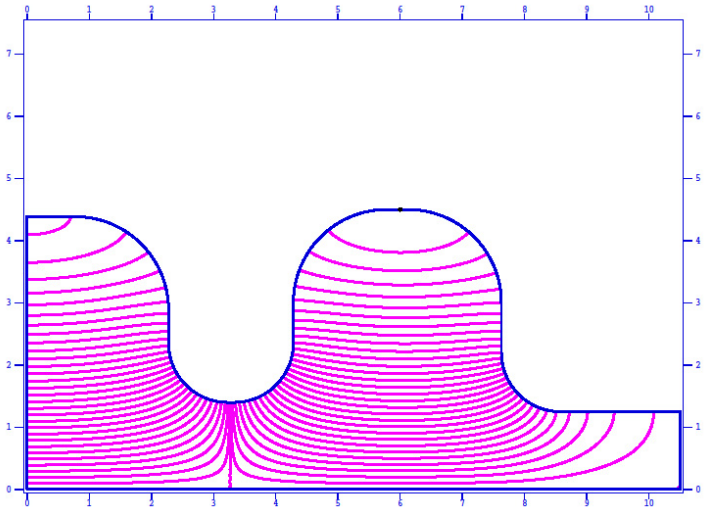

Fig. 3.4: Super Fish plot of RF gun cavity for new gun

The final predicted mode separation is 8.67 MHz with a field balance of 1.0. The field pattern thus obtained was then used for beam dynamics studies using ASTRA code [8]. Table 3.1 lists other parameters of RF gun cavity. The RF power input slot is in full cell and for the sake of symmetry a vacuum pumping port is made opposite the RF slot. The initial frequency of full cell is set higher and machining was done systematically to achieve target frequency. A routine check of frequencies gives better control over the fine tune frequency. At KEK we have sufficient experience in fabrication procedure for RF gun cavity cells. Four tuners are included in each cell to facilitate the fine tuning to finalize the parameters. In practice the mode frequencies are monitored using vector network analyzer and fine tuning is done so as to get the desired mode separation and field balance.

Table 3.1: Various parameters for proposed cavity

	Old RF Gun	New RF Gun	unit
Mode Separation	3.5	8.6	MHz
Q	15913	18275	
r/Q	438	412	
Z	29.6	34.9	MΩ/m

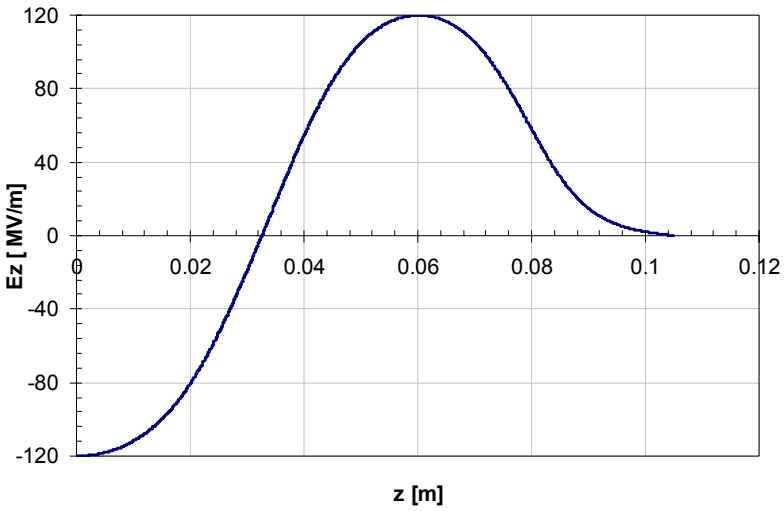

Fig. 3.5: Axial field plot for π mode field pattern

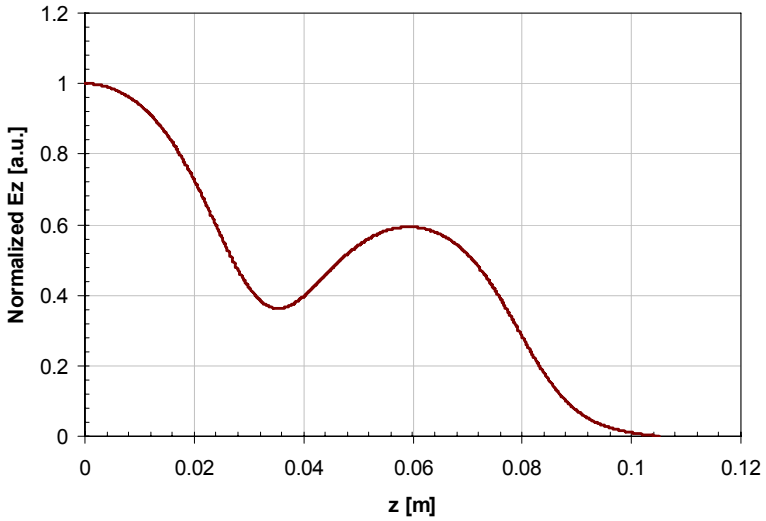

Fig. 3.6: Field pattern for zero mode fields

3.1.1: Comparison of Q value:

The old gun was a modified version of the BNL type gun. Over the years the design evolved with the experience gained at LUCX and ATF. The Q value also improved with new modifications. Table 3.2 shows the comparative values of Q obtained for various RF guns made by KEK. We also compare the new RF gun with BNL and LCLS gun.

Table 3.2: Comparison of measured Q

Gun	Measured Q	Coupling
LUCX	7900	0.6
ATF	12700	1.0
BNL [9]	12700	0.83
LUCX New (Curved Profile)	14,700	1.0

From the table it is clear that the new gun with modified profile has achieved the highest Q amongst all guns made at KEK. The Q value is higher than BNL or the new LCLS gun. This is a very useful achievement.

3.1.2: Increased stability due to large mode separation:

As seen above, the new profile has resulted in high Q. The shunt impedance is also increased from 29 MΩ/m to 35 MΩ/m. This will result in higher energy at the exit of the gun. On the other hand, the increased mode separation plays a very beneficial role in stabilizing the field balance over dimensional variations. Figure 3.7 shows the variation in field balance as a function of half cell radius for the old and new RF gun. The full cell radius was constant in this calculation. It can be seen that the field balance is less variant for large mode separation case.

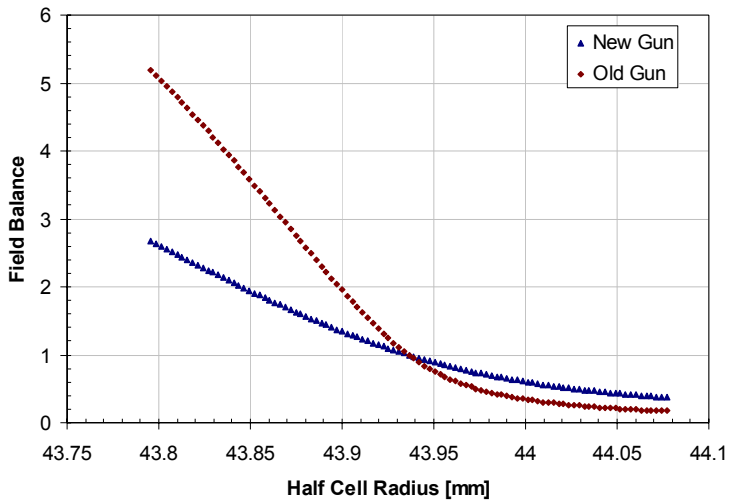

Fig 3.7: Field balance as function of half cell radius

It is observed that for 10 μm error in radius, the resultant variation in field balance is reduced from 20% for 3.5 MHz mode separation to 11% for 8.6 MHz mode separation gun. Thus the

dependence of field balance is less critical for dimensional errors. The variations in dimensions can be due to thermal variations and hence it means that the new gun delivers increased stability in field balance over thermal variations than the old gun.

Table 3.3: Variation in field balance

Mode Separation	Variation in the field balance for 10 μm error in half cell radius
3.5	20 %
8.67	11 %

3.2: Fabrication process and issues

Once the profile was finalized using a combination of Super Fish profiles for structure design and ASTRA runs to verify effect of parameters on the beam dynamics, fabrication issues were discussed at length. And a final process, based on prior experience at KEK was decided. Figure 3.8 shows the assembly drawing of the RF gun cavity that was fabricated. For the sake of clarity, laser port and cathode position are also shown in the same figure.

One of the first issues faced in the fabrication was that the internal profile of cavity is curved and hence turning of full cell had two options. One was to cut open along the center of the RF slot and turn uniform on two half cells to make a full cell. This option, usually practiced in many linac's, was not employed for the new gun to avoid brazing at the RF slot joint. This brazing is a complicated process and it was decided to go for second option. In second option, the full cell was divided into 2 sections with $1/3^{rd}$ going into half cell and $2/3^{rd}$ coming as a full cell with a slot opened in for RF feed port. In this option, a small step of less than 30 μm is expected in the full cell. The step is at a position where surface fields are less and hence will not be a source of dark currents.

This assembly drawing does not show locations of the tuners. 2 set of tuners were placed in each cell. The purpose of tuners is to help the fine tuning after the brazing is done so as to facilitate in achieving a desired field balance.

Oxygen Free High Conductivity (OFHC) Copper of grade C10100, JIS3510 (equivalent to ASTM-F-68) made by Hitachi was used to make the cells. The copper was subjected to Hot Isostatic pressing (HIP) process at 850 ^{o}C under high pressure. It has been experimentally checked at KEK [10, 11] that HIP processing reduces the micro-pores at the surface of copper

and the surface remains relatively clean after processing especially turning operation in which kerosene is used as a coolant.

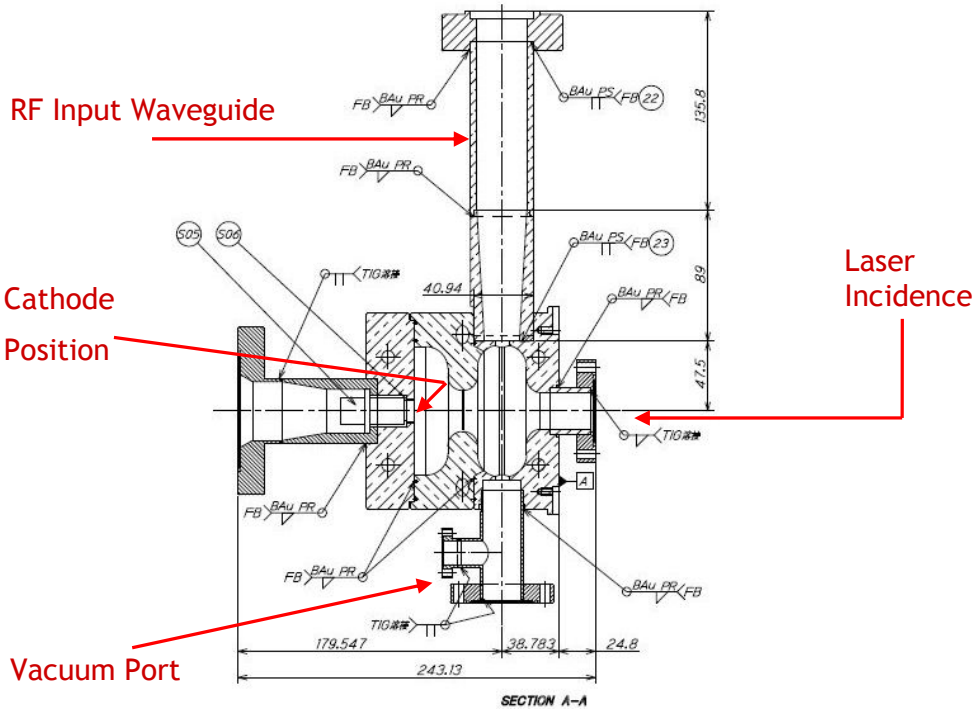

Fig. 3.8: Assembly drawing of RF gun cavity

The fabrication was done in-house at KEK machine shop. The actual diameter of the cavities was kept 1 mm less than the final desired diameter. End plate, half cell and full cell were turned and water cooling slots were bored in the cells. Water cooling end plugs were brazed and then the cavities were ready for precision machining, measurement and further processing. The mode separation between π and **0** mode and field balance, as well as the π-mode frequency needs to be monitored. The most crucial of these parameters is the π-mode frequency and it should be as close as possible to 2856 MHz. Hence, starting from the high frequency stage, cuts on diameter were taken.

The figure below shows the photograph of cavities at various stage of fabrication.

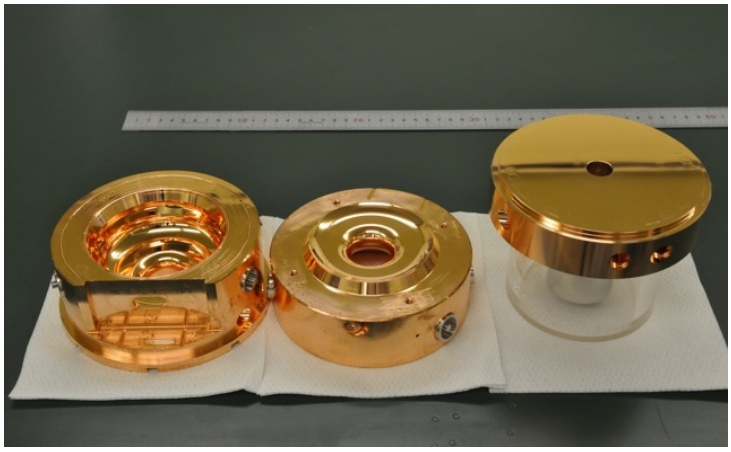

Fig. 3.9: Cavity after initial brazing

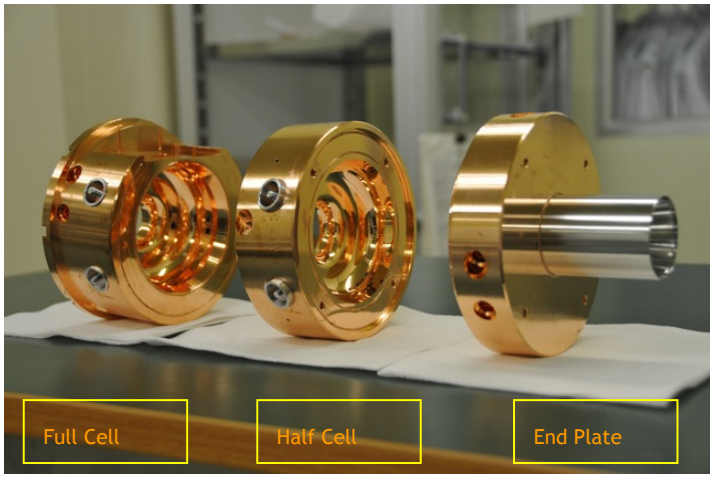

Fig. 3.10: Cavity after initial brazing side view

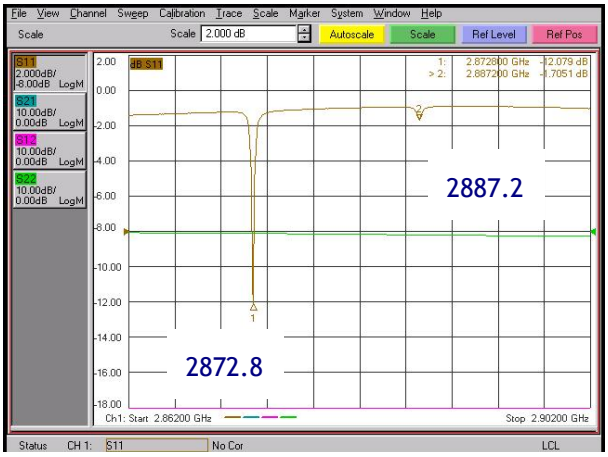

Fig. 3.11: VNA measurement after initial fabrication. The frequencies are very high than the target frequency.

3.3: Measurement and tuning

The measurements were done using Vector Network Analyzer. Mode frequency, individual cell frequency and field pattern using bead pull method was measured at each stage. Depending on the measurements, the next cut on surface was planned. At each stage of operation, frequency and axial field pattern inside the cavity was measured. This gave a clear idea of parameters and then the next stage of machine cut was simulated. Systematic cuts and measurements were done so at to achieve the desired parameters with least requirement of mechanical tuning using the set of tuners.

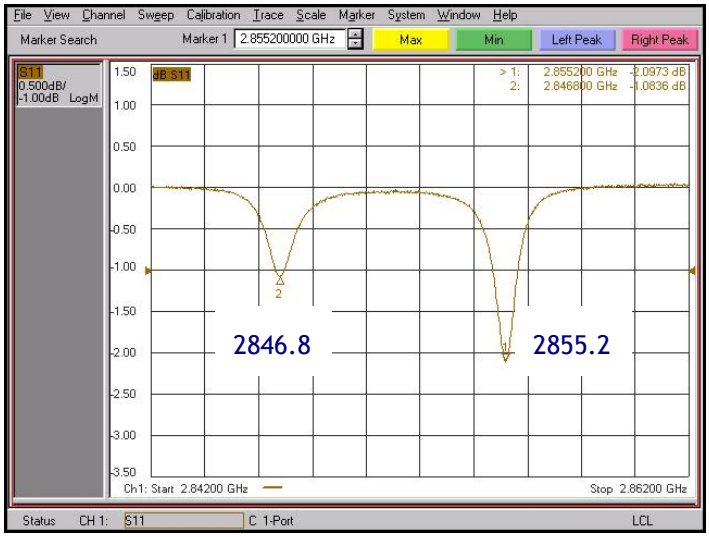

Fig. 3.12: VNA plot before cell to cell brazing. The frequencies are near to desired value and the field balance was almost reached.

Table 3.4: Data of measurements

	Half Cell Radius[mm]	Full Cell Radius [mm]	Measured Pi	Zero	Mode Sep	Simulated Pi	Zero	Field Balance Simulated	Measured
Cut1	43.370	44.515	2887.087	2876.837	10.250	2887.200	2876.900	0.730	**
Cut2	43.620	44.745	2873.370	2858.720	14.650	2873.970	2857.940	4.739	**
Cut 3	43.720	44.765	2865.450	2854.500	10.950	2865.596	2855.949	2.259	**
Cut 4	43.820	44.765	2861.480	2852.960	8.520	2861.611	2852.817	0.994	**
Cut 5	43.860	44.765	2860.120	2851.780	8.340	2860.777	2850.814	0.997	1.080
Cut 6	43.860	44.805	2858.485	2850.017	8.468	2858.741	2849.981	1.370	1.540
Cut 7	43.880	44.825	2856.020	2847.700	8.320	2856.107	2847.710	1.274	1.550
Cut 8	43.895	44.825	2855.200	2846.800	8.400	2855.631	2847.125	1.120	1.100
Brazing 1			2855.191	2846.644	8.547				1.047
Brazing 2	TUNED		2855.559	2846.825	8.734				**
Brazing 3	Tuned		2855.658	2846.920	8.738				0.955
Welding			2855.705	2847.017	8.688				0.956
FINAL TUNING			**2855.615**	**2846.987**	**8.628**				**0.989**

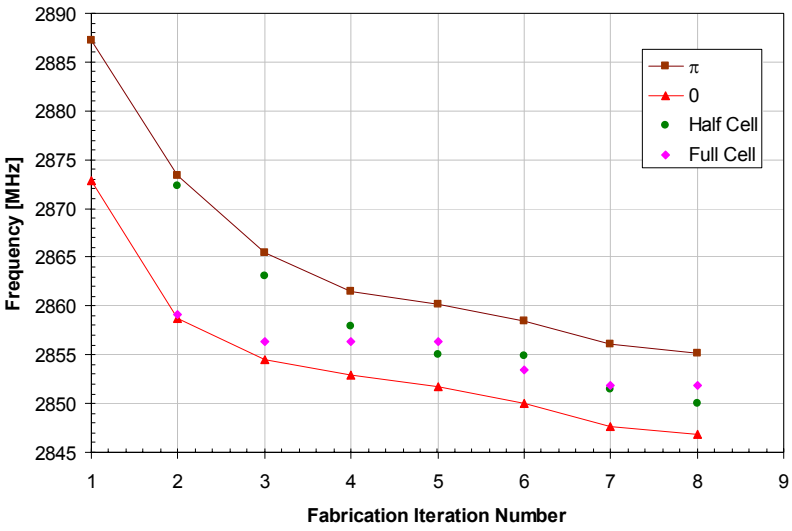

Fig. 3.13: Frequency as a function of cut number

The data of cut and frequency is shown in table 3.4 above. Once the desired frequency was reached, the turning process was stopped. Note that at this stage the π-mode frequency is less because the measurement is in air and at room temperature. The final cavity will have vacuum and beam operation is done at 33 ^{o}C. This was taken into consideration as shown later at the end of this chapter.

The brazing was done in hydrogen furnace. The difference in frequency before and after the brazing was less than 10 kHz. After the brazing, the parameters were measured and it was found that slight tuning is needed to match the frequency and the field balance. The cell has in-built tuners. The tuner can increase or decrease the frequency and the field balance.

The first brazing involved brazing of cell to cell, water cooling pipes and SS pipes at full cell end and pumping port end. The next brazing operation was of waveguide with the gun structure. After the brazing operations were successful, welding was done. The end flanges and tuner stubs were welded and the gun was leak tested using Helium mass spectrometer leak detector. No leak was found. The completed gun is shown in Fig. 3.15. Figure 3.16 shows the test result of VNA measurement.

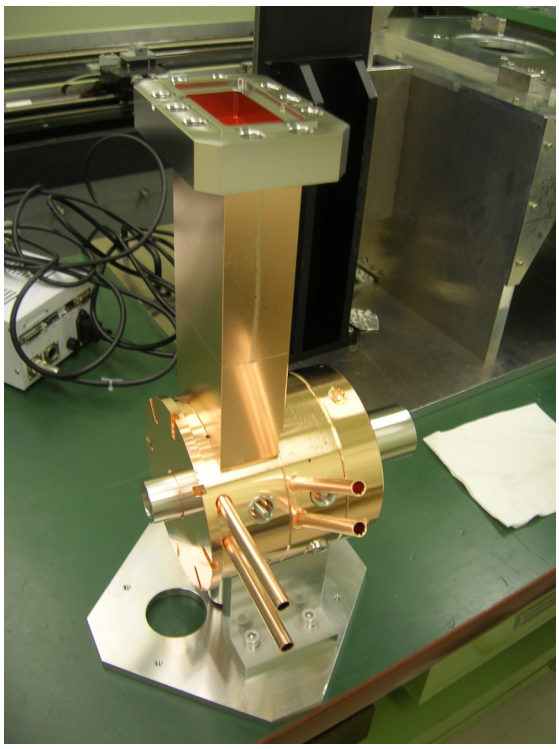

Fig. 3.14: Waveguide brazed to cells

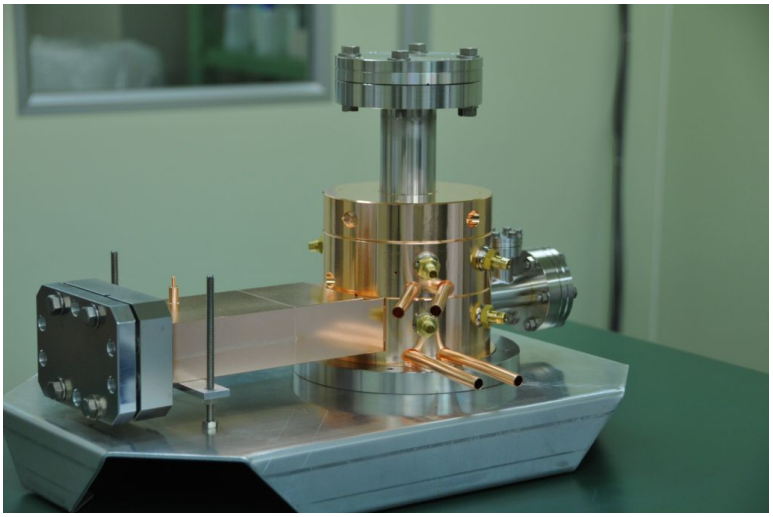

Fig. 3.15: Final gun with welding operations completed

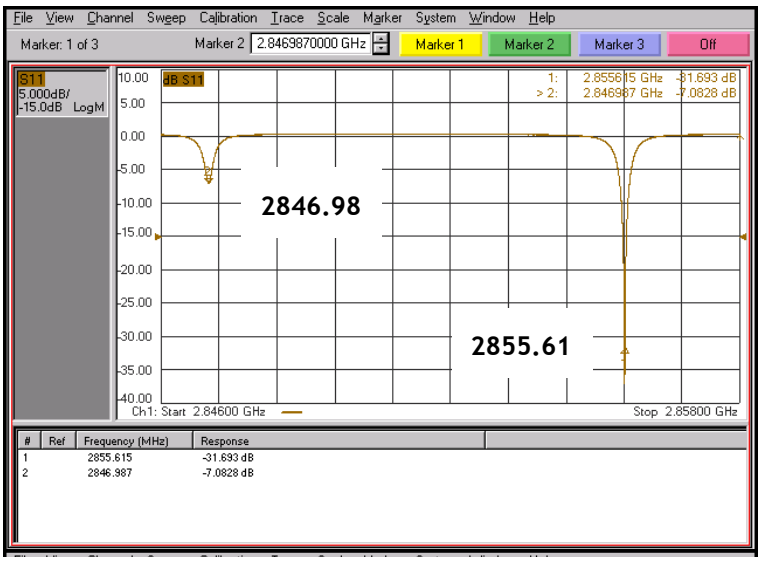

Fig. 3.16: VNA measurement of the final tuning of the gun.

The field balance was measured using a bead pull setup. Our setup is a semi automated setup with the bead motion controlled by stepper motor driven from a computer. The frequency shift is recorded manually and the calculations are done offline after the completion of experiment. Figure 3.17 shows the measurement setup while Fig. 3.18 shows the measured data. Simulated data is also shown for reference. Table 3.5 shows the measured parameters for the old and the new gun.

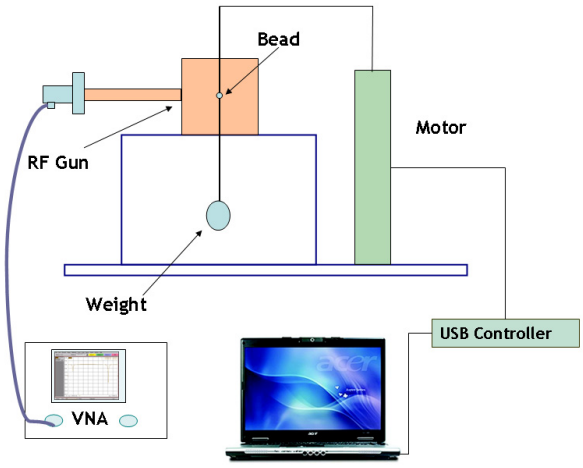

Fig. 3.17: Bead pull setup for cavity field measurement

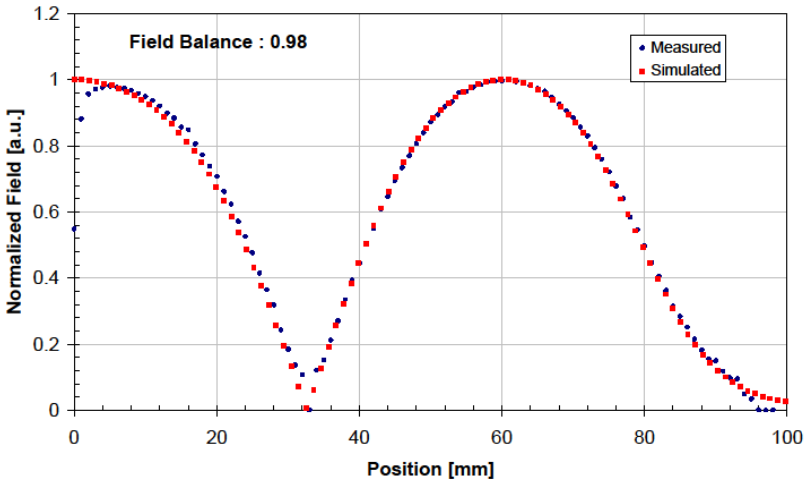

Fig. 3.18: Measured and simulated field distribution along the cavities

Table 3.5: Comparison of measured results for the old and the new gun.

	New Gun		Old Gun	unit
	Simulated	Measured	Measured	
Frequency	2855.64	2855.61	2855.74	MHz
Mode Separation	8.67	8.63	3.52	MHz
Field Balance	1.0	0.98	1.3	
Q	18000	14700	7900	
Coupling β	1.0	1.0	0.6	

From the table and the discussion in the sections earlier, we can conclude that the increased mode separation has been achieved with a field balance of 1.0. The new profile has helped to increase Q and we have achieved highest Q for RF gun at KEK. The large mode separation has made gun more stable over dimensional errors and hence we expect an increased stability in the field balance.

3.4: Tolerances and deviations

From Maxwell's equations for a pill box like cavity it is seen that the wave number 'k' is related to radius of cavity as:

$$k = \frac{J(0)}{R_c}$$

so,

$$R_c = \frac{J(0)\lambda}{2\pi} = \frac{J(0)c}{2\pi f}$$

For f = 2856 MHz, R_c = 0.04017 m.

Now we can use the same equation to find out variations in frequency with

a) dimensional errors:

$$f = \frac{J(0)c}{2\pi R_c}$$

$$\frac{\partial f}{\partial R} = -\frac{J(0)c}{2\pi R_c^{\,2}} = -\frac{f_c}{R_c}$$

$$\frac{\partial f}{\partial R} = -\frac{2.856\times10^{9}}{0.04017\times10^{-6}} = -71.097[kHz/\mu m]$$

So per micron variation in radius will result into change of around 71 kHz in frequency

b) temperature variations:

$$f = \frac{J(0)c}{2\pi R_c}$$

$$\frac{\partial f}{\partial T} = \frac{\partial}{\partial R}\{\frac{J(0)c}{2\pi R_c}\}\frac{\partial R}{\partial T}$$

$$\frac{\partial f}{\partial T} = -\frac{J(0)c}{2\pi R_c^{\,2}}\frac{\partial\{R(1+\alpha(T-T_0)\}}{\partial T} = -\frac{J(0)c}{2\pi}\frac{R\alpha}{R_c^{\,2}}$$

$$\frac{\partial f}{\partial T} = -\frac{J(0)c}{2\pi}\frac{\alpha}{R_c}$$

$$\frac{\partial f}{\partial T} = -f_c\alpha$$

$$\frac{\partial f}{\partial T} = -2.856\times10^{9}\times16.8\times10^{-6} = -47.98[kHz/^oC]$$

Hence for 2856 MHz, we expect around 48 kHz variations per degree Celsius.

3.4.1: Variation due air-to-vacuum difference:

All measurements are done in air at 23 deg. In reality the gun will be in vacuum. Hence the frequency needs to be adjusted assuming the difference in refractive index of air with respect to that of vacuum. The ratio of refractive index of vacuum to that of air is: 1/1.0002926 = 0.999707.

Hence 2856 MHz in vacuum will correspond to 2855.16 MHz in air.

The operating temperature of gun is set around 33^{o}C. This 10 deg temperature difference corresponds to frequency change by 0.480 MHz. Hence the value at which final tuning should be done was set as 2855.16 + 0.48 = **2855.64 MHz**. This will correspond to 33^{o}C operation in good vacuum condition.

References:

[1] C. Limborg et al., LCLS Tech Note, LCLS-TN-05-3

[2] S.G. Anderson et al, Proc. of PAC 2007, TUPMS028

[3] K. Hirano, M Fukuda et al., Nuclear Instruments and Methods in Physics Research, A 560 (2006) 233-239

[4] Abhay Deshpande, J Urakawa et al Nuclear Instruments and Methods in Physics Research, A 600(2009) 361-366

[5] Y. Kamiya et al. Proceedings of PAC 2007, pp 2808

[6] D. T. Palmer, Ph D Thesis, SLAC 1998

[7] K. Halbach and R. F. Holsinger, "SUPERFISH - A Computer Program for Evaluation of RF Cavities with Cylindrical Symmetry," Particle Accelerators 7 (1976) 213-222

[8] K. Flöttmann, A Space Charge Tracking Algorithm, ASTRA, http://www.desy.de/~mpyflo/

[9] J. Rose, Proceedings of PAC 2001, pp 2221

[10] H. Matsumoto et al, KEK pre-print 91–47, May 1991.

[11] H. Matsumoto, Proceedings of LINAC 1996, pp 626-630

Chapter 4: Beam dynamics simulations

Beam dynamics simulations are done to estimate the trends of parameter variations. One of the main issues in the simulations is which code is 'more accurate' and this debate is unending. At present, PARMELA, ASTRA, GPT are the three most widely used codes for beam dynamics simulations of RF guns. As far as published work is concerned, ASTRA seems to have an upper edge over PARMELA and GPT mainly because it is much simple to use, free-of-charge and has been bench marked using many new RF gun. PARMELA versus ASTRA comparison has been done with good precision and the results were found consistent. We decided to use ASTRA for the beam dynamics simulations of new RF gun.

This chapter presents simulation results for the new gun done using ASTRA code. We calculated the variation of emittance and energy spread as a function of laser injection phase. Also we obtained the simulation results which indicate the optimum laser size parameters to achieve low emittance value.

4.1: ASTRA code

In order to have a better estimate of parameters, beam dynamics was simulated using particle tracking code ASTRA. This helped to check the inter dependence of various parameters and thus to finalize operational parameters of the new gun. Before we look at the predictions from such simulations, let us have a brief look at details of the Astra code.

ASTRA is **A** **S**pace **C**harge **T**racking **A**lgorithm used to perform the particle in cell studies. ASTRA is developed by Prof K. Flöetmann from DESY and is available free of charge [1]. ASTRA is now routinely used for RF gun studies in many labs in world as it is very easy to use and gives results comparable to Parmela [2]. LCLS group has done a comparative study of ASTRA, PARMELA and other codes and conclude that ASTRA is same as PARMELA, but predicts emittance in better way [3]. For introducing the bending magnets, PARMELA is much easier than ASTRA. One of the most important features of ASTRA is that it includes the Schottky effect.

ASTRA tracks the particles taking into account the space charge field of the particle cloud. The tracking is based on a Runge - Kutta integration of 4^{th} order with fixed time step. To simulate the beam in better way, ASTRA divides the bunch into thin longitudinal slices and radial rings. This grid is Lorentz transformed into the average rest system of the bunch and field calculations are performed by integrating numerically over the rings, assuming a constant charge density inside a ring. ASTRA then adds up field contribution at the centre of ring and transforms back into laboratory frame. Grid selection is dynamic, in the sense it depends on bunch size. User can define only the number of slices and rings to be used. The particle count in each ring depends on the profile of the bunch.

ASTRA allows the user to define a Gaussian laser beam, incident on cathode and bunch generation from cathode. It can also simulate flat top or any other profiles. The Schottky effect can be incorporated in the simulations and the phase plot can be simulated. Solenoids, quadrupole and linac cells can be easily introduced. User can evaluate the phase space parameters at any location and it can be saved as a distribution file. This file can be used as input to other simulation, if the beam line is too long.

4.2: Simulation parameters

The solenoid used is capable of generating fields up to 0.32T. The field plot of solenoid is shown in Fig. 4.1.

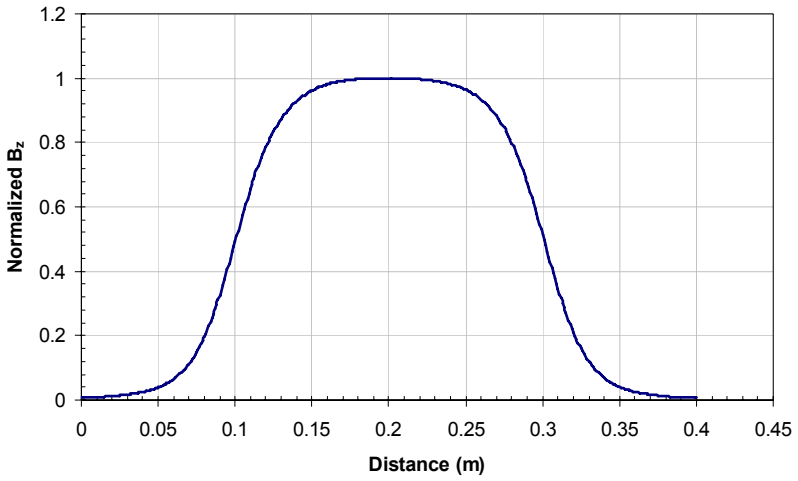

Fig. 4.1: Axial field pattern for LUCX solenoid

The Fig. 4.2 below shows magnetic field versus current characteristics

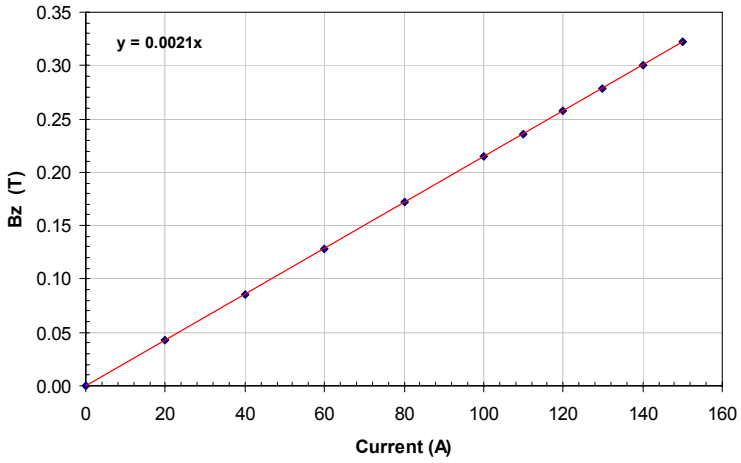

Fig. 4.2: Axial field strength as a function of current

The effect of variation of solenoid field on the emittance is important for the decision to use optimum field strength. Too high field will lead to very small beam size, high charge density and hence poor emittance at the focal point. Hence for a given set of initial parameters, the B_z for which emittance is minimum will have to be obtained using Astra.

4.3: Simulation 1: Energy as function of injection phase θ:

Input laser spot size parameters:

Transverse: 0.319 mm (rms) Longitudinal: 5.5 ps (rms)

The result of simulation is shown in Fig. 4.3. Since we launch beam with very low energy, there is a strong phase slippage. This plot shows the phase slippage. If we launch the beam at 90 deg at the cathode, the exit phase is very much higher and the phase slips prominently. Thus the exit energy is much less. Hence to obtain maximum energy gain at gun exit, injection phase should be between 25 deg to 50 deg.

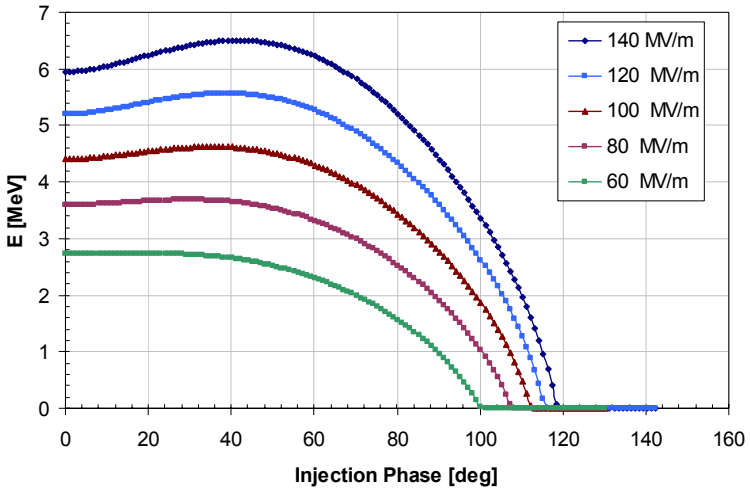

Fig. 4.3: Energy Gain for injection phase for various axial field strengths

4.4: Simulation 2: Emittance scans for solenoid variation

For given phase we can select E_Z from 100 MV/m to 140 MV/m. How ever as seen before, high E_Z results in higher kick at exit points leading to emittance dilution. If the E_Z is set too low, then the bunch at the cathode experiences very high space charge forces and results in emittance degradation. Hence we need a very high E_Z to quickly compensate the degradation near the cathode region. However too high E_Z results in high value of RF emittance contribution and hence results in emittance degradation. Therefore the choice of E_Z is important. The choice of B_z will also influence the emittance value. With increase in B_z, beam will tend to focus more but as the beam size reduces, space charge effect is dominant and emittance will dilute. At some point the RF effect and space charge effect are in balance leading to minimum emittance value. Thus the choice of parameters will affect the end result to a large extent.

In actual practice, very high axial fields are not used as this lead to heavy out gassing in the gun resulting in many vacuum faults. Hence, we fixed the axial field to a high value of nearly 120 MV/ m and performed the solenoid scan to find the minimum emittance. This value is therefore set as reference value and we did most of the parameter measurement at 120 MV/m setting. The results of simulation are as seen in Fig. 4.4 below.

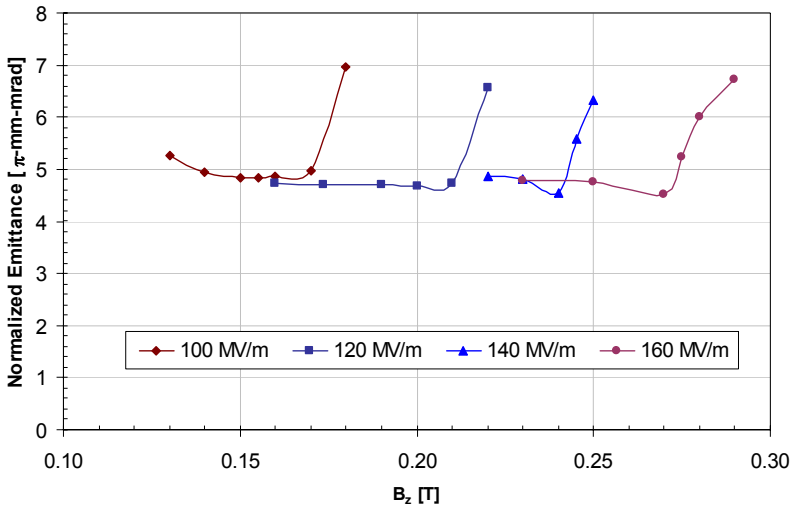

Fig. 4.4: Emittance versus magnetic field for various axial field strengths

4.5: Simulation 3: Effect of varying spot size:

In this case the spot parameters were varied. For a fixed value of pulse length, the transverse spot size was varied to check the minimum of emittance as a function of spot size. Then For the minimal setting of transverse spot size, the pulse length was varied to check the effect on emittance. The resultant plot is as seen in Fig. 4.5.

Clearly for a pulse length of 5.5 ps (rms), minimum emittance is obtained at transverse spot size 0.319mm (rms). Further at this transverse spot size value, a large pulse length can give a low value but the energy spread was high. Hence the optimum choice of parameters is:

Transverse: 0.319 mm (rms) Longitudinal: 5.5 ps (rms)

Physically, small transverse spot size results in emittance degradation due to high space charge. Large values of transverse spot size also results in bad emittance since the different transverse regions will receive different transverse kicks at the exit.

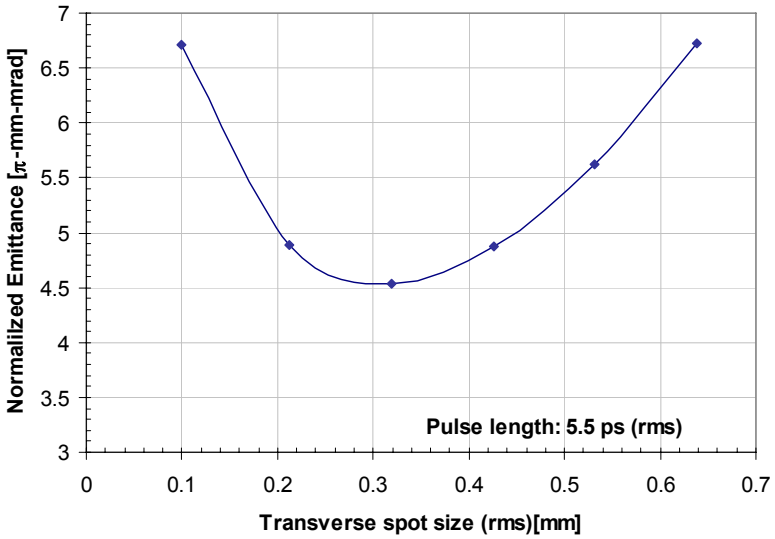

Fig. 4.5: Normalized transverse emittance as function of transverse spot radius

In practice, the laser spot size was measured using CCD camera system. In our setup it is not possible to vary the longitudinal spot size. The variation in transverse size is done using a telescope mechanism.

4.6: Simulation 4: Emittance as a function of injection phase

This simulation was done to check the stability of emittance over laser injection phase variations. The phase variations occur in system due to variation in low power electronic devices. For example, we found that the operational phase of our system shifts if the air conditioning unit is not functioning properly. In the event of total failure of the air conditioning unit, the phase shifts as large as 20 ^{o}C in short time. Since the operational phase is tuned to least energy spread position, shift in phase leads to increased energy spread and hence the beam quality can not be maintained to achieve the best results of emittance. The Fig. 4.6 shows the variation in normalized emittance as a function of injection phase. At each stage, the charge is maintained constant so that the change in emittance is not due to change in space charge effect. In operation, the charge setting was changed by changing the laser power for each setting and the data was then taken.

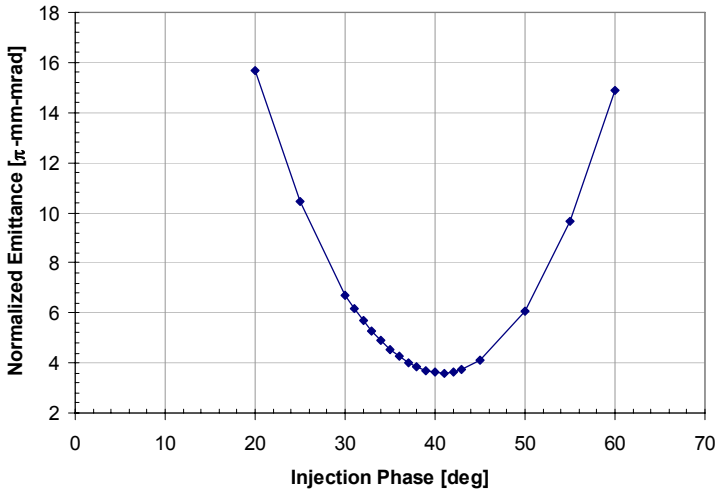

Fig. 4.6: The dependence energy and emittance on injection phase.

The physical explanation for this plot is as follow. To achieve maximum energy at the gun exit, the phase the bunch at the exit should be near 90 deg. But since the energy at the beginning of the half cell is nearly zero, there is a strong phase slippage mainly in the half cell. To avoid this, we retard the phase of injection, so that the exit phase is nearly 90 deg. If the injection phase is too early, the field at cathode is less and so the space charge dilutes the emittance. If we launch the bunch too late in phase, the RF field at the exit is very strong and this leads to a strong exit kick in transverse direction, thus diluting the emittance. The emittance dilution due to RF is low for low axial field while the space charge dilution is high for the low fields. This means that the selection of injection phase is a tricky issue and the user has to decide optimum point where space charge dilution and RF dilution to the emittance is balanced out and leads to least dilution.

4.7: Simulation 5: Energy spread as a function of injection phase

This simulation, shown in Fig. 4.7, was also done to check the effect of phase variations as above. The plot shows that the energy spread minimum is at slightly different injection phase as compared to the phase for maximum energy gain. This gives the user a choice of operation point to set. At LUCX, we usually set the operation point to minimum energy spread position.

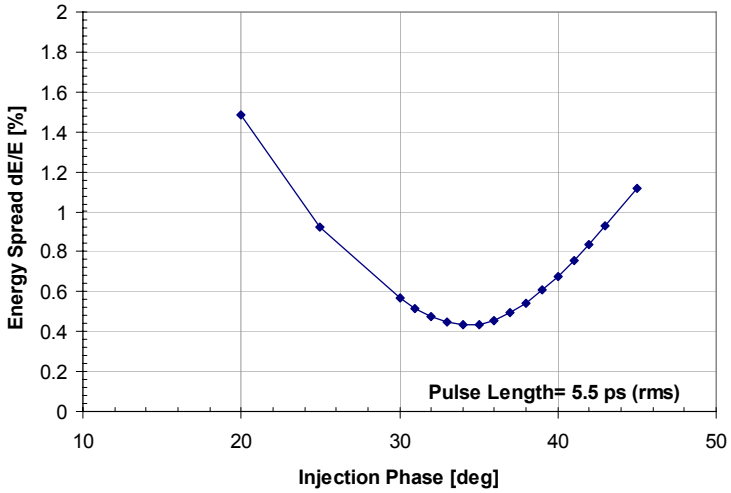

Fig. 4.7: Energy spread as a function of injection phase

In addition to the simulations, Kim gives an analytical way to estimate some of the above parameters [4]. Gao has reported some set of parameters based on Kim's theory for ATF RF gun [5]. It suffices to note that, the analytical estimates are approximated solutions and yield results bit far from observed values. This is mainly due to simplification of equations for simple and clear explanation.

References:

[1] K. Flöttmann, A Space Charge Tracking Algorithm, ASTRA, http://www.desy.de/~mpyflo/

[2] L.Young, J.Billen , PARMELA, LANL Codes,

[3] C. Limborg et al, Proceedings of PAC 2003, pp 3548-3551

[4] K. J. Kim, Nuclear Instruments and Methods in Physics Research A 275(1989) 201-218

[5] J. Gao, ATF Report, 2003

Chapter 5: Measurements and results

In order to measure the beam quality parameters, various standard methods were used. The main focus of measurement was to compare the parameters for the new RF gun with the parameters for the old RF gun, where ever possible. This will lead to understand whether the new gun is more suitable for future applications or not.

Emittance is one of the most important parameter for any gun. As always, a low value of emittance is desired. The emittance value depends on many parameters including the operational conditions. To test the dependence, emittance was measured as a function of solenoid field, laser injection phase, laser spot size and charge. These measurements played crucial role to fix the optimum operational parameters for the RF gun.

Variation in energy spread over the laser injection phase is a parameter that we focused upon. The larger mode separation helps to maintain a low energy spread value for large variations of injection phase. This was observed after careful experimentation.

The thermal emittance issue is discussed in this chapter. We try to estimate the thermal emittance using an indirect method. Direct measurement was not possible due to various limitations of the setup. We propose to measure the thermal emittance by direct method in near future and we are making changes in our setup accordingly. We conclude that the three step model as it exists today is not sufficient to explain the measured value of thermal emittance for semiconductor photocathode. Hence detailed study will be helpful to understand the complexities of factors involved, which affect the thermal emittance.

5.1: Installation and conditioning of the gun:

Once the gun was ready and tuned, it was installed on the LUCX setup. The uncoated cathode was mounted on the gun using load lock mechanism and then the gun was subjected to high power pulsing. Thus the cathode surface was cleaned using the RF fields. Fig. 5.1 below shows the installed RF gun on the system.

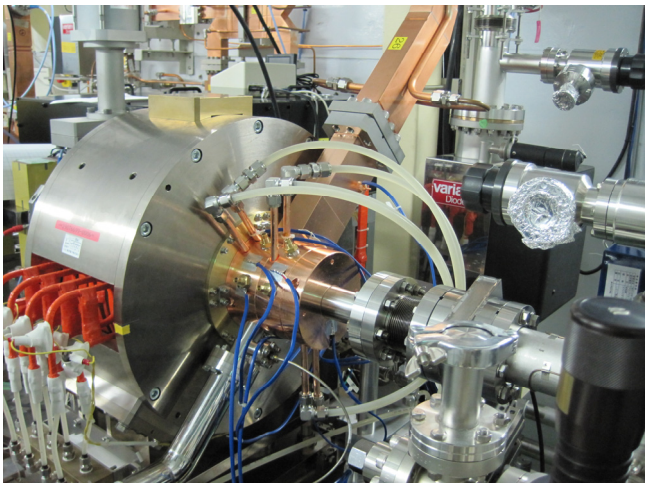

Fig. 5.1: New RF gun mounted on the LUCX beam line

Dark currents were observed and noted down. After about 150 hrs of conditioning at 10 MW power with 2 μs pulse width, cathode was removed and transferred using vacuum enclosure to the coating chamber. The cathode plus was coated with Cs_2Te and then it was re-installed back in the gun. Re-conditioning was done for about 100 hrs. The dark currents were again monitored. The initial quantum efficiency of the cathode was high and it reduced with time. From initial high of around 4% the QE went down up to 0.5% in about 30 days and then it stabilized around 0.4%. From earlier experience we expect the same QE for long time. So it is safe to assume, that the QE for operations will be ~ 0.4%. The dark current plot is shown in Fig. 5.2 below. The plots clearly show that the new gun shows less dark currents than the old gun, even with slightly higher quantum efficiency, especially for the high power.

In the figure, it is seen that the dark currents are high after we close the chamber. The dark currents reduce gradually with time. This reduction can be attributed to the improving vacuum condition. In reality it means that if we open up the chamber and then close it, there will be some degradation in the internal condition. In that case, it is essential to check the effect of Cs_2Te coating specifically to check if the coating of Cs_2Te material contributes to increase in dark

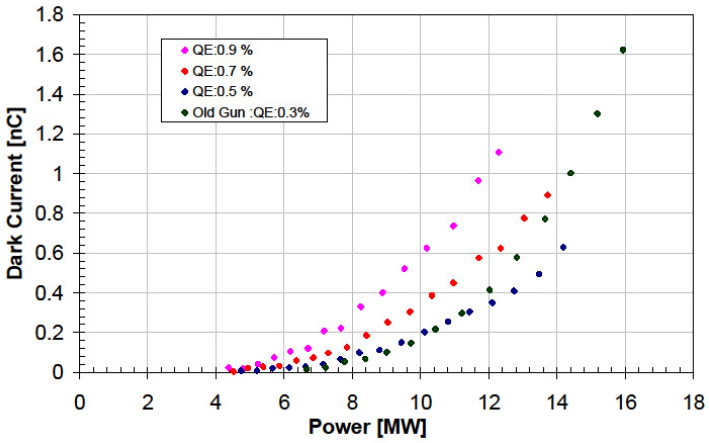

Fig. 5.2: Dark current measurements for old and new gun

currents. Dark current data was taken at similar intervals after closing the chamber before and after the coating. In both cases the vacuum condition was almost similar at the time of data taking. It was observed that the dark currents after coating with Cs_2Te are about 30-40% higher than the dark currents before coating. This implies that Cs_2Te coating may contribute in increasing the dark currents. More precise experimentation in much better controlled environment is needed to ascertain this result.

After the coating, the system was stabilized. Beam parameter measurements were done to check the beam quality. Some important results are discussed in the following sub-sections.

5.2: Solenoid field scans

As seen in chapter 4, the beam gets a transverse kick at the exit of the RF gun. This kick is due to the RF field and is proportional to the strength of the axial field and imparts a divergence to the beam leading to dilution of the emittance. To compensate for this dilution, Carlsten proposed to use a focusing solenoid immediately after the RF gun [1]. This solenoid field focuses the beam and compensates for the emittance dilution. For the fixed screen location, thus there will be a minimum emittance corresponding to some value of solenoid field. This minimum is measured by measuring the emittance at various solenoid field settings and then plotting the emittance as function of solenoid field. The plot in Fig. 5.3 shows the result of such measurement. The emittance is measured by quadrupole scan method. In this method, the strength of quadrupole doublet is varied. The beam is observed on a screen after the quadrupole doublet. Beam size is measured as a function of field strength and fit to the plot yields the emittance at that point. The beam energy is measured using the analyzer magnet and screen after the magnet. Since we know energy and geometrical emittance, the normalized emittance can be calculated.

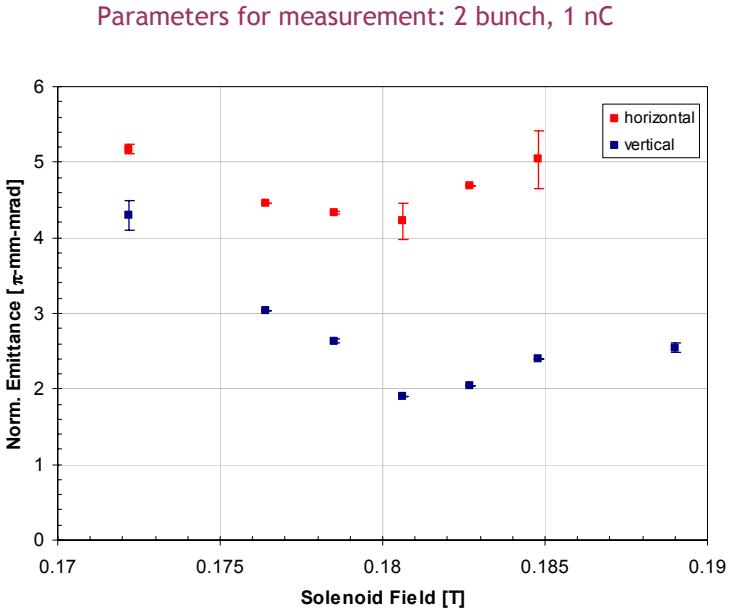

Fig. 5.3: Emittance versus solenoid field

The above measurement is done at 41 MeV. The minimum emittance measured was at solenoid field of about 0.181 T (corresponding to solenoid current of 86A). The normalized horizontal emittance is 4.22 ± 0.21 π-mm-mrad while the normalized vertical emittance is 1.89 ± 0.1 π-mm-mrad. The reported value for earlier gun was 15 π-mm-mrad (horizontal) and 7 π-mm-mrad (vertical). The emittance value has significantly dropped down. The horizontal emittance is higher than the vertical emittance as we have a chicane after the solenoid that bends the beam in the horizontal plane.

Table 5.1 shows comparison of least emittance measured at LUCX and ATF injector at KEK. The ATF damping ring has a modified BNL type RF gun with mode separation of 4 MHz as the source. ATF has reported emittance of 1.36 π-mm-mrad at 1 nC which is the least emittance reported for RF gun at KEK. The emittance of new gun at LUCX is slightly larger than the ATF gun, mainly because the precision alignment was not done at the time of measurements. The beam line was going to be modified after we installed the gun, so it was decided to do precision alignment using Laser tracker after the final modifications. So we expect that once we do the alignment, the emittance will go down. The ATF laser has slightly longer pulse length than the LUCX laser. This reduces the space charge repulsion and thus reduces the emittance.

Despite of the above drawbacks, we did measure an emittance value of as low as 1.25 π-mm-mrad (vertical) for the new gun, but it was not found repetitive. It means that, with good alignment and good tuning, the new RF gun can have a further low emittance. Efforts are on-

going to achieve a stable value of low emittance of 1.25 π-mm-mrad or further less at 1 nC. The result is shown in Fig. 5.4.

Table 5.1: Comparison of emittance measurements

	Normalized vertical emittance at 1nC (π-mm-mrad)
LUCX old gun with out chicane	7.0
LUCX old gun with chicane	4.0
LUCX new gun with chicane	1.89
ATF gun with chicane	1.36

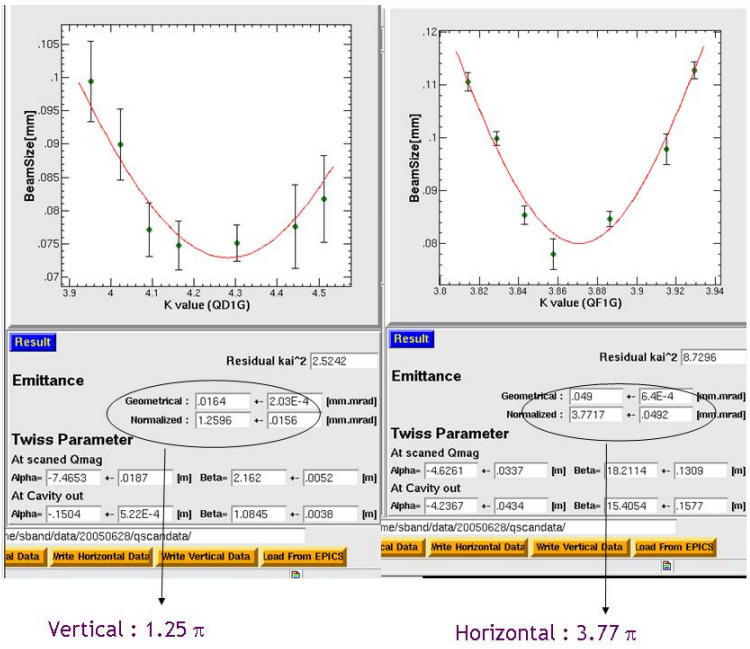

Fig. 5.4: Least measured emittance for the new RF gun. This emittance value is not very stable so we report 1.89 π-mm-mrad (vertical plane) as the stable, low emittance value.

Increasing the pulse length of the laser profile will further help in emittance reduction. It has been reported at LUCX [2] that using flat top laser reduces the emittance. This was reported by Spring-8 [3]. There fore using flat top laser can also be useful to reduce emittance. For thermal emittance measurements, a flat top laser profile will be more helpful because it ensures that the intensity variation over the area of illumination changes uniformly with changing beam size.

5.3: Emittance versus phase

The plot in Fig. 5.5 shows the variations in horizontal and vertical plane emittance as a function of the laser injection phase. Before the actual measurement is started, initial tuning is done. A scan of variation in bunch charge as a function of injection phase is done to fix the operational phase at so that the energy spread is minimized. Then the beam is passed through the linac and then through the bending magnet on to a screen located at the far end of LUCX. The image on screen correlates with the energy spread of the beam. The phase of linac is then adjusted to achieve the least energy spread setting. The detailed method is already explained in Chapter 2.

After doing the initial settings, the beam profile is seen on the screen immediately after quad doublet after the linac. Emittance is measured at this position using the quad scan method. For each injection phase setting the emittance is measured for various solenoid field strengths and the minimum emittance is noted. Then the phase of laser injection is changed and the above process is repeated. Thus the best setting is done at each point seen in the plot below and then the total results are plotted as shown in Fig. 5.5.

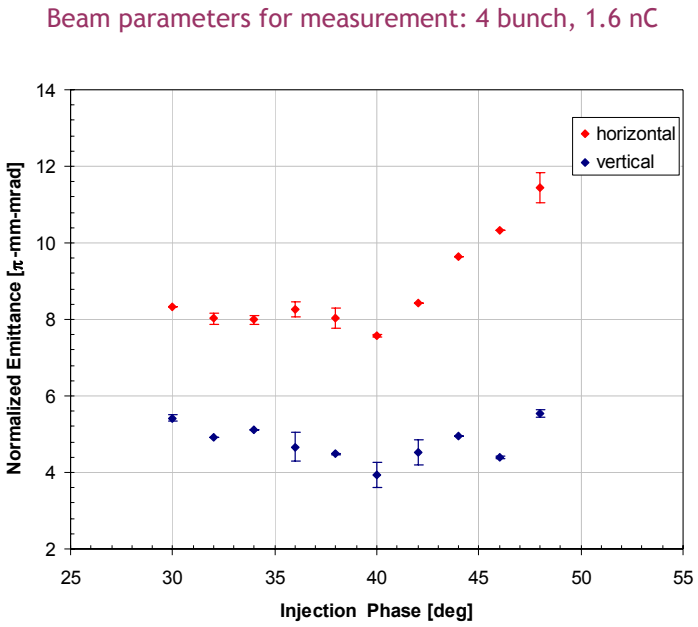

Fig. 5.5: Emittance variations with injection phase

It is important to note that, the charge is also a function of injection phase. This makes the above plot complicated. In order to check the actual effect of injection phase alone, the charge needs to be kept constant. To achieve this, the laser power is varied at each phase setting and nearly same charge is obtained. As expected, the emittance degrades for too early or too late injection.

5.4: Energy spread measurements

The energy spread is an important parameter. In our setup, we measure the energy spread using the analyzer magnet and screen as mentioned earlier. Calibration is done by changing the magnetic field and finding the position of the beam on the screen. Then the vertical axis calibration data is used to find out the energy spread.

With reference to the increasing mode separation, LCLS group had predicted lower emittance over phase variations [4]. The RF gun group at Swiss Light Source (SLS) has shown using simulations that with increase in mode separation, the energy spread variation over injection phase variations is low [5, 6]. In other words, this means the energy spread is stable for small variation of injection phase.

Figure 5.6 shows the variation of the energy spread as a function of the injection phase for a beam with a 1.6 nC charge. As the bunch charge is also a function of the injection phase, the charge is adjusted for each phase position by varying the laser power. For comparison, the figure also plots the measurement results for the old gun with less mode separation. The operating conditions and bunch parameters were same for both the measurements. The new gun clearly shows much more stable energy spread against the variations of the injection phase.

Increase in mode separation, can thus lead to maintain low value of spread over more phases. This brings additional stability to operation of RF gun over environmental parameters and thus increases the reliability of the gun.

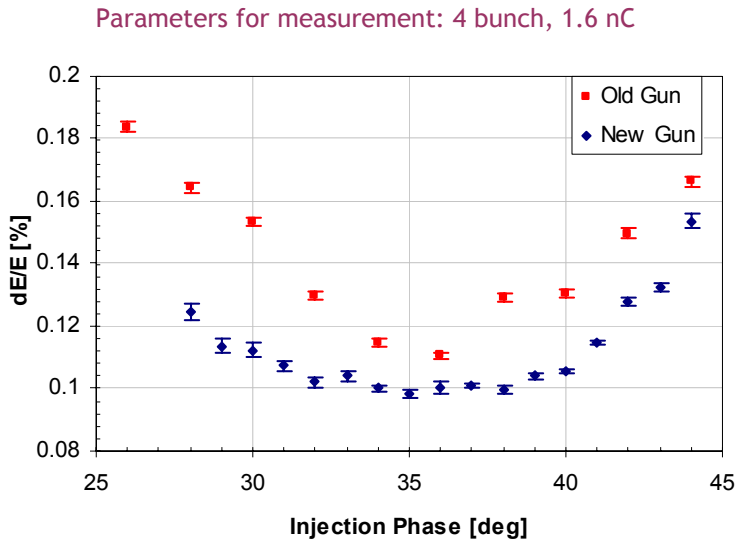

Fig. 5.6: Energy spread (rms) as function of injection phase

5.5: Emittance versus laser spot size

This measurement was done to find out the effect of variations in laser spot size on the emittance. The laser spot size was varied by changing the telescope-lens system. In our setup, the variation of spot size is not automated, so one has to shut down the system and then do the changes. Once the spot size is varied, all initial settings are needed to be repeated. So after we start up the machine, we perform a scan of bunch charge versus phase and fix the phase of injection to position to obtain minimum energy spread, by observation. Then we obtain the image on screen after analyzer and check if the phase location corresponds to minimum spread or not. At this point we fix the linac phase as well as the gun phase.

After doing these initial settings, the emittance is measured using quad scan method over a range of solenoid fields. The minimum of emittance obtained is then plotted in the graph below.

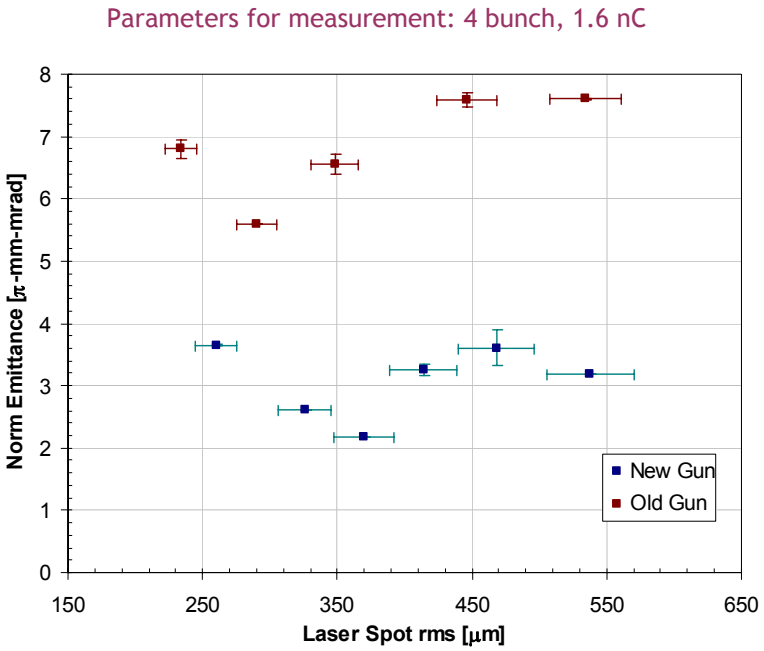

Fig. 5.7: Emittance for various laser spot sizes.

Fig. 5.7 shows that there is a laser spot size at which the emittance has minimum value. This is as expected and simulations done show a similar trend. The simulations done using ASTRA code predicted minima around 320 μm while experimentally we found that the emittance shows a low value around 350 ± 20μm. We think that this is therefore closest to minima. More data, especially for small and very large spot size is needed to find the true minima. At present, this was not possible because we generate minimum 4 bunches per train. For large spot size; the

bunches showed splitting and we could see multiple cores on screen. Hence emittance measurements were impossible.

As the laser spot size increases, the thermal emittance contribution will also increases; hence for actual operation a small spot size is preferred. Increase in the spot size, however exposes more photo cathode material to the laser spot and so high charge can be obtained. So if need arises, these facts can be considered to the benefit of user and careful choice of spot size can help to get high charge, low emittance beam.

5.6: Emittance versus charge

The emittance variation due to bunch charge is measured and plotted in Fig. 5.8 for the new and the old gun. As seen below, both the guns show similar patterns in variation. The plot can be extrapolated to zero charge state. The intercept on y-axis corresponds to the RF- *only* emittance contribution to the total emittance.

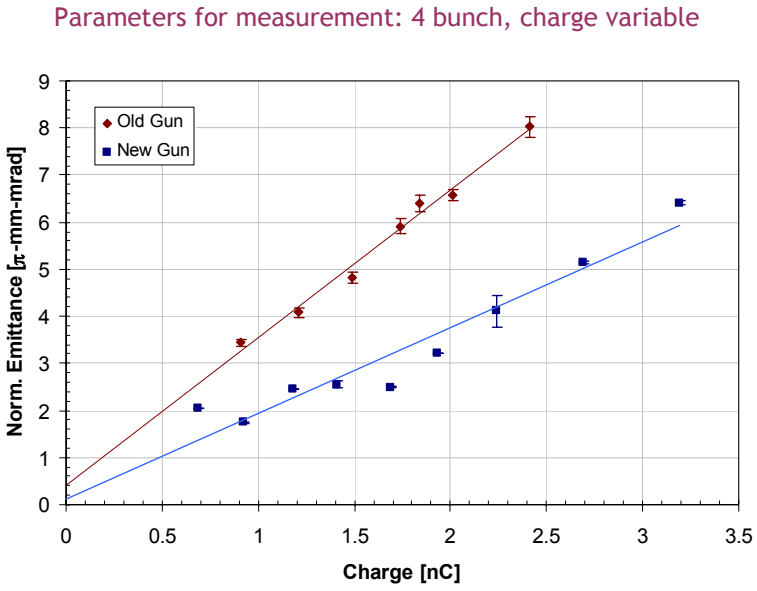

Fig. 5.8: Emittance variation with bunch charge

As seen from the above plot, for the new gun the zero charge emittance is less as compared to LUCX gun. This was expected as the laser ports are removed. Hence any asymmetry due to the slots is reduced and so the field pattern will be more uniform in new gun as compared to earlier gun.

5.7: Energy measurement for various injection phase

As explained earlier in chapter 4, due to low initial energy there is a phase slippage, mainly in the half cell. Hence the exit phase is much advanced as compared to the launch phase. To achieve a high energy at the gun exit, we need to have the bunch near the crest at the time of exit. To achieve this, the easiest way is to retard the launch phase. For late bunch launching, the phase slippage will be prominent and the exit energy will be very low. ASTRA code was used to predict this behavior. We used a direct measurement to find out the dependence of energy on the injection phase. The energy gain shown in Fig. 5.9 is measured immediately after the gun. For these measurements in our setup, we use the screen at the center of chicane magnet to measure the energy of beam. The injection phase is varied and the beam is seen to move on the screen. Chicane current is adjusted till beam comes at the screen center. The chicane current is correlated with beam energy and hence we find out the beam energy. For early injection phase, we expect high energy gain and low energy spread and the energy goes down, due to slippage as we go for late launch of the beam. The measurements shown below are for low klystron power. This was done due to repeated vacuum faults coming from klystron when operated at higher powers. In reality the gun can deliver high energy beam.

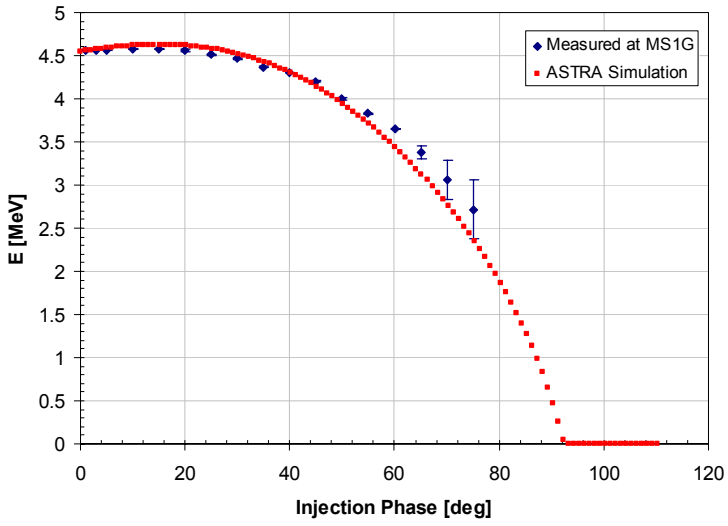

Fig. 5.9: Energy as a function of injection phase

5.8: Estimation of thermal emittance

The treatment shown here closely follows the analysis by Prof. K. Flöetmann [7] and by D. H. Dowell [8]. The method developed by Dowell, gets results very similar to Flöetmann's method. Yet as seen later, thermal emittance as seen from both the methods does not match with experiments done by various groups. The thermal emittance issues for Cesium Telluride type (semi conductor) cathode still remains unsolved issue. Before we go in more detail, let us look at the three step emission model on which most of the calculations of photo cathode gun are based. These explanations form the basis of thermal emittance measurements.

5.8.1: The three step model

We explain this model assuming the photoemission from Cesium Telluride. The schematic of energy level is shown in Fig. 5.10 below.

- ✓ **Step 1:** Photon absorption in cathode material and excitation of electron to conduction band (CB).

  The Threshold energy E_T is 3.5 eV while the band gap E_G is 3.3 eV. We use ultra violet laser with wavelength 266 nm i.e. E_{ph} is 4.66 eV. The optical absorption depth and the reflectivity of the surface are the main parameters which can affect this process. The reflection depends on angle of incidence as well as the surface condition

- ✓ **Step 2:** Transport of the electron to maximum of conduction band.

  The first maximum of density state of CB is at 4.05 EV and hence the laser photon with E_{ph}=4.66 eV is sufficient to excite electron to this level. The next maximum is at 4.9 eV and hence it is not considered for the calculations.

  The transport phenomenon is the most complex part with electron-electron interactions dominant for metal photo cathode. For semi conductor cathode, electron-phonon interactions are also dominant and the calculations are further complicated.

- ✓ **Step 3: Escape of electrons to vacuum:**

  When electrons overcome the affinity E_A, which arises from surface potential barrier, they escape to vacuum. The surface barrier is the energy difference between vacuum level E_{vac} and the bottom of conduction band. Hence E_T = 3.5 eV = E_{vac}.

$E_T = E_G + E_A$, and therefore, $\mathbf{E_A = 0.2\ eV}$

The electrons before the escape have average energy E= 4.05 eV, hence after escape in vacuum, the energy will be:

$E_K = E_{CB} - E_G - E_A$ and therefore, $\mathbf{E_K = 0.55\ eV}$

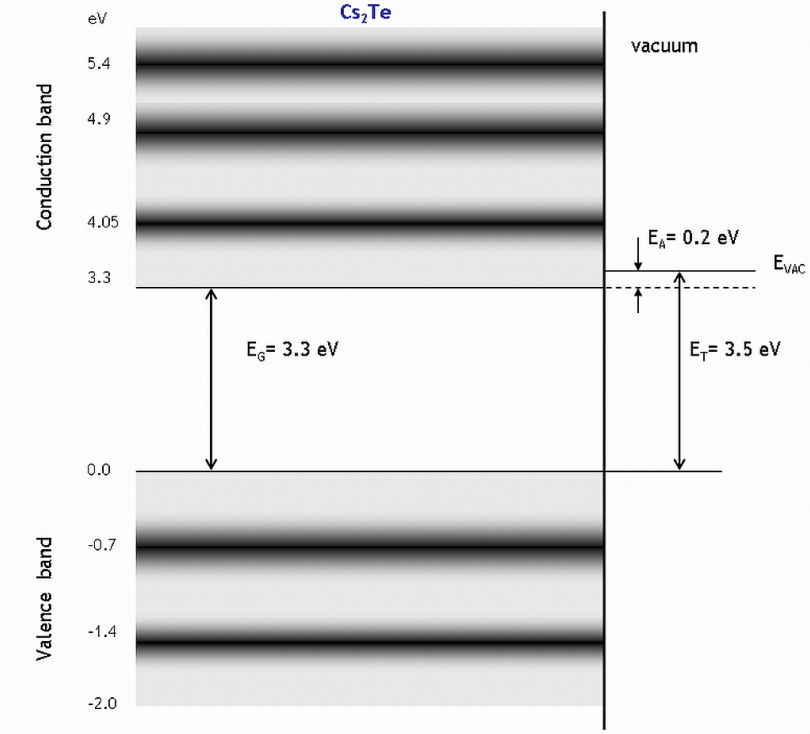

Fig 5.10: Band structure of Cs_2Te

5.8.2: Relation for thermal emittance

Following the three step model, we can define thermal emittance as:

$$\varepsilon_{th} = \frac{1}{m_o c}\sqrt{\langle x^2\rangle\langle p_x^2\rangle - \langle xp_x\rangle^2}$$

At cathode there is no correlation in phase space, so $x.p_x$ term is zero. Hence,

$$\varepsilon_{th} = \sigma_r \frac{p_{x,rms}}{m_o c}$$

Now, we define the geometry at cathode to find out the momentum component. We define, ϕ and θ as the azimuth and meridian angle for electrons emitted with momentum p. The components of momentum are:

$p_x = p.\sin\phi.\cos\theta$ $\qquad$ $p_z = p.\cos\phi$

Particles with longitudinal momentum $p_z = \sqrt{2m_0E_A}$ will be stopped by the potential barrier. These are the electrons with azimuth angle ϕ larger than

$$\phi_{\max} = \arccos\sqrt{\frac{E_A}{E_{Kin}}} \qquad (5.1)$$

Hence,

$$p_{x,rms} = \sqrt{\frac{\int_0^{\phi_{\max}}\int_0^{2\pi} p_x^2 \sin\phi.d\phi.d\theta}{\int_0^{\phi_{\max}}\int_0^{2\pi} \sin\phi.d\phi.d\theta}}$$

And hence,

$$\varepsilon_{th} = \sigma_r\sqrt{\frac{2E_{Kin}}{3m_0c^2}}\sqrt{\frac{2+\cos^3\phi_{\max}-3\cos\phi_{\max}}{2(1-\cos\phi_{\max})}} \qquad (5.2)$$

If we assume that the emission takes place behind the barrier into half sphere over cathode,

then $\phi_{\max} = \tilde{\pi}/2$ and so:

$$\varepsilon_{th} = \sigma_r\sqrt{\frac{2E_{Kin}}{3m_0c^2}}$$

Hence, $\varepsilon_{th} = \sigma_r\sqrt{\frac{2(E_{CB}-E_G-E_A)}{3m_0c^2}}$

5.8.3: Comparison for metal and semi conductor

For metal cathode we can readily define work function and Schottky effect. For photo emission from metal photo cathode,

$$\varepsilon_{th} = \sigma_r \sqrt{\frac{h\nu - \phi_{eff}}{3m_0c^2}}$$

$$\phi_{eff} = \phi_W - e\sqrt{\frac{eE_{axial}}{4\pi\varepsilon_0}}$$

Where the second term in ϕ_{eff} is the Schottky reduction term and we define, $E_{metal} = h\nu - \phi_{eff}$;

For semi conductor, the Schottky effect can be seen as change in the surface potential barrier. For Cs_2Te like photo cathode $E_{semi\text{-}conductor} = h\nu - E_G - E_A$

Where in: $2E_{kin} = h\nu - E_G - E_A$ can help correlate the equations derived independently by two papers.

For the sake of completion, it is worth to point out that for thermionic cathode emitter,

$$\varepsilon_{th,n} = \sigma_r \sqrt{\frac{k_B T_e}{m_0 c^2}}$$

Based on the theory mentioned above, measurements done by various groups were analyzed and the details are listed by Dowell [6] and shown in Table 5.2 on next page. It can be seen that, the proposed theory does not agree well with the measured data for metal as well as semi conductor cathode.

5.8.4: Measurement method

We have adopted Clendenin's method, which though not correct for Cs_2Te cathode, throws some light on the topic [9].

We check the effect of change in work function which changes the Quantum Efficiency, QE. We define QE as the ratio of emitted electrons to the no of incident photons. Since all the photons are not converted to exactly same no of electrons QE is less than 1.

Table 5.2: Summary of properties of cathodes from Ref. 6

Thermionic	Temperature (K) k_BT (eV)	Radius (mm)	Current Density (A/cm^2)	Work Function(eV)	Thermal Emittance/beam size (microns /mm(rms))
CeB_6	1723 0.1486	1.5	42	2.3	0.539

Metal	λ (nm) E (eV)	QE	Vacuum (torr)	Work Function (eV)	Thermal Emittance/beam size (microns /mm(rms))	
					Calculated	Measured
Copper	250 , 4.96	1.4×10^{-4}	10^{-9}	4.6	0.5	1.0±0.1
Mg	266, 4.66	6.4×10^{-4}	10^{-10}	3.6	0.8	0.4±0.1
Semi Conductor	λ (nm) E (eV)	QE	Vacuum (torr)	E_G+E_A (eV)	Thermal Emittance/beam size (microns /mm(rms))	
					Calculated	Measured
CsTe	211, 5.88 264, 4.7 262, 4.73	~ 0.1	10^{-9}	3.5	1.2 0.9 0.9	0.5±0.1 0.7±0.1 1.2±0.1
GaAs	532, 2.33	~ 0.1	?	1.4±0.1	0.8	0.44±0.01

For the change in work function the Quantum Efficiency changes as an exponential function.

$$\frac{QE}{QE_0} = \exp\left(\frac{-\Delta\Phi}{kT_e}\right) = \exp\left(B\sqrt{E_c}\right)$$

$$B = \frac{e}{k_B T_e}\sqrt{\frac{e}{4\pi \in_0}}$$

$$\ln(QE) = B\sqrt{E} + \ln(QE_0)$$

Where, k_B is the Boltzmann constant and T_e is the effective temperature of the exited electrons at the emission.

For the measurements, we incident a laser pulse on the cathode surface. The laser intensity is measured using a photo diode. So we know the laser energy deposited. The emitted charge is measured using the current transformer (ICT). We measure the charge as a function of injection phase. The result is shown in Fig. 5.11. Since we know the charge and the laser power, we know the quantum efficiency as a function of phase. Since we know the axial field strength, we also

know the field at cathode as a function of injection phase. Then we plot, log QE as a function of square root of Electric field and fit the line to equation below, as shown in Fig. 5.12.

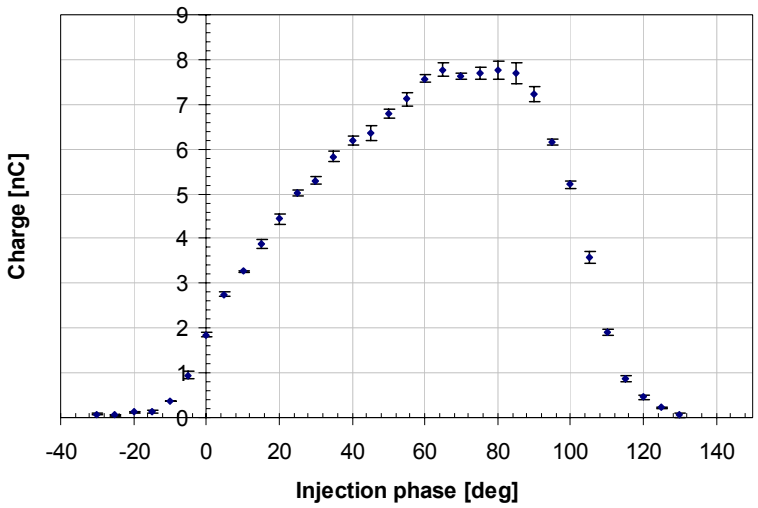

Fig. 5.11: The bunch charge as a function of injection phase.

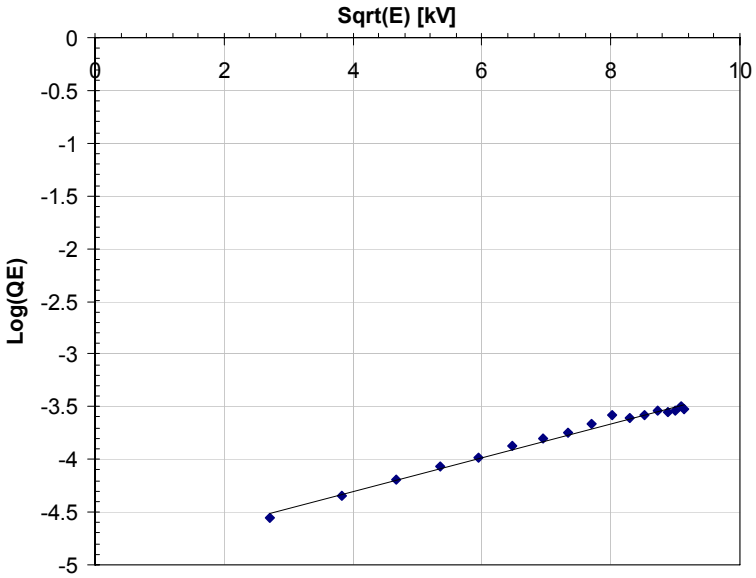

Fig. 5.12: Plot of square root of axial field as a function of logarithm of quantum efficiency. The fit of this plot determines the parameter B.

Fit to the curve yields the parameter B, which gives the effective temperature T_e. A set of data over varied values of laser powers will yield similar set of values and hence the error can be found out.

Using the fit we get the slope **B**: $0.1618 \times 10^{-3} \pm 0.00395 \times 10^{-3}$

The slope is related to the temperature (strictly speaking longitudinal temperature) as:

$$\frac{k_B T_e}{e} = \frac{1}{B}\sqrt{\frac{e}{4\pi\varepsilon_0}} = \frac{3.7925\times10^{-5}}{B}$$

Hence: T_e: 0.2343 eV

Since, this analysis is using thermionic cathode terminology; we use formula for thermionic emitter thermal emittance [10].

$$\varepsilon_{th,n} = \sigma_r \sqrt{\frac{k_B T_e}{m_0 c^2}}$$

Using this data, we find thermal emittance as a function of laser radius as shown in Fig. 5.13. For our settings, we estimate that the thermal emittance per unit beam size is found to be 0.525 microns/mm. The estimated upper limit for thermal emittance per unit beam size is 0.847 microns/mm. The upper limit is achieved if we assume the cosine term in Equation 2 equal to 1. However, as seen from Equation 1, this may not be the case, as it will imply infinite kinetic energy to the electrons. Hence, we estimate the cosine term effect assuming the values of E_{kin} to be 0.55 eV and E_A is 0.2 eV. These values come from the band structure for Cs_2Te shown in Fig. 5.1. If we include the affect of the cosine term then the thermal emittance is 0.437 microns/mm. This value is close to the measured value. It implies that to find out the actual thermal emittance, we need to find out E_{kin} and E_A as accurately as we can. The proposed experiment in next section focuses to measure these parameters and then fit to get good estimate of thermal emittance.

Thus although our method is not a direct method, the measured thermal emittance is close to the theoretical estimate. The method does follow a similar trend and fall short of the predicted values. More data and direct measurements are needed to find out the thermal emittance. More data will establish a clear trend and thus finding the limit of thermal emittance may be possible by studying phase plot alone. Thus the estimation of thermal emittance will become very easy.

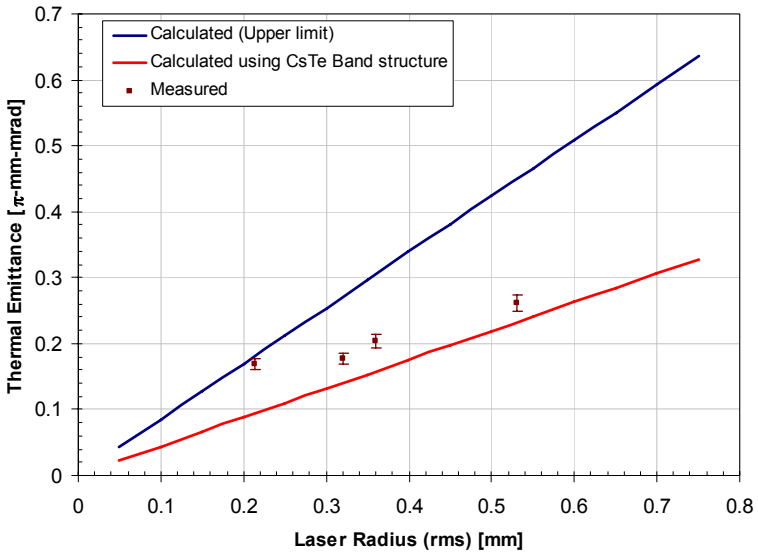

Fig. 5.13: Comparison of theory and measurement. The blue curve shows upper limit while the red curve shows the emittance inclusive of the cosine factor in Equation 5.2. The measured data is using method described earlier.

5.8.5: Possibility of direct measurement

Now we propose to measure the thermal emittance directly from observation. If we reduce the charge per bunch very low to around 5 pC per bunch, then the space charge effect is negligible and hence we get the thermal emittance. The main problem in this method is to measure the low emittance value. We propose this experiment in our setup. The main drawback will be that the quad scan method may not be so effective in measuring very small beam size and the error may be high. Hence the emittance value may not be correct. The other problem in our setup comes from the beam size variation. We use a Gaussian beam profile and changing the beam size will change the illumination pattern significantly. A flat top laser profile, on the other hand will give less radial intensity variations with change in aperture.

As before,

$$\varepsilon_{th} = \sigma_r \sqrt{\frac{2E_{Kin}}{3m_0c^2}}$$

Hence a derivative of this result will be: $E_{Kin} = 1.5 m_0 c^2 \left(\frac{d\varepsilon_{th}}{dr} \right)^2$

Therefore, a plot of thermal emittance as a function of radius will give the value of electron energy in the vacuum. This can be re-used back in the theory to compare the results.

We conclude that, the thermal emittance measurement needs to be studied in great details. We find that the method given by Ref. 7 is inappropriate for our case. We propose to measure thermal emittance in near future with more direct method proposed. The measurement will also help in contributing inputs to on-going theoretical development for semi conductor photo cathode theory. It is also essential from point of view of further reduction of observed emittance of photo cathode gun that we study.

References:

[1] B. E. Carlsten et al., Nuclear Instruments and Methods in Physics Research, A 285 (1989) 313-319

[2] Sheng-Guang Liu, Junji Urakawa et al 2010 Chinese Phys. C 34 584

[3] H.Dewa, T.Asaka, et al. in Proceedings of FEL 2006, BESSY, Berlin, Germany, pp. 649–652.

[4] C. Limborg et al., LCLS Tech Note, LCLS-TN-05-3

[5] J.Y. Raguin, R.J. Bakker, Proceedings of FEL 2005, pp 324

[6] D.H. Dowell et al., Nuclear Instruments and Methods in Physics Research A 528 (2004) 316.

[7] K. Floetmann, Tesla-Fel-97-01 (Feb., 1997)

[8] D.H. Dowell and J. F. Schmerge, PRST-AB, 12, 074201 (2009)

[9] Jim Clendenin, SLAC PUB 7760

[10] J. D. Lawson, The physics of Charged Particle Beams, Clarendon Press, Oxford, 1988, p 210.

Chapter 6: Multi bunch beam loading compensation

The generation of multi bunch beam with least possible energy difference needs very careful design of system and good tuning. At LUCX we are trying to establish the generation of very long bunch trains and we wish to achieve 8000 bunches per train. The future of compact x-ray sources will depend on how long trains with high charge and low energy difference. After more research, in few years these sources will be generating x-ray beams with high flux.

In this chapter, we present a brief theory for the multi bunch beam loading compensation using delta T method. We present the simulation results based on the existing theory. Then we list down the actual experimental methods for generation of multi bunch beam. We already succeeded in generating 100-bunches with 0.5 nC per bunch at 40 MeV with peak to peak energy difference less than 0.7%. In other experiment we generate low energy beam of 5 MeV. In this case we succeed to generate 300-bunches with 0.55 nC per bunch with peak to peak energy difference less than 0.85%. These results are very important results for our efforts to make 8000-bunches per train as a first step. We hope to achieve this goal by the end of this year (2010).

6.1: Standing wave RF gun

The multi bunch generation is one of the main challenges in our experiment. It is essential to generate a multi bunch beam to overcome the x-ray flux issue. For generating high photon flux after collision with laser, we need a high charge bunch. But then, if we increase the charge to a very high stage, say 200nC, then the energy spread will be become too high. Since the beam passes through chicane, a positional difference can occur and some part bunch will hit the wall of chamber or the linac and thus damage the system. Obviously it is not desirable. It is not achievable, as well, due to the limitation of the laser system. The better option is to reduce the charge per bunch and increase the number of bunches. In this option, the multi bunch beam loading has to be compensated. In this chapter we discuss the scheme for such compensation. There is also a third option, where in we can maintain a single bunch with say 2nC charge and increase the rep rate of system to very high rate of around 300 Hz. The main problem in this case will be the heat dissipated in the gun and linac will be high and so it may be tough to keep the structure tuned at same frequency. Therefore the best option is to go for multi bunch beam with low charge per bunch and moderate rep. rate of say up to 50 Hz. This system will then generate high flux x-rays after the collision.

We plan to achieve 2nC in 100-bunch beam and 0.5nC in 8000 bunch beam as a first step for multi bunch beam experiments. Till now, we have achieved 0.5nC in 100-bunch at 40 MeV and 0.55nC in 300 bunches at 5 MeV. The acceleration of 2nC per bunch with 100 bunches per train requires higher power from Klystron and we are now making a new modulator for our new Klystron. At low energy, we stopped at 300 bunches due to the Pockels cell problem. Recently, we replaced the Pockels cell and so we can generate longer bunch train in near future. In this chapter, we first have a brief overview of the theory for the multi bunch beam loading compensation and then we will see the details of experiments and achieved results. In the theory part, we consider standing wave (RF gun) and travelling wave (linac) case and then we check the effect of power multiplier in such system.

6.1.1: Loading for standing wave structure

Derivation of unloaded energy gain:

For single resonant cavity as seen in Fig. 6.1, we define P_i is the incident power, P_L the reflected power, P_c the power dissipated in the cavity and P_e the emitted power. We define the fields associated with the power by:

$$P = kE^2$$

Where we define the reflected wave as E_L, emitted field from the coupling aperture E_e, and the incident wave from the klystron as E_i [1][2],

We can imagine E_L, as a superposition of E_e and E_i as:

$$E_L = E_e - E_i \qquad (6.1)$$

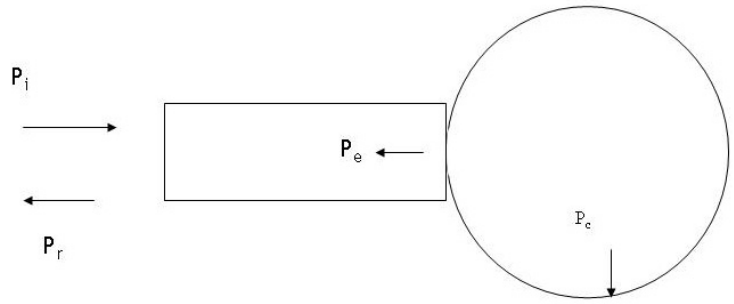

Fig. 6.1: Standing wave cavity model

By the conservation of power,

$$P_i = P_L + P_c + \frac{dW_c}{dt} \qquad (6.2)$$

$$P_c = \frac{\omega_0 W_c}{Q_0}$$

Where, W_c is the energy stored in the cavity at time t, ω_o is the resonant frequency and Q_0 the unloaded quality factor. Using Eq. (6.2), together with the fact that power is proportional to the square of the field we can derive equations for field as:

$$E_i^2 = (E_e - E_i)^2 + \frac{E_c^2}{\beta} + \frac{2Q_0}{\omega_0 \beta} E_e \frac{dE_e}{dt} \qquad (6.3)$$

Where β is the cavity coupling coefficient defined as $kE^2 = \beta P_c$. By rearranging Eq. (6.3) and introducing the cavity filling time t_f, one gets Eq. (6.4).

$$t_f \frac{dE_e}{dt} + E_e = \frac{2\beta}{1+\beta} E_i$$
$$t_f = \frac{2Q_L}{\omega_0} = \frac{2Q_0}{\omega_0(1+\beta)} \qquad (6.4)$$

If we take E_i to be 1, the emitted field E_e is obtained by solving Eq. (6.4) as

$$E_e = \frac{2\beta}{1+\beta}(1 - e^{-t/t_f}) \qquad (6.5)$$

Hence,

$$P_L = kE_L^2 = k(E_e - 1)^2 = k\{\frac{2\beta}{1+\beta}(1 - e^{-t/t_f}) - 1\}^2$$
$$P_L = \{\frac{2\beta}{1+\beta}(1 - e^{-t/t_f}) - 1\}^2 P_i \qquad (6.6)$$

$$\frac{P_L}{P_i} = \{\frac{2\beta}{1+\beta}(1 - e^{-(t-m_3)/t_f}) - 1\}^2 \qquad (6.7)$$

where the parameters β, t_f, and m_3 correspond to the cavity coupling coefficient, the cavity filling time, and the input timing, respectively.

In a steady state condition,

$$P_c = P_i - P_L = P_i - (\frac{1-\beta}{1+\beta})^2 P_i = \frac{4\beta}{(1+\beta)^2} P_i$$

If t_{bl} is the bunch length such that $t_{bl} << t_f$ then

$$P_c = 4\frac{\beta}{(1+\beta)^2} P_i (1 - e^{-t/t_f})^2 \qquad (6.8)$$

If we assume ZT^2 is the Shunt Impedance, then

$$ZT^2 = \frac{V^2}{P}$$

$$V_{acc} = \sqrt{P_C ZT^2}$$

Hence

$$V_{acc} = \frac{2\sqrt{\beta P_i R_0 T^2}}{(1+\beta)}(1-e^{-t/t_f}) \qquad (6.9)$$

6.1.2: The beam loading term

Instead of single bunch now let us assume *n* bunches. The inter bunch spacing is t_b. The effective beam loading is given by [2]:

$$V_b = V_{b0}(\frac{1}{(1-e^{-\tau})} - \frac{1}{2})$$

For transient case:

$$V_b = V_{b0}(\frac{1-e^{-(t-t_{inj})/t_f}}{(1-e^{-t_b/t_f})} - \frac{1}{2})$$

$$V_{b0} = 2kq$$
$$V_{b0} = \frac{w_0 Z T^2 q}{2Q_0}$$
$$V_{b0} = i_0 Z T^2 \tau_0 \quad \text{where } \tau_0 = t_b / t_{f0} \qquad (6.10)$$

Therefore for RF Gun the energy gain V_{RFG}

$$V_{RFG} = \frac{2\sqrt{\beta P_c Z T^2}}{(1+\beta)}(1-e^{-t/Ta}) - V_{b0}(\frac{1-e^{-(t-t_{inj})/T_a}}{(1-e^{-t_b/T_a})} + \frac{1}{2}) \qquad (6.11)$$

Equation 6.11 is the formula to calculate the energy gain for standing wave structure where V_{b0} is given by equation 6.10. From equation 6.11 it can be seen that the bunch-by-bunch energy for multi bunch beam depends on the bunch to bunch spacing, the injection time and input power. A balance between the filling time and injection time should be reached so that the bunch to bunch energy difference is minimum. This method of minimizing the energy spread by varying the injection time is called as ΔT (Delta T) Method for beam loading compensation [3].

Subsequent section shows the simulations done for the new RF gun operated in multi-bunch mode.

6.2: New RF gun: Total charge: 160 nC, No power multiplication

Let us now launch a 0.5 nC per bunch beam with 300-bunches per train using the parameters of new RF gun and the theory developed in section 6.1. To understand clearly the Delta T (ΔT) method of beam loading compensation we launch the first bunch at 3 different timing and check the effect of early, late and optimum injection time on the energy per bunch in the train.

Table 6.1: RF gun cavity parameter

Q for RF Cavity	14700
beta for RF cavity	1.0
Filling Time for RF Cavity	0.766 us
Number of bunches per train	300
Bunch Spacing	2.8 ns
Per Bunch Charge	0.55 nC
Total Charge	160 nC

Table 6.2: Output bunch to bunch parameter

Injection Time [us]	E_{ave} [MeV]	$E_{peak\text{-}to\text{-}peak}$ [MeV]	$E_{p\text{-}p}/E_{ave}$ %
2.0	5.13	0.118	2.5
2.45	5.21	0.00241	0.018
3.0	5.35	0.01664	1.65

In this case RF power input to the RF gun has 4μs pulse width and no power compression. Fig. 6.2 shows the loading curves for various injection times. When the first bunch passes through the structure, some power in the cavity goes to the bunch and the cavity power reduces. Hence, the next bunch in the train will see less power and thus have slightly less energy than the first bunch. This pattern can continue and thus we have a bunch-to-bunch energy difference. This situation is indicated by Curve 1 (for 3 μs) in the Fig. 6.2. On the other hand, if we launch the first bunch much earlier, then the first bunch gets low energy and takes away some part of the cavity power. By the time the next bunch arrives, the cavity power is enhanced due to filling of power and the subsequent bunches will have more energy. In this case, as well, we get a bunch-to-bunch energy

difference. This is indicated by Curve 3 (for 2 μs) in Fig. 6.2. If the bunch injection time is adjusted such that by the time the next bunch arrives, the loss in power is compensated by the filling power, then the next bunch will have same energy as the preceding bunch. Hence all the bunches in the train can have more or less same energy and the bunch-to-bunch energy difference will be less. This case is indicated by Curve 2 (for 2.45 μs) in Fig. 6.2. The method is called ΔT method of beam loading compensation. We use this method for our experimentation.

We achieve a small peak to peak energy variation if we inject at optimum timing. This is seen in Table 6.2. Fig. 6.3 shows the bunch to bunch energy variation for the case of best injection timing of 2.45 μs for this simulation.

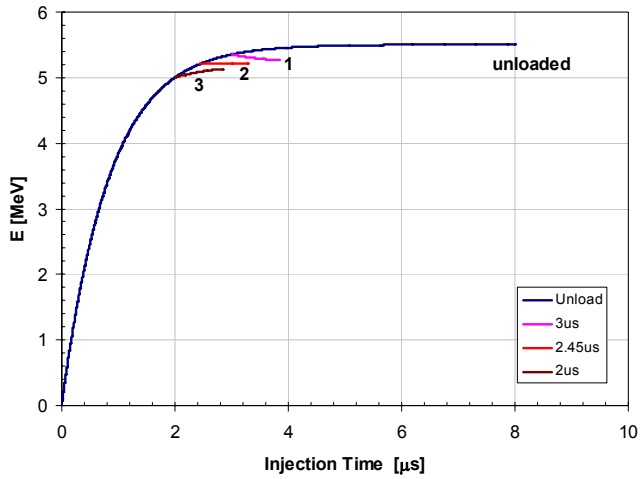

Fig. 6.2: New RF gun beam loading compensation

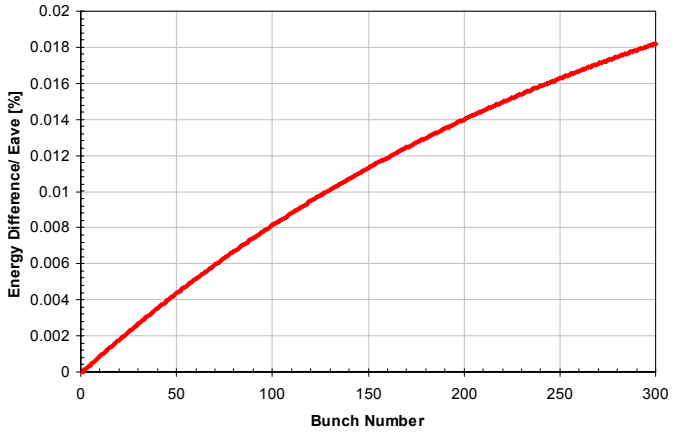

Fig. 6.3: Bunch-by-bunch energy for 300 bunch with 0.55nC per bunch

These results are later verified using the LUCX measurement setup. It should be noted that, for sake of clarity, three cases shown above are where the shift in the injection time is large. In real operation, the shifts are not so large. We use, the time delay units to change the injection time and the minimum delay we can set is 2.8ns and in multiples of this delay.

6.3: Beam loading for travelling wave constant gradient (TWCG) linac

The LUCX system consists of RF gun followed by a 3 meter long travelling wave constant gradient linac. Since the beam from RF gun is input to this linac and the injection at the linac should also be studied so as to get clear picture of compensation using delta T method.

Let us have a quick look at the equations that govern the energy gain and beam loading for the TWCG linac [4].

In presence of beam the power loss per unit time is:

$$\frac{dP}{dz} = \left(\frac{dP}{dz}\right)_{cav-wall} + \left(\frac{dP}{dz}\right)_{beam}$$

$$\frac{dP}{dz} = -2\alpha(z)P(z,t) - i(t)E(z,t)$$

The most general solution for above equation is:

$$\begin{aligned} V(t) = {} & E_0 L \frac{(1-e^{\frac{-wt}{Q}})}{(1-e^{-2\tau})} U(t) - E_0 L \frac{e^{-2\tau}}{(1-e^{-2\tau})}(1-e^{\frac{-w(t-t_f)}{Q}})U(t-t_f) \\ & + \frac{ri_0}{2}\{\frac{wLe^{-2\tau}}{Q(1-e^{-2\tau})}(t-t_i) - \frac{L}{(1-e^{-2\tau})}(1-e^{\frac{-w(t-t_i)}{Q}})\}U(t-t_i) \\ & - \frac{ri_0}{2}\{\frac{wLe^{-2\tau}}{Q(1-e^{-2\tau})}(t-t_i-t_f) - \frac{Le^{-2\tau}}{(1-e^{-2\tau})}(1-e^{\frac{-w(t-t_i-t_f)}{Q}})\}U(t-t_i-t_f) \end{aligned} \qquad (6.12)$$

For $t_i = 0$; $t = t_f$ and after 1 filling time:

$$V(t) = E_0 L + \frac{ri_0}{2}\{\frac{wLe^{-2\tau}}{Q(1-e^{-2\tau})}t - \frac{L}{(1-e^{-2\tau})}(1-e^{\frac{-wt}{Q}})\} \qquad \text{for } 0 \le t \le t_f$$

$$= E_0 L - \frac{ri_0}{2}\{1-\frac{2\pi e^{-2\tau}}{(1-e^{-2\tau})}\} \qquad \text{for } t \ge t_f \qquad (6.13)$$

6.3.1: Calculation for E_0L for above time regions

Consider the E_0L term in general equation.

$$V(t) = E_0 L\frac{(1-e^{\frac{-wt}{Q}})}{(1-e^{-2\tau})}U(t) - E_0 L\frac{e^{-2\tau}}{(1-e^{-2\tau})}(1-e^{\frac{-w(t-t_f)}{Q}})U(t-t_f)$$

For $t \le t_f$:

$$V(t) = E_0 L\frac{(1-e^{\frac{-wt}{Q}})}{(1-e^{-2\tau})}$$

$$\because E_0 L = \sqrt{(1-e^{-2\tau})}\sqrt{PZT^2 L} \qquad (6.14)$$

$\therefore$

$$V_a(t) = \sqrt{PZT^2 L}\frac{(1-e^{-2\tau\frac{t}{t_f}})}{\sqrt{(1-e^{-2\tau})}} \qquad (6.15)$$

For $t \ge t_f$:

$$V(t) = E_0 L\{\frac{(1-e^{-2\tau\frac{t}{t_f}})}{(1-e^{-2\tau})} - \frac{e^{-2\tau}}{(1-e^{-2\tau})}(1-e^{\frac{-w(t-t_f)}{Q}})\}$$

$$at\ \ t = t_f$$

$$V(t) = E_0 L\{\frac{(1-e^{-2\tau})}{(1-e^{-2\tau})} - 0\}$$

$$= E_0 L$$

(6.16)

Hence:

$$V_a = \sqrt{P_c Z T^2 L(1-e^{-2\tau})} \qquad (6.17)$$

The loading term can be calculated and hence the final V (t) can be calculated.

$$V_{Load} = -\frac{i_0 R_a}{2(1-e^{-2\tau})}\left[(1-e^{-2\tau\frac{(t-t_2)}{t_f}}) - 2\tau e^{-2\tau}\frac{t-t_2}{t_f} + \tau(1-e^{-2\tau})\frac{t_0}{t_f}\right] \qquad (6.18)$$

Hence,

$$V_{ACC} = \sqrt{P_c Z T^2 L(1-e^{-2\tau})} - \frac{i_0 Z T^2}{2(1-e^{-2\tau})}\left[1-e^{-2\tau\frac{(t-t_2)}{t_f}} - 2\tau e^{-2\tau}\frac{(t-t_2)}{t_f} + \tau(1-e^{-2\tau})\frac{t_b}{t_f}\right] \qquad (6.19)$$

Equation 6.19 gives the loaded energy gain for TWCG linac structures.

Till now we have assumed the RF power to be like square wave with no pulse compression. However as seen from Fig. 2.7 of chapter 2, the LUCX uses a pulse compressor. So let us now see how to introduce a pulse compression unit in our loading calculations.

We use Resonant Ring Compressor System (RRCS) at LUCX. The compression starts at 3 μs and there after in 1 μs time, the power can go up to 3.2 times the original power. This power is then split as shown in Fig. 6.4 below and then it goes to the gun and linac.

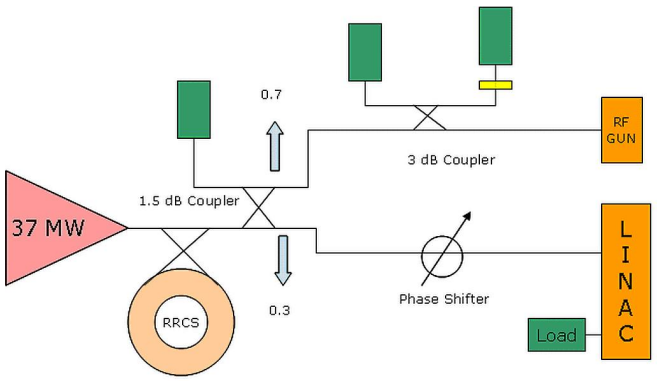

Fig. 6.4: Power distribution at LUCX

6.4: LUCX accelerator with 100 bunch at 50 MeV

In the simulation results shown in Fig. 6.6, the power comes from RRCS system and we input high power to RF gun and linac. The power that goes in linac is shown in Fig. 6.5. Corresponding energy gain is also seen in the same figure. The linac receives power for 1 μs and acceleration takes place only during this time. The beam has to be injected in this time window.

In the following explanation we assume a high input power of about 90 MW entering the linac tube. The power is much higher than the present deliverable power to the linac. We explain this situation a little later. For the time, assume that 90 MW power is entering the linac. Fig. 6.6 shows the beam loading characteristics for above linac in the region of interest. We launch a multi bunch beam at 3 positions. Curve 1 corresponds to injection at 3.3 μs and curve 3 corresponds to injection at 3.25 μs. As seen from plot, in both these cases, bunch to bunch energy variation is high. The launch time of 3.27 μs yields very good compensation as seen in Fig 5.

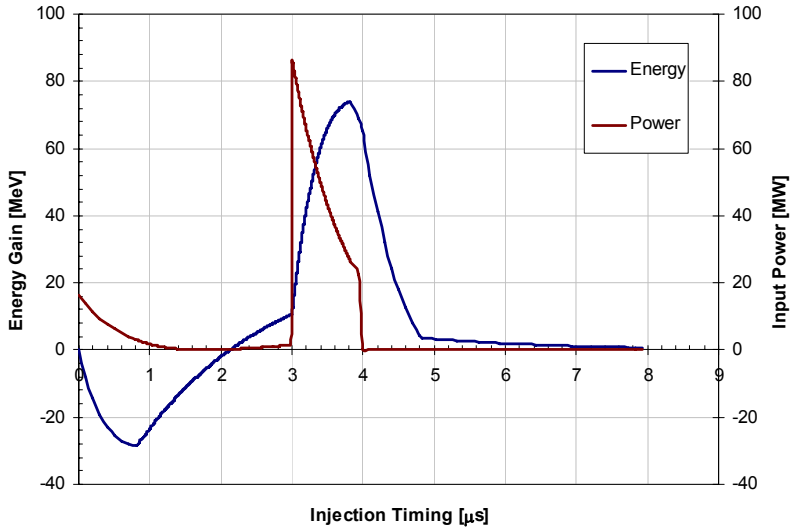

Fig. 6.5: Energy Gain Curve with power multiplier scheme in the travelling wave linac.

Fig. 6.7 shows the total beam loading that we are attempting to compensate using the ΔT compensation technique as described earlier in the chapter [5]. Once again, we show early, optimum and late injection to find out if we can indeed compensate the 2nC per bunch with 100 bunches per train. We find that we can compensate to get a low peak-to-peak energy difference with 50 MeV average energy, if we use a high input power of 90 MW going into the linac.

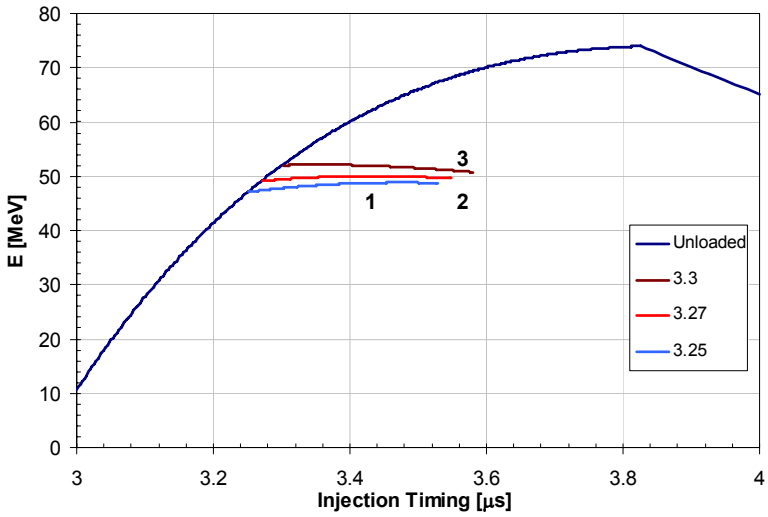

Fig. 6.6: Beam loading compensation in the region of interest for 2 nC per bunch, 100-bunches per train.

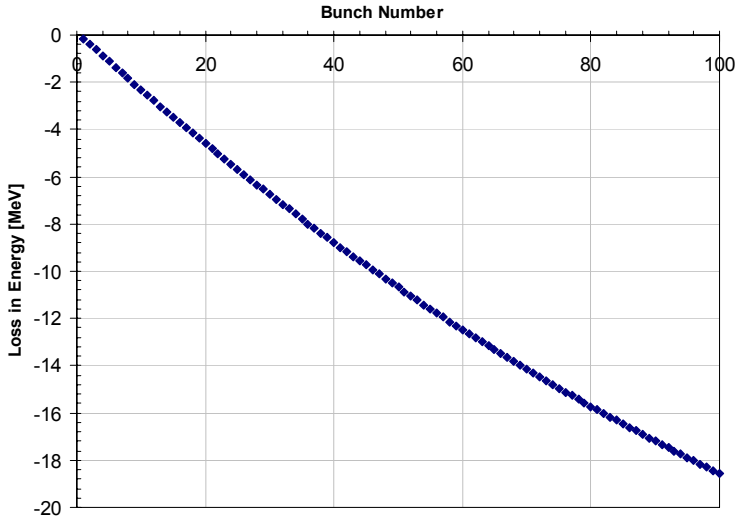

Fig. 6.7: Bunch by bunch energy variation for 100 bunches with 2nC per bunch charge

Now let us check if we can use the existing low power scheme to achieve beam loading compensation. In this case we can achieve a good beam but at low energies. This is clearly seen in Fig. 6.8 which shows the comparison of 2nc per bunch, 100-bunches per train acceleration for two different input power levels. For the case of existing RF system setup with one klystron and hence low power of about 36 MW at the linac port, we achieve good compensation but the beam energy is less than 30 MeV. For the modified RF system where we will have 2 klystrons driving

gun and linac independently, we expect around 90 MW or more power at the linac port with RRCS scheme. In this case we get good compensation at 50 MeV.

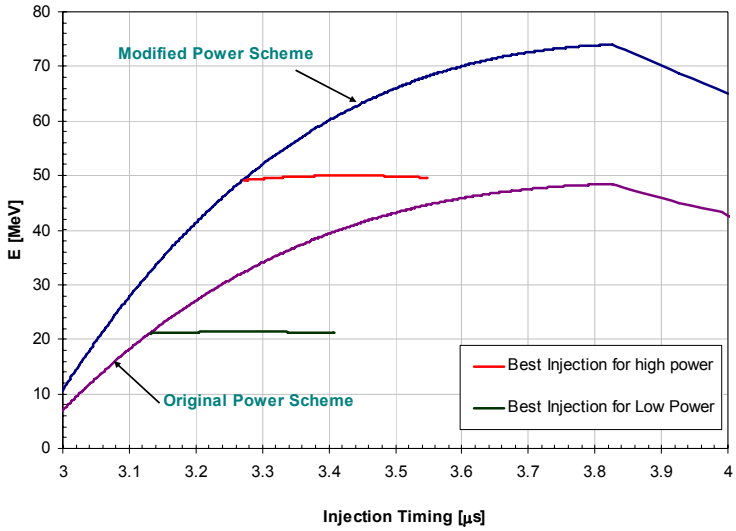

Fig. 6.8: Comparison of compensation scheme for different input power.

Thus in order to achieve high energy and a high charge beam with low peak to peak energy variation, we need to use a higher input power. Accordingly, a major change was proposed in the RF system. We decided to purchase one more klystron and modulator for RF gun. This will make RF gun system independent of linac system and we will have more control on timing in the gun and the linac. This will also lead to high power in the gun and the linac and so we can achieve high charge beam loading compensation with almost similar energy levels as of today. The new scheme is shown in Fig. 6.9.

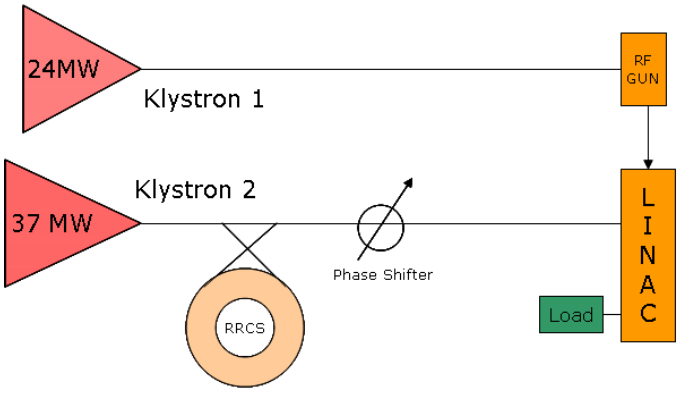

Fig. 6.9: Proposed power distribution system

The other change that was worked out was to achieve longer bunch train. The linac offers very

heavy beam loading as seen in Fig. 6.7. If we increase the number of bunches in train, this loading becomes more severe and the beam does not come out of the linac. This means that very long bunch trains with high charge per bunch can not be accelerated to high energies using the TWCG linac. In order to study the acceleration of many bunches in one train, we proposed to remove the linac and use the gun to accelerate 8000 bunches [6]. In reality, the existing laser system did not support more than 300 bunch operation and so we could verify our simulations up to 300 bunch generation.

6.5: Experiment No. 1: 100 bunch, 40 MeV

The experimental setup for generation of multi bunch beam is shown in Fig. 6.10. There is an analyzer magnet after the linac followed by beam position monitor, integrated current monitor and an OTR screen. We can use the combination of these instruments and find bunch to bunch energy variations when the bunch passes through the BPM. The analyzer magnet and screen is used to fix the energy of the bunch. For this case the beam position is known using the BPM signal. Now we launch a multi bunch beam. If the energy of a bunch is different from the average energy corresponding to the analyzer magnet setting, it will pass through a different location through the BPM. The BPM will record the position and the change in position with respect to mean position can be used to find the deviation in energy for bunch by bunch case. Thus using the screen, BPM and magnet we can measure the variations. The ICT is used to monitor if there is beam loss during the measurement.

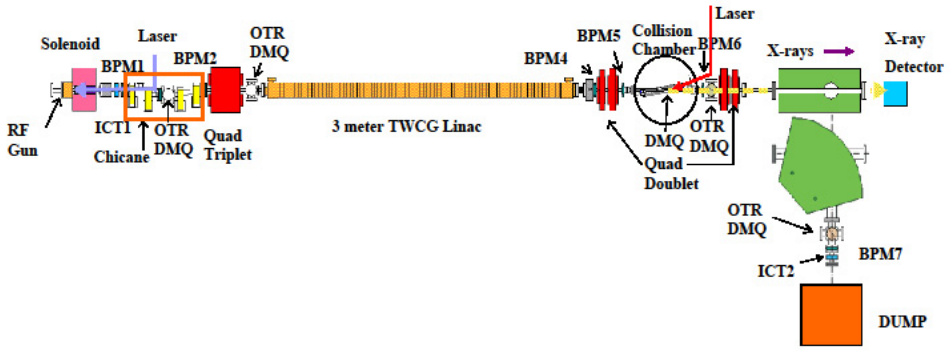

Fig. 6.10: Experimental setup for 40 MeV, 100 bunch beam

The linac is used to accelerate bunches to high energy. RRCS is used to enhance the power available at the linac input port. The pulse width of input power is about 1 μs and hence very long bunch train can not be accelerated.

The initial settings are done and the energy spread is minimized in 4-bunch mode. The phase plot is used to fix the gun injection phase and then the image of beam is obtained on screen MS4G after the bending magnet. The linac phase is now adjusted to get minimum energy spread. To achieve this, the acceleration of bunch is done off-crest. This reduces the energy gain but minimizes the energy spread.

After above mentioned initial tuning, we launched 100-bunch beam with 0.4nC per bunch charge. Then by varying the injection timing, we compensated this 40nC beam to get minimum peak to peak energy variation. The Fig. 6.11 shows the result of such measurement. Figure 6.12 shows the waveforms of BPM and ICT measurements recorded using an oscilloscope.

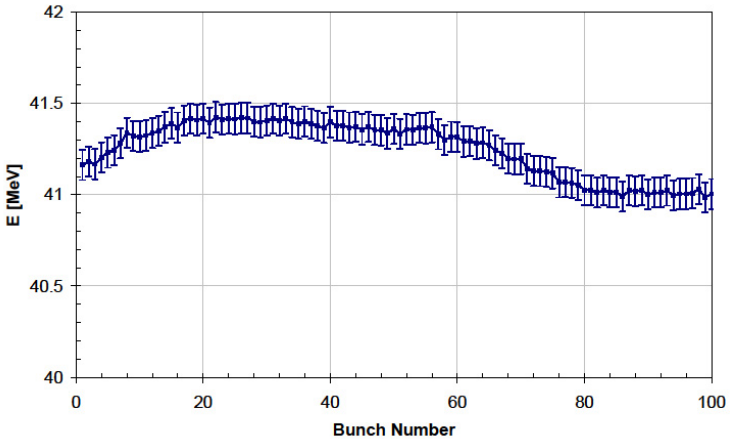

Fig. 6.11: Beam loading for 40 MeV in 100 bunches

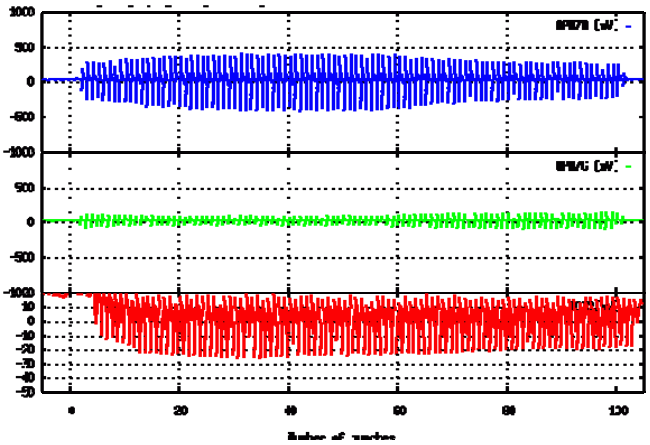

Fig. 6.12: Oscilloscope waveforms recorded during the measurement. The red waveform is for ICT monitor and it indicates bunch intensity at the location near the screen.

Table 6.3: Comparison of beam loading

P [MW]	Total Charge [nC]	$\%dE_{p-p}/E$
39.2	40	0.7
40.6	42	1.4
42.1	42.5	0.9

The table 6.3 shows that as we increase the charge we need more power to compensate for the beam loading effect. This is an expected conclusion and this is the reason why we need a high power klystron if we want to increase bunch charge or number of bunches.

6.6: Experiment No. 2: 300 bunches, 5 MeV

As we plan to go for large number of bunches with high charge per bunch, the linac can not be used due to heavy beam loading in the linac section. The position of beam will be displaced and some part of bunches may strike the cavity wall thus damaging the linac. Hence, we decided to remove the linac and use low energy beam for this experiment. The linac was removed and a long drift tube was introduced in the location of linac. After initial out gassing, the system was turned on. Figure 6.13 shows the new setup with out the linac.

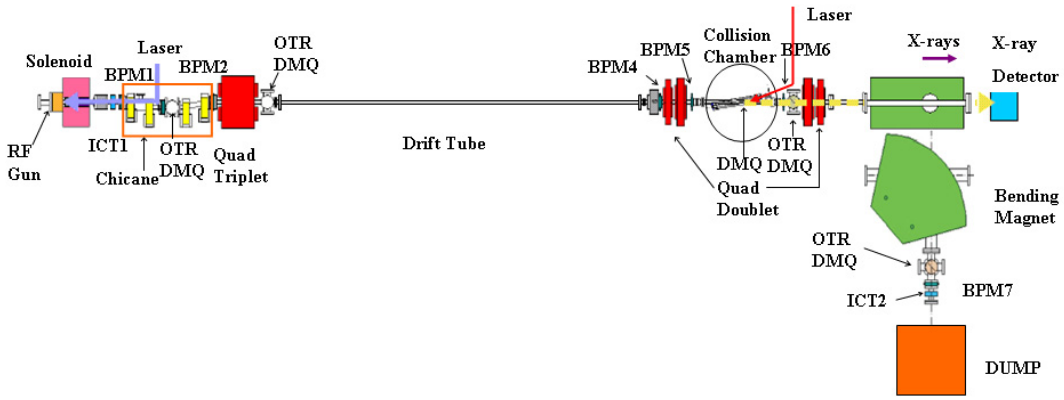

Fig. 6.13: Modified layout with the linac replaced by a drift tube

The purpose of this experiment was to try for long pulse train acceleration which needs long pulse power. So we decided not to use RRCS scheme and instead input entire klystron output pulse to the RF gun. In reality this resulted in heavy out gassing and hence we restricted to 2 μs pulse width. Figure 6.14 shows the input waveforms. The dark blue line is the forward power going to

the RF gun while the light blue line is the reflected waveform. The pink curve is the cavity power waveform. From the cavity power waveform, the filling time can be evaluated. We found that the filling time for this measurement was 0.76 μs. After careful tuning, the beam was successfully accelerated to the dump with no loss. Figure 6.15 shows that the beam indeed goes through till the dump. How ever we found that the beam may have a long tail due to dispersion in the bending magnet.

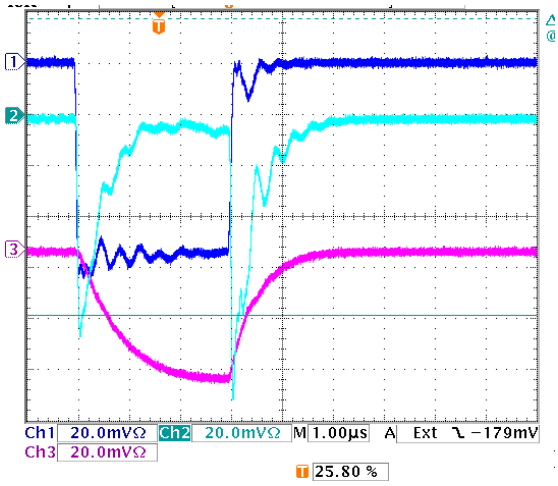

Fig. 6.14: Power waveform for low energy experiment. RRCS is turned off.

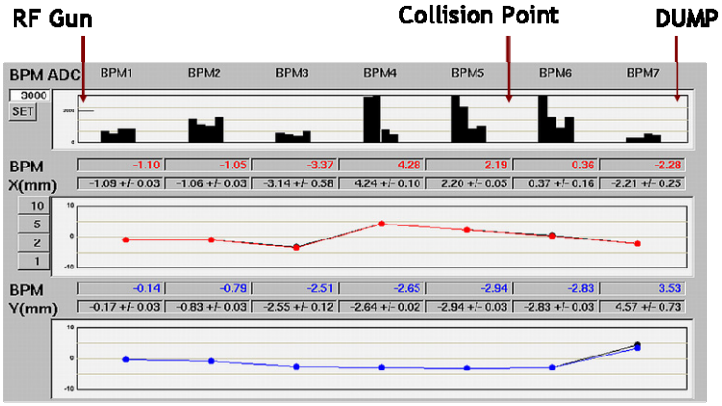

Fig. 6.15: Snap shot of beam position for 5 MeV beam.

After these initial settings, we planned the final experiment for 300 bunch beam. The Pockels cell for laser is capable of generating long pulse trains, however above 300 pulses, the waveform showed ringing and hence we can not use it for longer pulse train more than 300. For more bunches per train a new Pockels cell was required. So we decided to limit the experiment up to 300 bunches. The beam was carefully tuned starting from 4 bunch mode and gradually the bunch

number was increased to 36, 100, 150, and 230 and then finally to 300 bunches. Careful tuning was done at each stage to ensure that the beam goes to the dump. The charge of bunch was then gradually increased to 0.55nC per bunch. Figure 6.16 shows the results for 100-, 230-, and 300-bunch mode operation. The 100-bunch mode was performed at a charge of a 40 nC charge; the 230-bunch mode, at 80 nC; and the 300-bunch mode, at 160 nC. Figure 6.17 shows oscilloscope waveforms for the 300-bunch case.

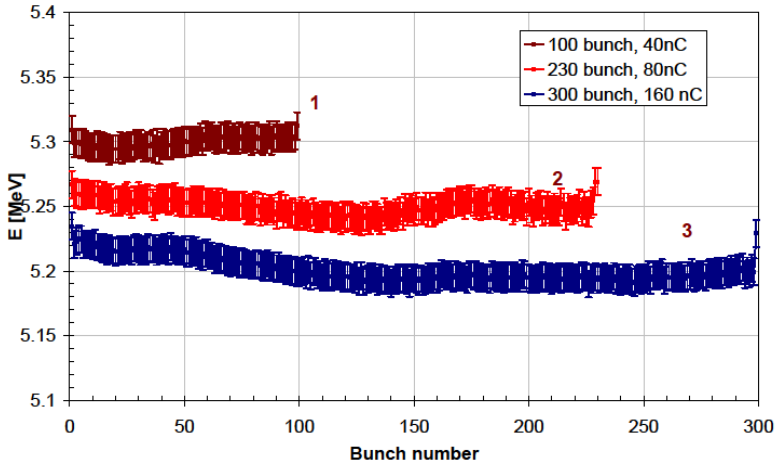

Fig. 6.16: Curves 1, 2, and 3 plot 100-bunch mode at 40 nC, 230-bunch mode at 80 nC, and 300-bunch mode at 160 nC, respectively.

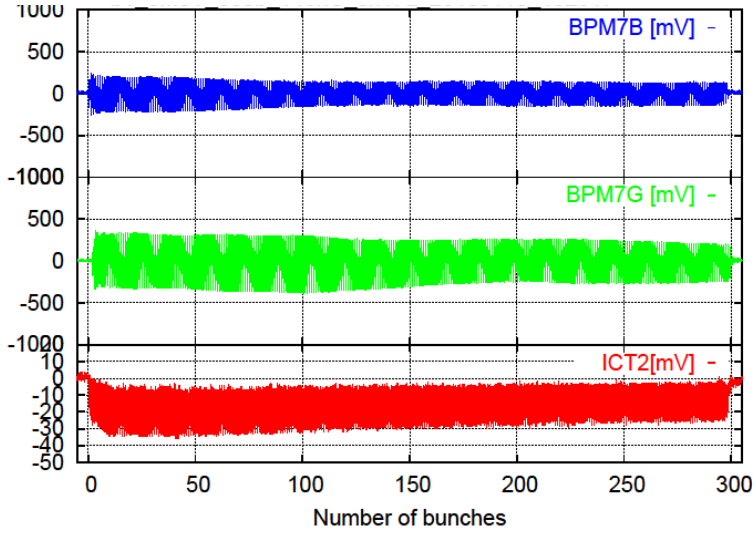

Fig. 6.17: Oscilloscope data for 300-bunch experiment. The upper two waveforms indicate position of bunches in the BPM while the last curve shows the current transformer waveform.

As seen from above plot, we generated successfully 300 bunch beam at 5 MeV with 160nC total charge. The peak to peak energy difference goes on increasing as we increase the bunch number. For present case, 100 bunch beam leads to 0.36% while 300 bunch beam leads to 0.85% peak to peak variations. Fig. 6.18 shows the comparison of calculated and measured values for same input conditions.

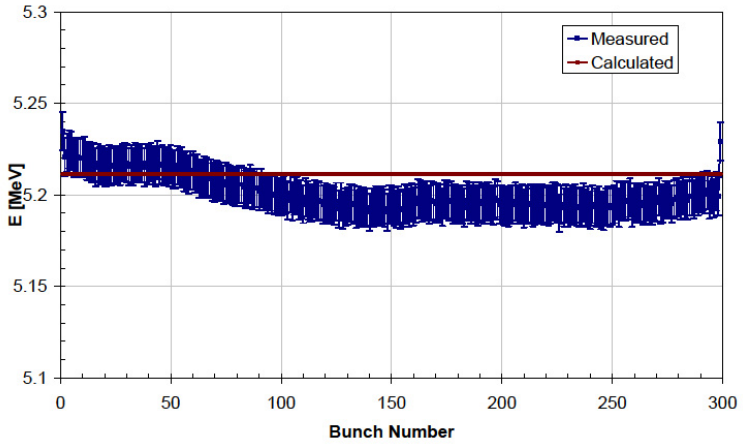

Fig. 6.18: 300 bunch 160nC total charge generation

Table 6.4: Measurement results for multi-bunch beam

Number of bunches	100	100	300
Energy [MeV]	41.5	5.3	5.25
Charge per bunch [nC]	0.5	0.5	0.55
Peak-to-peak energy difference [%]	0.7	0.36	0.85

Thus we successfully generated a long bunch train with high charge. The next target is to achieve 2nC per bunch charge and accelerate it successfully at 45 MeV. This will be possible by this year end when we make independent Klystron based power system for gun and linac. There after we plan to achieve 3000 bunches at 5 MeV with 0.5nc to 1nC charge per bunch. The final target is to accelerate 8000 bunches with 0.5nC or more bunch charge. Then we do multi bunch collisions with laser to achieve multi pulse x-rays.

References:

[1] K. Hirano, M Fukuda et al., Nuclear Instruments and Methods in Physics Research, A 560 (2006) 233-239

[2] P.B. Wilson, High Energy Electron Linacs: Applications to Storage Ring RF Systems and Linear Colliders, SLAC-PUB-2884, 1991.

[3] S. Liu et al., Nuclear Instruments and Methods in Physics Research, A 584 (2008) 1-8

[4] J. Wang, Ph D Thesis, SLAC-R-339

[5] Abhay Deshpande et al. Nuclear Instruments and Methods in Physics Research A 600(2009) 361-366

[6] Abhay Deshpande et al Proceedings of PAC 2009, MO6RFP065

Chapter 7: Results

This chapter summarizes the work done and lists down the important achievements of the work. We found that the new RF gun helped to achieve a good quality beam with low emittance value. We were successful in accelerating 300-bunches per train using the gun. This result is a boost for our future work.

7.1: Results

The improvement of the LUCX beam line was initiated in 2009 and it was planned to change the RF gun, the power delivery scheme, the laser system and extend the beam line to incorporate new experimental setup. The first three changes were to make a high charge multi-bunch beam with good quality and transport it to the collision point. The new laser system will then make it possible to use high power for collision with this high charge beam. The target is to achieve 2nC per bunch, 100 bunch beam in the collision region with energy nearly 45 MeV. The collision will then result in increase of flux from 10^5 to 10^7 or more photons / sec.

In this thesis, details of mode separated RF gun, beam parameter measurements and multi bunch beam generation is reported. Let us summarize in brief some achievements of the work.

A) The New RF gun was designed to change the mode separation from 3.5 MHz to 8.6 MHz. The internal profile of the gun cavity was changed to achieve a high Q structure. We successfully designed a curved internal profile and achieved an unloaded Q of 14,700. This is highest Q amongst all the RF guns we made. It is higher than the standard BNL gun and also the new LCLS gun design. The increased mode separation has enhanced the stability of the structure over thermal variations. The dark current of the new gun is found to be less than that of the old gun especially at higher power. This will help in tuning the system to low background during operation.

B) The increased mode separation has made it possible to operate the gun with less energy spread variations over injection phase variations with high energy output. This stability is one of the key features of the new gun. The emittance is reduced significantly and a good tuning will ensure further low emittance beam. The stable value of normalized emittance at the time of writing this report was 1.89 π-mm-mrad in the vertical plane. This value will further go down after we do good alignment and good tuning.

C) By removing the 3 meter long linac, we successfully generated 300-bunches with 160 nC total charge. The peak to peak energy difference for this measurement was less than 0.85% with average energy of 5.2 MeV.

D) With the linac in use, we generated 100-bunches with 40 nC total charge and peak to peak energy difference less than 0.7% at 41 MeV energy. Thus we established multi bunch beam generation for high energy-less bunches case as well as low energy-long

train case. This result is a big boost in our effort to deliver long trains with high charge in the measurement area.

E) The new RF gun design is thus found to be satisfactory and we found that the beam quality is enhanced after installation of new gun. Further tuning and conditioning will help achieve further better beam quality and will prove as a good injector for our experimentation.

Appendix 1

The 3.5 cell RF gun

After the successful design and development of the new RF gun with high Q and high shunt impedance, we decided to make a longer RF gun based on the profile of new RF gun. The main motivation for this new proposal is to make the acceleration system much more compact than the present one. In present setup, we use 1.5 cell standing wave (SW) RF gun and 3 meter long travelling wave linac to achieve 45 MeV. The total acceleration length is thus around 3.3 meter. With the proposed 3.5 cell SW RF gun, we will achieve 10-12 MeV electron beam energy at the gun exit. The 3 meter linac will be replaced by 0.8 meter long π-mode SW high gradient linac. The design of linac is on-going. In this way, we will achieve 45 MeV, 8000-bunches with total charge of 4 μC in about 1.2 meter acceleration length. This will make system compact.

Here we discuss the design and measurement results of the 3.5 cell RF gun. The gun fabrication was finished in Aug. 2010 and was ready for installation.

As discussed in the main thesis, we plan to make a very compact system to accelerate 8000 bunches to the collision area. To make the accelerating system more compact we adopted a new strategy. First we planned to make a 3.5 cell RF gun. The energy of bunches after the gun will be about 10 MeV. Next, we plan to make a π-mode standing wave linac with 50 MV/m gradient. The 10 MeV bunches will be accelerated using this standing wave linac to achieve 8000-bunches with 0.5 nC per bunch charge at 45 MeV in the collision area. The active acceleration length will be thus reduced to 1.2 meters.

The design of 3.5 cell RF gun is similar to the new gun. We added two identical cells. The RF input is in last cell so that we can use the same input setup at LUCX. To enhance the pumping, we make two vacuum ports in 1st full cell. In addition there will be a vacuum port in full cell no. 3, as always opposite to the RF waveguide slot. Fig. A1.1 shows the Super Fish profile of the long RF gun.

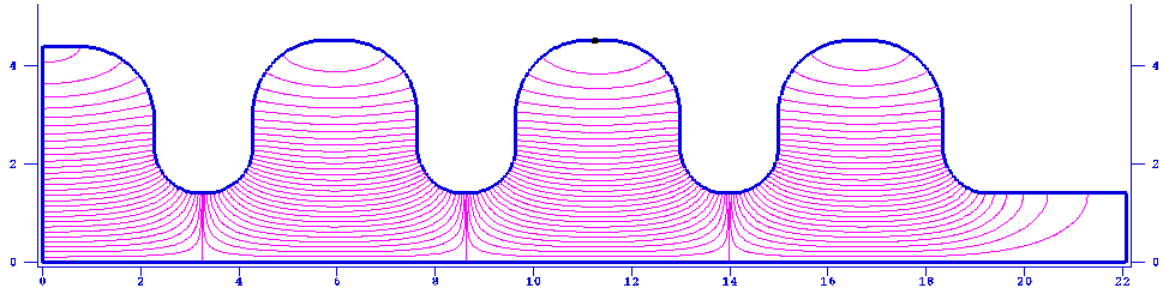

Fig. A1.1: The 3.5 cell RF gun profile

Since this gun has 4 cells, we expect 4 modes of excitation with π mode being the operational mode. We will get 2π/3, π/3 and 0 modes as well. Fig. A1.2 shows the fabricated structure. Table A1.1 shows the simulation and initial measurement results.

Table A1.1: Measured frequencies of various modes for 3.5 cell gun

	Cell Frequency				Mode Frequency			
	HCF	FC1F	FC2F	FC3F	π	2π/3	π/3	0
Simulation	2949.63	2849.61	2850.14	2852.36	2855.59	2853.09	2847.94	2843.57
Measured	2849.62	2849.63	2850.1	2852.33	2855.85	2852.95	2848.21	2843.75

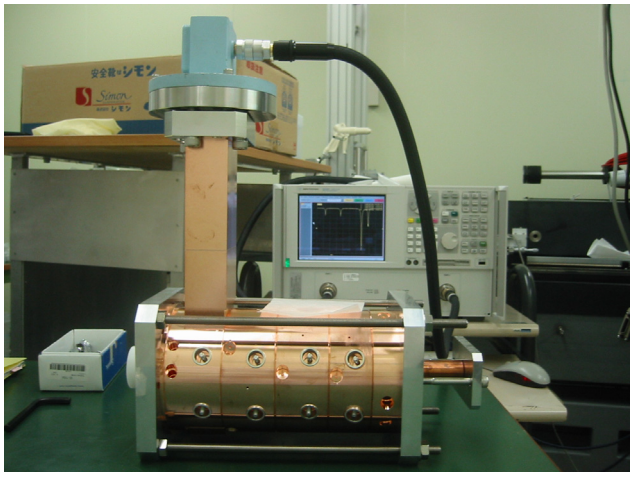

Fig. A1.2: 3.5 cell gun during measurement

In the above photograph, half cell is towards right end while the full cell is on left side. Figure A 1.3 shows the measured mode spectrum recorded using Vector Network Analyzer (VNA).

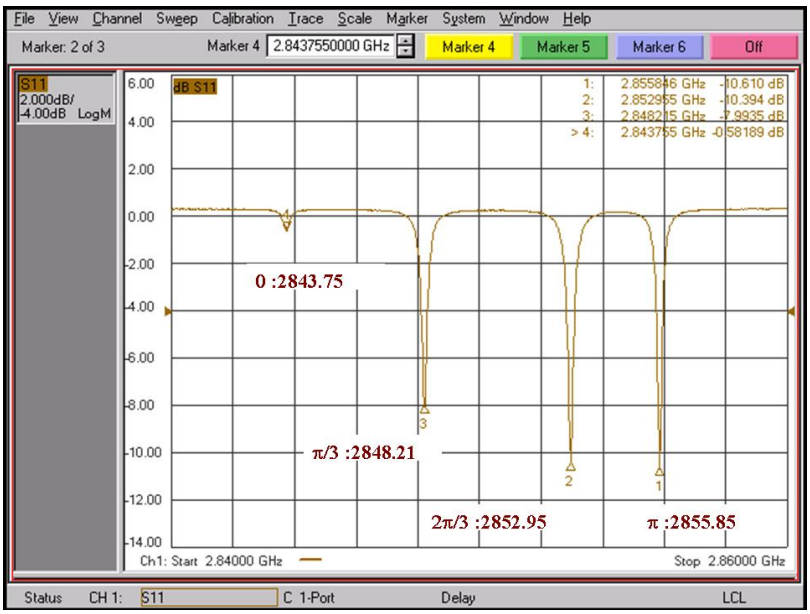

Fig. A1.3: Mode spectrum of 3.5 cell RF gun

The gun was be fabricated, brazed and tuned in Aug 2010. The final processing is planned in Sept. 2010.

Appendix 2

Future plans

The work initiated at LUCX to generate high bunch charge with long bunch trains and to make high gradient structures has tremendous potential in research as well as industry. The traditional accelerator for cancer therapy application or industrial application is based on four decade old technology. A compact RF gun can yield about 15 MeV energy in 30 cm length, thus making it possible to make the acceleration unit compact and more effective for applications. In this appendix, we discuss design details of the compact x-ray source using π/2 mode linac. We also discuss an example of simple application for patient treatment based on a high gradient linac.

A 2.1: π/2 mode compact source at 3 GHz in India

It is proposed to build an Inverse Compton X-ray source similar to LUCX as a collaborative work between KEK and 'SAMEER' research lab in India. SAMEER stands for Society for Applied Microwave Electronics Engineering and Research and is a research laboratory of Government of India focusing on application of accelerator physics for medical treatment. We have already developed and installed medical linac and completed 30,000 patient treatments in 2 yrs. The operation frequency of SAMEER linac is 3 GHz. The main difference is that the linac used is π/2 mode standing wave linac [1, 2, and 3]. Such structure with high shunt impedance can yield high energy beam in small length with less power. The proposed beam line will look as in Fig. A2.1 below. The main parameters for gun and linac are in Table A2.1.

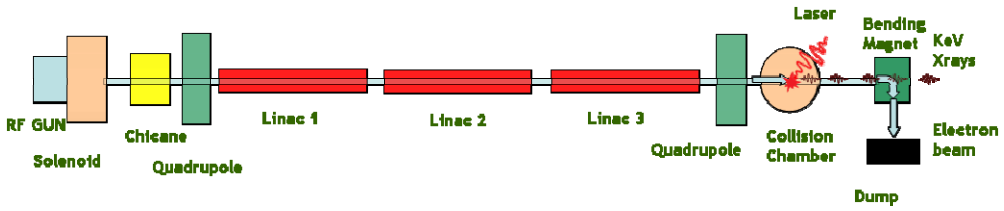

Fig. A2.1: Proposed lay out of π/2 linac based beam line

Table A2.1: Gun and linac parameters

Parameter	RF GUN	SAMEER Linac
Frequency in MHz	2998	2998
Mode of Operation	π	π/2
No of Cells	1.6	23.5
Cavity	Standing Wave	Standing Wave
Input Power	10 MW with 6 μs (peak)	5 MW in 6 μs peak
Repetition Rate	50 Hz	200 Hz
VSWR	1.0	1.4
Q	14000	15000
Shunt Impedance (ZT^2)	40 MΩ / m	87 MΩ /m
Peak Electric Field	120 MV/m	30 MV/m

A2.2: Linac design

The basic design parameters of linac tube are given in Table A2.2. The cavity designed for the linac tube is shown in Fig. A2.2 while the Super Fish profile for single cell is shown in Fig. A2.3 [4]. The linac operates at π/2 mode, hence every alternate cavity has no accelerating fields and plays role in coupling the power only. These coupling cells are moved out of main axis of linac thus making the linac a side coupled structure. In case of on-axis coupled structure, the length of cells can be reduced to reduce the over all length of the structure.

Fig. A2.2: Linac cavity at various stage of fabrication

Table A2.2: Measured linac parameters for existing 15 MeV linac tube

Parameter	Simulated	Measured	
π/2 frequency,	2997	2998	MHz
Side to main coupling	0.03	0.0267	%
Shunt Impedance,	100	87	MΩ/m
Q (unloaded)	16000	15000	
VSWR	1.4	1.56	

The choice of π/2 operation mode was made due to the fact that for this mode frequency is much stable against the dimensional errors in fabrication and against temperature related variations. The shunt impedance of an on axis coupled π/2 mode linac is less as compared to the π mode. But by choosing the off-axis structure, one gets the advantages of π-mode like shunt impedance. These structures are therefore very popular in making moderately high current, stable beam linac structures, mainly used for medical applications. The structure design is very complicated from fabrication point of view but we have successfully established the fabrication, tuning and measurement procedure for the linac. All components are fabricated and brazed in-house at

SAMEER campus in India. The 15 MeV linac structure contains 24 accelerating cells and 23 coupling cells. The existing linac tube has two and half buncher cavities for bunching the beam from the dc gun.

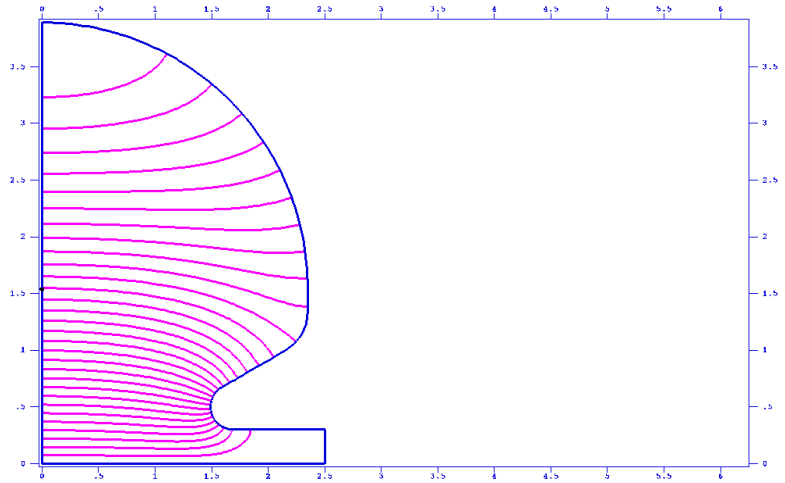

Fig. A2.3: Super Fish plot of a single cell

The unloaded Q of the structure was found to be 15000 with shunt impedance of 87 MΩ/m measured using bead perturbation technique. Fig. A2.4 shows the brazed linac tube. The electron gun is diode type with dispenser cathode having current density of 2 A/cm^2. This gun will be replaced by RF photocathode gun as mentioned in the next section. The RF window is water cooled with ceramic of thickness 2.77 mm. The window is capable of handling 10 MW peak power.

A2.3: RF photo cathode gun

The existing gun in the SAMEER linac is a diode gun and the electron bunches are formed in the buncher cavities which are a part of the main linac. The main disadvantage of such a gun is that, the users do not have any control over the bunch structure. Choosing RF photocathode gun can help get a very good control on bunch and the bunch train structure. The main parameter that is against such a gun is the cost factor of a RF photo cathode gun which is much higher as compared to a thermionic gun. At present we propose to use photocathode gun based on new LUCX gun scaled to the new operating frequency of 3.0 GHz as shown in Fig. A2.5. In our setup, long pulse RF will drive the gun and hence to avoid dilution of emittance due to excitation of zero modes, we propose to increase the separation between operational π and zero modes to 10 MHz or more while maintaining the field balance of half cell fields to full cell fields near unity.

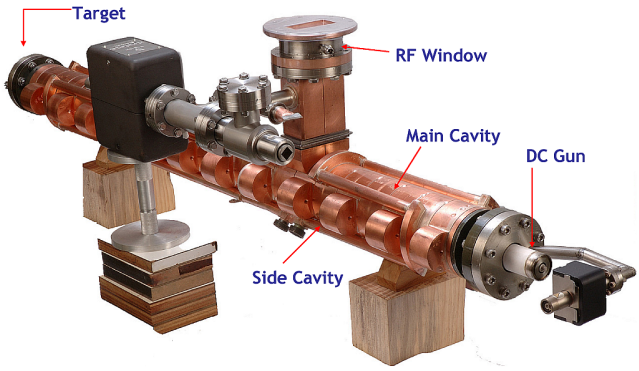

Fig. A2.4: SAMEER made side coupled linac tube. The diode gun is on the right end of the figure. RF Window is on top and the in-built target for bremsstrahlung X-rays is on left opposite end and not visible in this photograph. The gun will be replaced by RF photocathode gun.

A solenoid will be provided to achieve emittance compensation after the exit from the gun and a good quality, low emittance beam with emittance less than 2π-mm-mrad is expected at the entrance point of the first linac. The profile of the proposed RF gun cavity is shown in Fig. A2.5 and the main parameters are listed in Table A2.3.

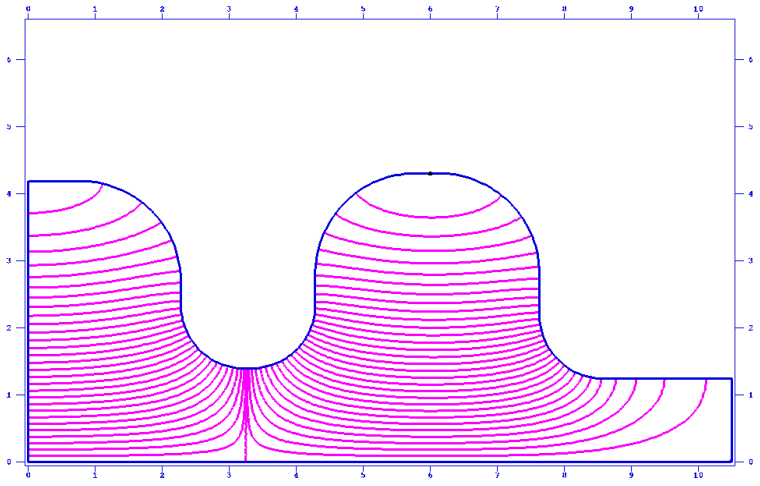

Fig. A2.5: RF gun cavity profile using Super Fish code

A2.4: Lasers and the collision chamber

The X-ray source system will have two laser systems. One laser is used to generate the electrons by hitting the photocathode. The beam of electrons is then subjected to very high fields near the cathode in the RF gun cavity and the degrading effect of space charge forces is quickly compensated to get a low emittance beam out of the gun. The beam is then accelerated to 45 MeV energy using three linac tubes. Then using a quadrupole doublet the beam is focused to make the

beam size of the order of 50 μm in the collision chamber. The second laser system produces continuous streams of infrared laser pulses with bunch spacing same as that of the incoming beam train and these laser pulses collide with the electron bunches.

Table A2.3: RF gun cavity parameters

π mode Frequency	2998	MHz
Zero mode Frequency	2988	MHz
Mode Separation	10	MHz
Field Balance	1.0	
Q	15,000	

The gun laser is a mode locked pulsed laser with 7W at 1064 nm to generate the laser pulses at 375 MHz. Using Pockel cells 2250 pulses will be selected, amplified and down converted to 266 nm using a BBO crystal. The pulse width of this UV laser pulse will be around 5.5 ps (rms). With Cesium Telluride (Cs_2Te) photocathode, assuming quantum efficiency of 1% this laser will be sufficient to produce around 220 pC per bunch charge at the cathode.

The collision chamber laser will be a 1064 nm mode locked pulsed laser to produce uniformly spaced, 2.66ns pulses. The collision chamber contains a laser cavity in which the amplitude of the laser pulses will be enhanced and the collision will take place at the center of the cavity. The chamber design will be as per the collision chamber work at LUCX, KEK.

Proper synchronization and low jitter operation will enhance the ultimate performance of the X-ray source. The chamber will have horizontal and vertical movement using motorized system. This is essential to move the laser beam to collide with the electron beam. The angle of collision plays an important role to decide the energy of exit photons. With 20 deg collision at 45 MeV it will be possible to generate 35 KeV Compton X-rays. Further it is possible. The parameters of the proposed source are given in Table A2.4 below.

A2.5: Ultra light radio therapy linac

The present day technology (developed in 1970's) has made it possible to deliver 6 to 18 MeV X-ray photons to the patient for cancer therapy. The dose rate of such radiation oncology machine is around 300 rads/min at 1 meter (RMM). In principle the linac is capable of high dose delivery,

but the clinical radiation issues restrict the dose rates to the limit where the exposure is just sufficient not to harm other tissues of the patient. It is essential from patient's health point of view.

Table A2.4: Parameters of X-ray source

Parameter	Value	
Electron Beam Energy	45	MeV
No of bunches	2250	per train
Charge per bunch	220	pC
Bunch spacing	2.66	ns
Transverse beam size	< 60	μm
Collision Angle	20	degree
X-ray energy	35	keV
X ray flux	4.1×10^8	photons /sec / 1% bw

Apart from the dose rate and stability, the isocenter height (height from floor to isocenter) and the gantry weight are two other parameters important from hospital and doctor point of view. The technology for linac in radiation machine is 40 yrs old technology and it can be replaced easily with new work done in high gradient linac in past few years. Mitsubishi Corporation have already made use of C-band linac based gantry which has easier motions and hence better dose control in latest dose delivery techniques like Intensity Modulated Radiation Therapy etc.

We propose a new setup with RF gun based compact linac. In our proposal, we will make a small 3 and ½ cell (or longer) RF gun with laser port at 45 deg. for side-wise incidence. This removes the chicane. The out put beam will be focused at the Gantry center location of rotary joint. The beam will bend at this place and follow the gantry. With total 3 bends it will be possible to hit the beam to target and produce high dose rates. The main feature of this system is that the gantry will contain nothing but the bending magnets and drift tubes. This will reduce the gantry weight significantly and a small gantry can be made. The isocenter height can be chosen as per convenience. The current, most available standard isocenter height is ~ 130 cm, how ever around 120 cm or even low can be achieved in the new technique.

Figure A2.6 shows the SMR make existing gantry. Figure A2.7 shows the new proposal. This proposal also is an out come of the experience gained at LUCX.

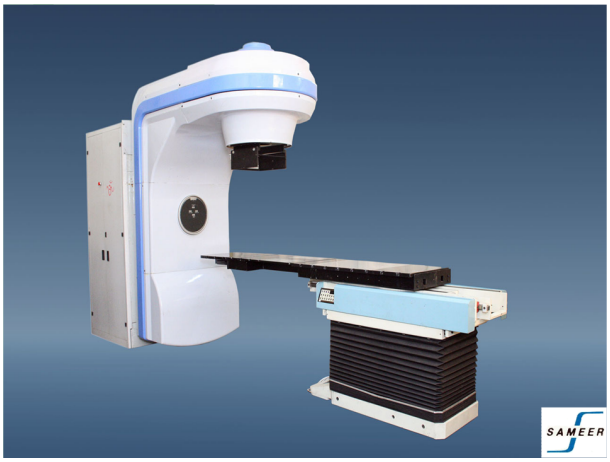

Fig. A2.6: SAMEER medical therapy linac

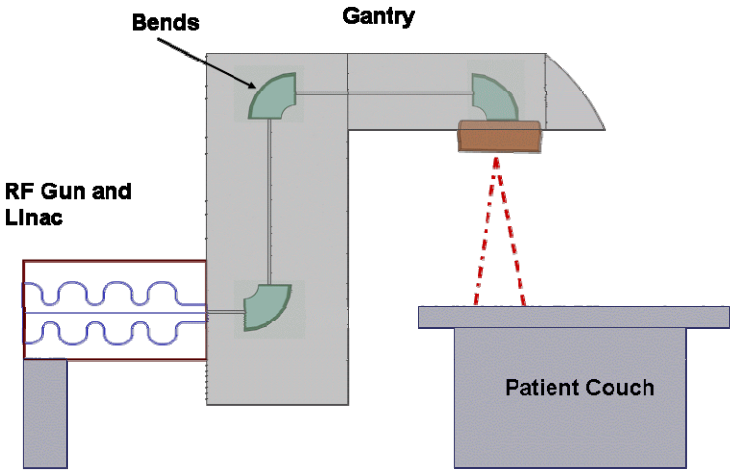

Fig. A2.7: Proposed layout of compact gantry system

References:

[1] Abhay Deshpande, Tanuja Dixit et al, Proceedings of InPAC 2005, pp 85

[2] R Krishnan et al, Proceedings of PAC-2009, May 2009, FR5REP083.

[3] Tanuja Dixit et al, Proceedings of PAC09, May 2009, WE5PFP016

[4] Abhay Deshpande et al. Nuclear Instruments and Methods in Physics Research (2010), doi:10.1016/j.nima.2010.02.023

Appendix 3

Modifications of LUCX

The existing setup of LUCX was modified after discussions and the beam line modification started in January 2010 and completed in April 2010. The beam line was extended to incorporate a new experimental station as shown in Fig. 7.1 [1]. A new experiment with Coherent Diffraction Radiation is proposed [2] at the new station area. The beam now bends twice in the x-plane and then transports to the vertical bending magnet, now pushed much farther than earlier. This has made the collision chamber region easily accessible and the beam moves in different transverse plane than the out going x-rays. Hence the back ground signal may reduce. Figure A3.1 shows the modified layout of LUCX. There is no change in components till collision chamber, so the setup for earlier experiment is maintained as it. As of Aug. 2010, the beam tuning is going on and experimentation will start after radiation safety inspection.

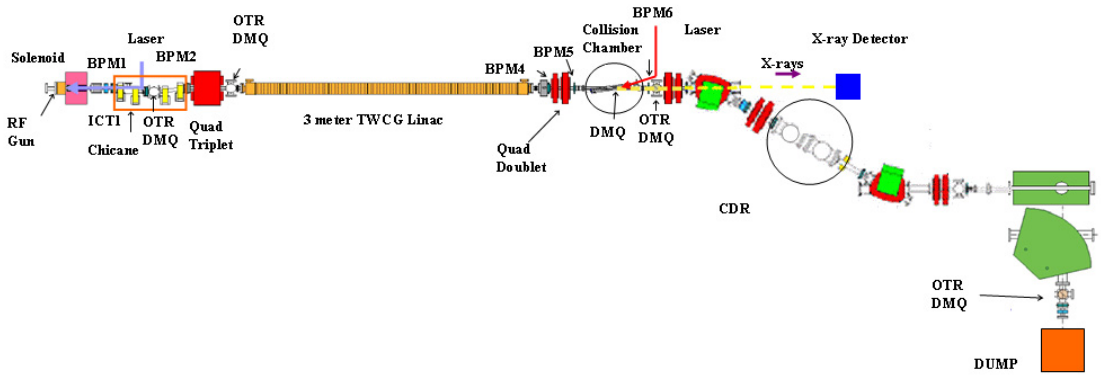

Fig. A3.1: The new beam line. The position of bending magnet is shifter further ahead so that the cathode to the dump distance is increased. Two additional bends are introduced. The additional setup for coherent diffraction radiation (CDR) experiment is included after first bend.

References:

[1] M. Fukuda et al. Nuclear Instruments and Methods in Physics Research A,

doi:10.1016/j.nima.2010.02.024

[2] A. Aryshev et al. Proceedings of IPAC 2010 MOPEA053

Bibliography

Chap. 1

[1] F. Hinode et al. ATF Design and Study Report, KEK Report 1995-4

[2] K. Hirano, M Fukuda et al., Nuclear Instruments and Methods in Physics Research, A 560 (2006) 233-239

[3] J. Gao, KEK ATF Internal Report, ATF-04-01, 2004.

[4] Liu S. et al., Nuclear Instruments and Methods in Physics Research, A 584 (2008) 1-8

[5] K. Sakaue et al., Rev. Sci. Inst. 80 (2009) 123304.

[6] K. Sakaue, Ph D Thesis, Waseda University 2009

[7] D. T. Palmer, Ph D Thesis, Stanford University 1998

[8] L. Xiao, D H Dowell et al. SLAC Pub 11213 (2005)

[9] S. G. Anderson et al, Proc. of PAC 2007, TUPMS028

[10] J.Y. Raguin, R.J. Bakker, Proceedings of FEL 2005, pp 324

[11] Y. Park, RF gun at PAL-Postech, AAWS-2010 http://kocbeam.kek.jp/

[12] J. H. Hong, I S Koo et al, Proceedings of IPAC 2010 TUPEC014

[13] Abhay Deshpande, J Urakawa et al Nuclear Instruments and Methods in Physics Research, A 600(2009) 361-366

[14] C. Limborg et al. LCLS Tech Note, LCLS-TN-05-3

[15] D. H. Dowell et al. Nuclear Instruments and Methods in Physics Research, A 528, 316-320 (2004)

[16] Quantum Beam Project, http://kocbeam.kek.jp

Chap. 2

[1] K. Hirano, M Fukuda et al., Nuclear Instruments and Methods in Physics Research, A 560 (2006) 233-239

[2] Liu S. et al., Nuclear Instruments and Methods in Physics Research, A 584 (2008) 1-8

[3] K. Sakaue et al., Rev. Sci. Inst. 80 (2009) 123304.

[4] X. J. Wang et al. Nuclear Instruments and Methods in Physics Research A 375 (1996) 82-86

[5] L. Xiao, D H Dowell et al. SLAC Pub 11213 (2005)

[6] Y. Park, RF gun at PAL-Postech, AAWS-2010 http://kocbeam.kek.jp/

[7] J. H. Hong, I S Koo et al, Proceedings of IPAC 2010 TUPEC014

[8] S. H. Kong et al. J. Appl. Phys., 77(11), (June 1995)

[9] R. A. Powell et al. Phys. Rev. B, Vol. 8, Number 8 (Oct 1973)

[10] K. Sakaue, Ph D Thesis, Waseda University 2009

[11] S. Yamaguchi et al. KEK Pre-print 94-87 (1994)

[12] Z. D. Farkas, SLAC-TN-73-08 (1973)

[13] P. B. Wilson, SLAC-TN-73-15 (1975)

Chap. 3

[1] C. Limborg et al., LCLS Tech Note, LCLS-TN-05-3

[2] S.G. Anderson et al, Proc. of PAC 2007, TUPMS028

[3] K. Hirano, M Fukuda et al., Nuclear Instruments and Methods in Physics Research, A 560 (2006) 233-239

[4] Abhay Deshpande, J Urakawa et al Nuclear Instruments and Methods in Physics Research, A 600(2009) 361-366

[5] Y. Kamiya et al. Proceedings of PAC 2007, pp 2808

[6] D. T. Palmer, Ph D Thesis, SLAC 1998

[7] K. Halbach and R. F. Holsinger, "SUPERFISH - A Computer Program for Evaluation of RF Cavities with Cylindrical Symmetry," Particle Accelerators 7 (1976) 213-222

[8] K. Flöttmann, A Space Charge Tracking Algorithm, ASTRA, http://www.desy.de/~mpyflo/

[9] J. Rose, Proceedings of PAC 2001, pp 2221

[10] H. Matsumoto et al, KEK pre-print 91–47, May 1991.

[11] H. Matsumoto, Proceedings of LINAC 1996, pp 626-630

Chap. 4

[1] K. Flöttmann, A Space Charge Tracking Algorithm, ASTRA, http://www.desy.de/~mpyflo/

[2] L.Young, J.Billen , PARMELA, LANL Codes,

[3] C. Limborg et al, Proceedings of PAC 2003, pp 3548-3551

[4] K. J. Kim, Nuclear Instruments and Methods in Physics Research A 275(1989) 201-218

[5] J. Gao, ATF Report, 2003

Chap. 5

[1] B. E. Carlsten et al., Nuclear Instruments and Methods in Physics Research, A 285 (1989) 313-319

[2] Sheng-Guang Liu, Junji Urakawa et al 2010 Chinese Phys. C 34 584

[3] H.Dewa, T.Asaka, et al. in Proceedings of FEL 2006, BESSY, Berlin, Germany, pp. 649–652.

[4] C. Limborg et al., LCLS Tech Note, LCLS-TN-05-3

[5] J.Y. Raguin, R.J. Bakker, Proceedings of FEL 2005, pp 324

[6] D.H. Dowell et al., Nuclear Instruments and Methods in Physics Research A 528 (2004) 316.

[7] K. Floetmann, Tesla-Fel-97-01 (Feb., 1997)

[8] D.H. Dowell and J. F. Schmerge, PRST-AB, 12, 074201 (2009)

[9] Jim Clendenin, SLAC PUB 7760

[10] J. D. Lawson, The physics of Charged Particle Beams, Clarendon Press, Oxford, 1988, p 210.

Chap. 6

[1] K. Hirano, M Fukuda et al., Nuclear Instruments and Methods in Physics Research, A 560 (2006) 233-239

[2] P.B. Wilson, High Energy Electron Linacs: Applications to Storage Ring RF Systems and Linear Colliders, SLAC-PUB-2884, 1991.

[3] S. Liu et al., Nuclear Instruments and Methods in Physics Research, A 584 (2008) 1-8

[4] J. Wang, Ph D Thesis, SLAC-R-339

[5] Abhay Deshpande et al. Nuclear Instruments and Methods in Physics Research A 600(2009) 361-366

[6] Abhay Deshpande et al Proceedings of PAC 2009, MO6RFP065

Appendix 2

[1] Abhay Deshpande, Tanuja Dixit et al, Proceedings of InPAC 2005, pp 85

[2] R Krishnan et al, Proceedings of PAC-2009, May 2009, FR5REP083.

[3] Tanuja Dixit et al, Proceedings of PAC09, May 2009, WE5PFP016

[4] Abhay Deshpande et al. Nuclear Instruments and Methods in Physics Research (2010), doi:10.1016/j.nima.2010.02.023

Appendix 3

[1] M. Fukuda et al. Nuclear Instruments and Methods in Physics Research A,

doi:10.1016/j.nima.2010.02.024

[2] A. Aryshev et al. Proceedings of IPAC 2010 MOPEA053